

POLITECNICO DI TORINO

I Facoltà di Ingegneria

Corso di Laurea in Ingegneria Nucleare

TESI DI LAUREA

Field quality analysis to monitor the industrial series production of the dipole magnets for the Large Hadron Collider

Relatore
Prof. Ing. Giovanni Del Tin

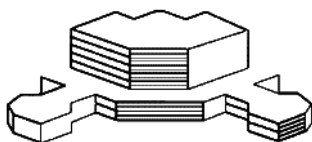
Relatori esterni
Dott. Ezio Todesco (C.E.R.N.)
Dott. Walter Scandale (C.E.R.N.)

Candidato
Stefano Pauletta

Luglio 2002



Special thanks for the financial and logistic support to:



ASP, Associazione per lo Sviluppo scientifico e tecnologico
del Piemonte



CERN, Centre Européenne pour la Recherche Nucléaire

Contents

Introduction	v
1 CERN and the Large Hadron Collider project (LHC) ...	1
1.1 CERN	2
1.1.1 Particle accelerators	2
1.1.2 CERN accelerator complex	5
1.1.3 The Large Electron Positron Collider (LEP)	6
1.1.4 From LEP to LHC	6
1.2 The LHC Project	8
1.2.1 Machine performance	8
1.2.2 Machine basic layout	9
1.2.3 Superconducting technology for accelerator magnets	11
2 The LHC main dipoles	13
2.1 Main features and parameters	14
2.2 Main components	16
2.2.1 Superconducting coils	17
2.2.1.1 Superconductivity	17
2.2.1.2 The cables	19
2.2.2 Mechanical structure	20
2.2.2.1 Collars	20
2.2.2.2 Iron yoke	21
2.2.2.3 Shrinking cylinder	21
2.2.3 Cryostat	22
2.3 Magnet assembly	23
2.3.1 Coils	23
2.3.2 Collared coil	24
2.3.3 Cold mass	25
3 Magnetic design of the dipole coil	27
3.1 Coil design	28
3.1.1 Definition of field harmonics	28

3.1.2	Field harmonics of a current line	30
3.1.3	Generation of pure multipole fields	33
3.2	The LHC dipole coil	37
3.2.1	Coil straight part design	39
3.2.2	Coil heads design	40
4	Modeling of magnetic field quality	43
4.1	Magnetic measurements at room temperature	44
4.1.1	Equipment and procedure	45
4.1.2	Warm magnetic measurement data	47
4.1.3	Monitoring magnet construction through field quality	51
4.2	Field quality analysis methods	54
4.2.1	Models for construction errors	54
4.2.2	Multipoles decay	56
4.3	Geometrical models for the coil straight part	60
4.3.1	Symmetric model	61
4.3.2	Asymmetric model	63
4.3.2.1	Azimuthal coil size variations	63
4.3.2.2	Non-nominal polar shims and polyimide sheet insertion in the coil midplane	65
4.3.2.3	Non-nominal coil radial dimension	67
4.3.3	Sensitivity results	67
5	A tool to monitor collared coil industrial series production	71
5.1	Statistical analysis of magnetic measurements at room temperature	72
5.1.1	Available data	73
5.1.2	Measurement data subdivision	74
5.1.3	Normality test and considerations on variability among the manufacturers	76
5.1.4	Control bounds and test choice	80
5.1.4.1	Control bounds for straight part averages	83
5.1.4.2	Control bounds for variations along the straight part	85
5.1.4.3	Control bounds for CS, NCS and C_1 in position 3 and 19	87

5.1.4.4	Control bounds for magnetic length, coil waviness and field parallelism between coil apertures	90
5.2	A macro to monitor the homogeneity of industrial production	92
5.2.1	Layout	92
5.2.2	Macro test procedure	94
5.2.3	Analysis results	95
6	Applications of field quality analysis to production cases	97
6.1	Wrong magnetic measurement	98
6.2	Assembly error	100
6.2.1	Simulations	102
6.3	Anomalous multipole variations along the axis	105
6.4	Torsion of the collared coil	112
	Conclusions	115
	Acknowledgements	119
	Bibliography	121
A	Stationary circular motion for a particle beam	125
B	Geometric models for symmetric computations	127
C	Fortran codes for field quality computations	131
D	Statistical notes and normality test results	143

E The macro used to monitor collared coil production . . 147

F Measurement data of Firm1 defected collared coils . . . 161

Introduction

Particle physics is the study of the basic constituents of matter and of the forces involved in their interactions. [1] Particle physicists have found that they can describe the fundamental structure and behavior of matter within a theoretical framework, called *the Standard Model*. [2] In order to derive evidence of it, many experiments have then been brought on during the past years by making particles interact at high energy. [3] But to reach deeper and deeper insight of matter constituents, accelerating machines which collide particles (*colliders*) must be built and run at higher and higher energies.

The *Centre Européenne pour la Recherche Nucléaire* (CERN) is the European Center for the Nuclear Research and it has been founded in 1954. Since then, particle accelerators and colliders have been built and run to give scientists the instruments needed for their studies. The latest project under construction now at CERN is the Large Hadron Collider (LHC), which will mainly accelerate and collide two 7 TeV proton beams.[4][5][6]

Strong magnetic fields are needed in circular accelerators to bend the particle motion on a circular trajectory.[2][5] Due to the beam energy foreseen for the LHC and since protons will be made to circulate in the former LEP tunnel, dipolar magnetic fields of more than 8 T have to be reached.[7][8] To feature such field strength at a reasonable cost, the superconducting technology is applied to dipole magnets, which use NbTi superconductors and operate at less than 2K. Due to the large number of dipoles needed for the LHC construction (1232), this component will be industrially series-produced.[9]

In superconducting magnets, the field quality is mainly affected by conductors position with respect to the aperture where particles circulate.[7][10][11] Since beam dynamics requires that the dipolar field homogeneity must be assured up to 10^{-5} of the main field component [12], the position of conductors must then be controlled with a precision of the order of 50 μm . [13] The tight mechanical tolerances imposed to the manufacturing of dipoles are then one of the most critical aspect to be monitored during the industrial production. But the manufacturing process cannot be monitored in terms of the constraints

imposed by beam dynamics, since they are too loose if referred to a single magnet. In fact, beam dynamics specifications are given in terms of mean and standard deviation of the whole production. On the other hand, to detect production drifts or manufacturing errors more stringent acceptance criteria are needed to check the field quality featured by a single magnet and to point out its differences from the previous production.

Magnetic measurements at room temperature provide a fast and economical way to monitor dipoles production since they give relevant indications on the conductor positioning inside the superconducting coil.[7][10][14][15][16] By comparing at an early stage of production the field quality featured by a new magnet with that achieved by the previous ones, it is possible to monitor production homogeneity and to detect assembly errors or the use of faulty components which possibly affects the measured sub-assembly.[9] Also indications on possible tooling wears can be derived.[17][18]

The present work focuses on the monitoring of the magnet industrial series-production homogeneity by mean of magnetic measurements.[16][17][19][20] In order to implement an automatic tool for such analysis, measurements performed on the pre-series *collared coil* sub assembly are statistically analyzed to derive control bounds for the field quality achieved by each magnet.[20][21] The analysis tool must apply computed acceptance criteria and point out deviations from the expected magnetic content. It must be simple and it must present analysis results in a fast readable manner (preferably by colored alarms). Since it must be used at the manufacturer, it must be compatible with the most used software and it must contain updatable control bounds which can be modified according to the history of the industrial production (cross section design modification, tooling change, etc...).

Magnets which feature a wrong magnetic structure can be analyzed once deviations have been pointed out by the automatic tool. Attempts must be made to trace measurement discrepancies back to their mechanical causes by applying field quality analysis methods.[7][13][17][22] Computations are needed to ponder the likeliness of a set of manufacturing errors used to describe deformations affecting the assembly and a geometric model to compute conductor real positions must then be derived. These and other anal-

ysis methods can then be applied to real cases encountered during collared coil pre-series production to give indications of the non-nominalities which affect them.[7][17]

In the first chapter of this work a brief description of CERN and of the LHC project is given, while the second chapter focuses on the dipole magnet, its design and the manufacturing process. The magnetic design of the dipole coil is then presented in chapter three together with some issues about multipolar expansion theory. Magnetic measurements and field quality analysis methods are described in the first part of chapter four.

The original part of the work starts in the second part of chapter four that describes the geometrical model implemented to compute conductor positions inside the coil; sensitivity tables are then computed for manufacturing errors assumed to be likely during magnet production. The first part of chapter five focuses on the statistical analysis of magnetic measurements needed to derive field quality acceptance criteria, while in the second part the automatic tool to monitor magnet production homogeneity is presented. In chapter six we analyze some cases encountered during collared coil pre-series production such as a not-reliable measurement or manufacturing errors. Finally, some conclusions are drawn, where the main results obtained in this work are summarized.

Chapter 1

CERN and the Large Hadron Collider project (LHC)

CERN is the European Organization for Nuclear Research, the world's largest particle physics centre, on the border between France and Switzerland, just outside Geneva. A brief presentation of its activities into particle physics is given in the first part of this chapter, where particle accelerators are shortly described. Some hints are also given about the former CERN project, the Large Electron Positron collider. The second part of the chapter is devoted to the new project under construction, the Large Hadron Collider (LHC) which will use the superconducting technology for accelerator magnets.

1.1 CERN

The European Organization for Nuclear Research (CERN) is an intergovernmental organization with 20 Member States founded in 1954 [1]. It has its seat in Geneva but straddles the Swiss-French border (see Figure 1.1). Its objective is to provide for collaboration among European States in the field of high energy physics research and to this end it designs, constructs and runs the necessary particle accelerators and the associated experimental areas.



Figure 1.1 Areal view of the region where CERN is located. LEP tunnel follows the white circle.

1.1.1 Particle accelerators

CERN facilities permit scientists from all the world to study how particles interact and the nature of the forces involved. During the past, CERN has managed to build and run several particle accelerators, in order to achieve deeper insight in particle physics.

Particle accelerators are machines that accelerate charged particles to high kinetic

energies by applying electro magnetic fields. In fact, a charged particle moving through an electro magnetic field is acted on by the Lorentz's force:

$$\vec{F} = q\left(\vec{E} + \vec{v} \wedge \vec{B}\right) \quad (1.1)$$

where \vec{F} is the electro-magnetic force exerted by an electric field \vec{E} and a magnetic field \vec{B} on a particle of charge q and velocity \vec{v} .

As one can argue from equation (1.1), charged particles can be accelerated by passing through an electric field. For a voltage difference $V[V]$, a particle of charge $q[C]$

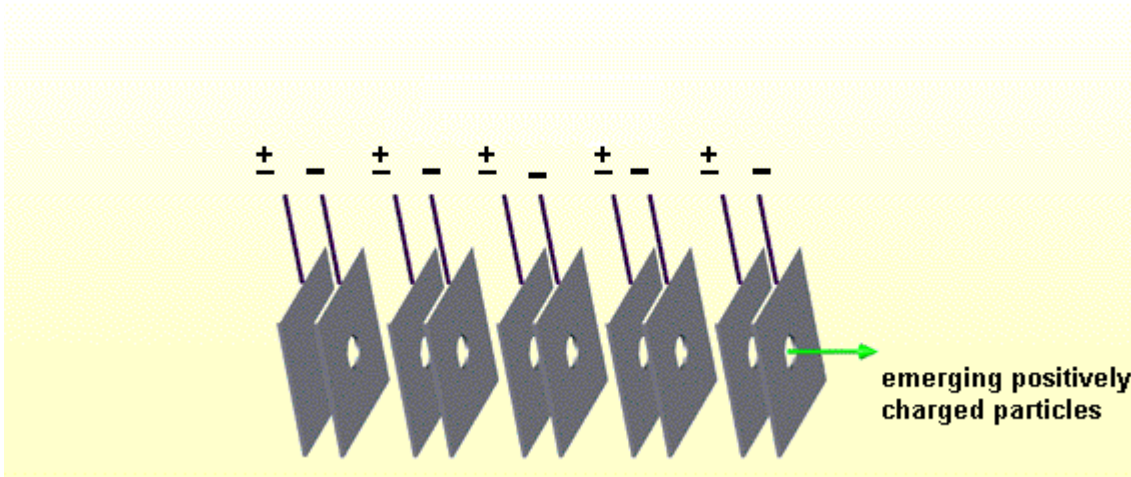


Figure 1.2 Schematic of the LINAC basic principle: charged particles enter the accelerating device from left, undergo the accelerating stages and exit from right with increased kinetic energy.

increases its energy by an amount $W[J] = qV$. This is the basic principle used in linear accelerators (LINAC). In a linac many steps of voltage difference between two following metal plates accelerate particles (see Figure 1.2). Between two following couple of charged plates, particles must be shielded against the electric field of the previous plate

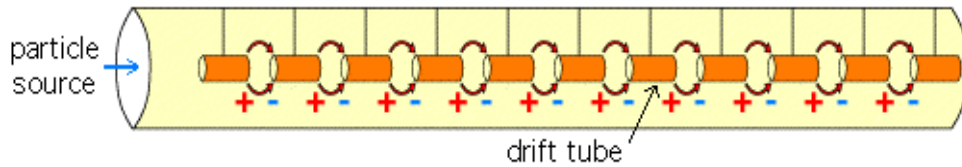


Figure 1.3 .Schematic view of a LINAC with drift tubes: charged particles are shielded from the counter accelerating field in the drift tube once they have left an accelerating stage

until the next accelerating step is reached. Particles are shielded by a so-called *drift* tube, in which they drift without undergoing any acceleration (see Figure 1.3). [2]

From equation (1.1), it can also be argued that if a magnetic field is applied normally to the particle trajectory, the particle motion can be deviated on a circular trajectory. If the particles move in a circular path that passes through one set of accelerating steps, high beam energy levels can be obtained. This is the basic principle of circular accelerators. From equation (1.1) it can be derived the following expression (see Appedix A for complete treatment):

$$B = \frac{E}{qRc} \quad (1.2)$$

which relates the bending magnetic field magnitude B , the beam energy E , the circular trajectory radius R , and the speed of light c . So when the particle beam is being accelerated and its energy level is getting higher and higher, one has to synchronize the magnetic field with the accelerating electric field in other to keep particles on a closed circular trajectory. Machines of this kind are called synchrotrons.

Particles can be studied to understand the nature of forces that govern the matter. By annihilating the particle beam against a target and analyzing the interaction data, the whole machine works as a microscope. The beam energy level is chosen depending on the goals of the experiment and detectors measure the energies and directions of motion of the particles that emerge from the collisions in other to obtain knowledge about the process being studied. But since the energy of a particle beam can convert into mass, as Einstein's equation $E = mc^2$ states (E is the beam energy, m the particle mass and c is the speed of light), if the incoming beam is simply slammed into a stationary target, much of

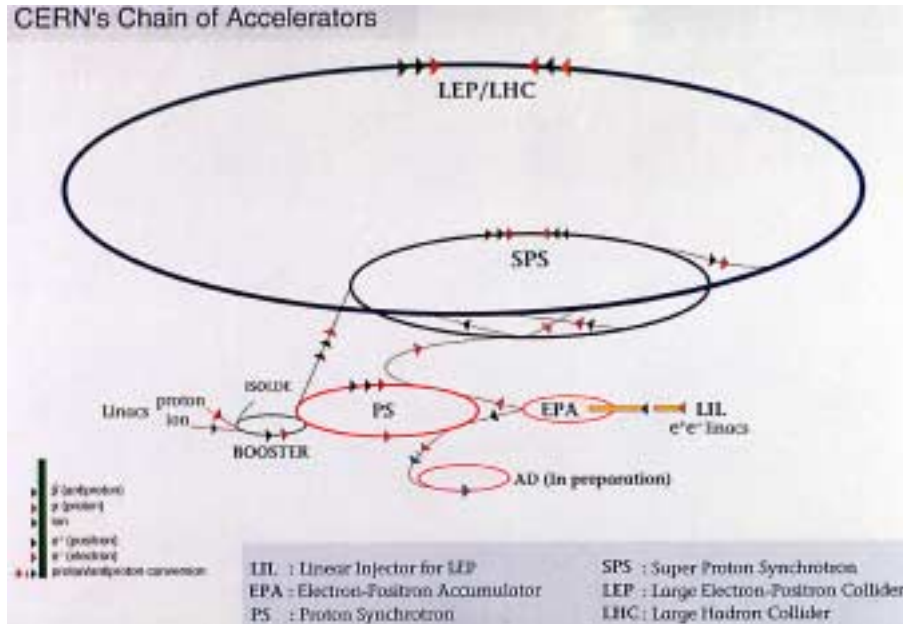


Figure 1.4 CERN accelerator complex schematic view.

the projectile energy is taken up by the target's recoil and not exploitable. Much more energy is available for the production of new particles if two beams travelling in opposite directions are collided together. Most of the world particle physics projects now under way concentrate on such colliding beam machines, called *colliders*.

1.1.2 CERN accelerator complex

CERN's accelerator complex includes particle accelerators and colliders, can handle beams of electrons, protons, antiprotons and heavy ions (see Figure 1.4). Each type of particle is produced in a different way, but then passes through a similar succession of acceleration stages, moving from one machine to another. The first steps are usually provided by linear accelerators, followed by larger circular machine. CERN has 10 accelerators altogether, the biggest having been the Large Electron Positron collider (LEP), undergoing decommissioning, and the Super Proton Synchrotron (SPS).

1.1.3 The Large Electron Positron Collider (LEP)

The LEP machine at CERN has been the largest particle collider in the world. In a ring 27 km in circumference, buried about 100 m underground, electrons and positrons (anti electrons) have raced round in opposite directions as they were being accelerated to almost the speed of light. Electrons and positrons have been made to collide, giving scientists the possibility to study particles originated from their interaction to validate the *Standard Model*, which represents a physical theory that summarize and unify the current state of knowledge about fundamental particles.

LEP began operation in the summer of 1989 and for six years the collision energy of its electrons and positrons was tuned exactly to the value needed to produce the neutral carrier of the weak force, the Z^0 (50 GeV per beam). Since the autumn of 1995, the energy has been increased to almost double its earlier value. In the summer of 1996, LEP ran at the exact value needed to produce pairs of the charged carriers of the weak force, the W^+ and W^- particles (90 GeV per beam).[3] Detection of millions of Z^0 s and hundreds of W s has allowed the LEP experiments to make extremely precise tests of the Standard Model of particles and their interactions (for further reading on this matter see [2]). LEP Dismantling Project has been in its operational phase since late 2000.[6]

1.1.4 From LEP to LHC

LEP was an electron - positron collider and it was one of the facilities around the world which aim was to get deeper insight in the properties of Z and W particles. Since the existence of the weak force carrier has been demonstrated, now scientist must study particle interactions in the range of TeV and to get deeper knowledge in the nature of matter constituents. With proton-proton collision, scientists can analyze a wider range of particle interaction than with an electron - positron collider and to look for new physical discoveries. So, in December 1994 CERN's Council officially approved the construction of the Large Hadron Collider (LHC) - a superconducting circular accelerator, which will be installed in the existing LEP tunnel - to provide proton-proton collisions at beam energy of 7 TeV.[23]

However to reach a beam energy of 7 TeV re-using the LEP tunnel is not easy, as one can derive from equation (1.2). In fact, if the desired beam energy E is 7 TeV, in order to follow the circular LEP tunnel for which R is 27 km, protons (with a charge q of $1.6 \cdot 10^{-19}$ C) would need a magnetic bending field B of around 8 T: magnets designed with conventional technology do not reach such field levels at a practicable cost. To achieve the desired bending magnetic field, the superconducting technology has to be applied. Furthermore, since the two head-on collisioning beams are made of protons, the LHC machine will need two beam tubes with opposite magnetic bending field to let positively charged particles to go in opposite directions. On the other hand, LEP needed only one beam tube (electron and positrons can circulate in opposite directions along a circular trajectory undergoing the same bending magnetic field due to their opposite charge).

1.2 The LHC Project

The Large Hadron Collider (LHC) is the next accelerator being constructed on the CERN site. The LHC machine will mainly accelerate and collide 7 TeV proton beams but also heavier ions up to lead. It will be installed in the existing 27 km circumference tunnel, presently housing LEP. The LHC design is based on superconducting magnets which operate in a superfluid helium bath at 1.9 K. Since to accelerate two proton beams one need two beam tubes with opposite bending field, magnets have been chosen as twin -aperture structures (i.e. each magnet contains two beam tubes). The 1232 magnets used to bend particles motion (called *dipoles*) and the 386 magnets designed to focus the beam (called *quadrupoles*) use NbTi superconducting cables for their coils. The magnets operate in superfluid helium at 1.9 K at a field varying between 0.54 T and 8.4 T for the dipoles, and at a field gradient up to 223 T/m for the quadrupoles.[5]

1.2.1 Machine performance

The main performance parameters for proton-proton operations are shown in Table 1.1. For a collider machine, we can define its luminosity as a quantity proportional to the observation rate of the nuclear interaction events.[3] The design luminosity for the LHC machine is $10^{34}\text{cm}^{-2}\text{s}^{-1}$ with simultaneous collisions at the two high-luminosity insertions (see Section 2.2.2).

Table 1.1 LHC performance parameters

Parameters	Design value	Measuring unit
Energy at collision (per beam)	7	TeV
Energy at injection (per beam)	0.45	TeV
Dipole field at 7 TeV	8.4	T
Coil inner diameter	56	mm
Distance between aperture axis (1.9 K)	194	mm
Luminosity	1	$10^{34}\text{cm}^{-2}\text{s}^{-1}$
Circulating current/beam	0.54	A
Bunch spacing	7.5	m

Table 1.1 LHC performance parameters

Parameters	Design value	Measuring unit
Bunch separation	25	ns
Beam lifetime	22	h
Luminosity lifetime	10	h
Energy loss per turn	7	keV
Total radiated power per beam	3.8	kW
Stored energy per beam	350	MJ
Filling time per ring	4.3	min

In addition to proton-proton operation, the LHC will be able to collide heavy nuclei (Pb-Pb) produced in the existing CERN accelerator complex, giving an energy of 1150 TeV in the centre of mass.[5]

1.2.2 Machine basic layout

The basic layout of the LHC mirrors that of LEP (see Figure 1.5): there are 8 arcs 2500 m long spaced by 8 straight sections each approximately 530 m long, available for experimental insertions or utilities. The two high-luminosity insertions are located at diametrically opposite straight sections, point 1 (ATLAS) and point 5 (CMS), for the two large LHC proton-proton experiments. Point 2 and 8 are for beam injection into both rings, and additionally host respectively the heavy-ion experiment ALICE and the B physics experiment. The beams cross from one ring to the other only at these four locations. The remaining four straight sections do not have beam crossings but contain the beam dump insertion (Insertion Point 6, to safely remove the beam from the collider at the end of a physics run), RF systems (IP 4, to accelerate each beam), and collimation systems (IP 3 and 7).[5]

Each of the eight arcs is composed of 23 arc cells and all arc cells are made of two identical half cells. The layout of an arc half-cell is shown in Figure 1.6. It consists of three 15 m twin aperture dipoles (*MB*) and one 3 m quadrupole (*MQ*).

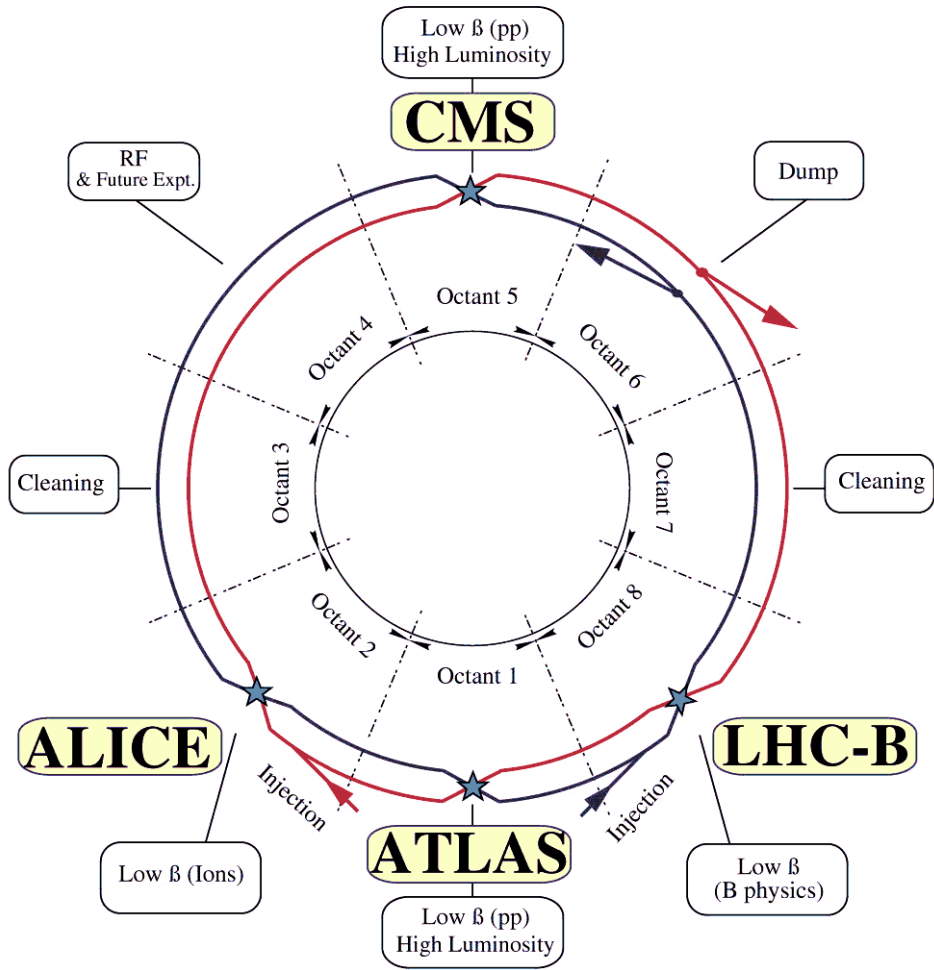


Figure 1.5 Schematic layout of the LHC with the 8 straight section available for experimental insertions or utilities.

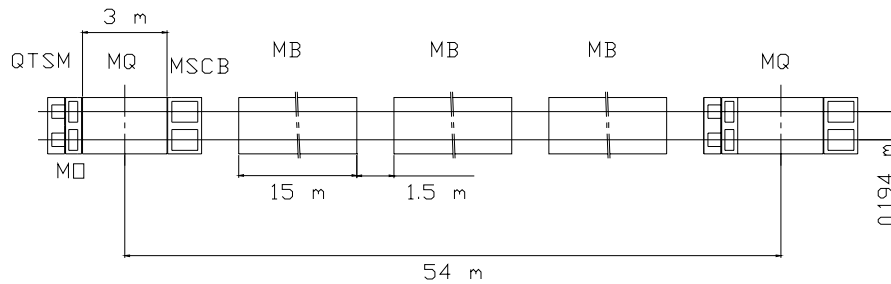


Figure 1.6 Layout of the arc half-cell. Length are given in metres. MB: dipole magnet; MQ: quadrupole magnet; MO: arc octupole magnet; QTSM: technical service module; MSCB: arc sextupole/dipole corrector. Components are not in scale.

1.2.3 Superconducting technology for accelerator magnets

As previously stated, the superconducting technology will be applied for the main magnets of the LHC project (see Section 1.1.4, [9]). There are three large operational accelerators based on superconducting magnets: the Tevatron (Fermilab), HERA (Desy) and RHIC (Brookhaven). They make use of classical NbTi superconductors cooled with normal liquid helium at a temperature of 4.2 K, and their operational fields are relatively low (in the range of 4-5 T). For the LHC, it is attractive to retain the well-proven industrial fabrication methods of cables and coils made of NbTi already experienced, but the only way of obtaining fields of 8 T or above with sufficient margin is to cool the magnets at a temperature below 2.17 K. In fact, below 2.17 K, helium takes the so-called superfluid state, with much lower viscosity and much greater heat transmission capacity than normal helium. These properties permit a drastic reduction of the helium flow through magnets.[9]

On the other hand, the enthalpy of all metallic parts and in particular of the superconducting cables is reduced by almost an order of magnitude between 4.2 and 1.9 K (LHC design temperature), with a consequent faster temperature rise for a given deposit of energy. Since forces on a conductor increase with B^2 and so does the electromagnetic energy, one of main difficulties is limiting the conductor motion to avoid energy release

that could bring NbTi conductors to a transition from the superconductive state to a normal conductive state (see Section 2.2.1.1), with possible damages to the superconducting magnetic coils. These problematics calls for particular care in limiting conductor motion already in the coil design stage as it will be pointed out further on (see Section 2.2.2).

Chapter 2

The LHC main dipoles

In order to curve the trajectory of particles accelerated up to an energy of 7 TeV, the LHC machine will make use of superconducting magnets featuring a dipolar field in the range of 8 T at an operating temperature of 1.9 K with a high degree of uniformity. Since the LHC machine requires 1232 main dipoles (called also main bending, MB), this component will be industrially series produced. Its features and parameters are presented in the next pages, with particular interest in the mechanical structure and in the assembly procedures.

2.1 Main features and parameters

The main parameters of the dipoles are listed in Table 2.1: the main features of design [5] are the following ones:

- design field: 8.4 T;
- NbTi superconductor operating in superfluid helium at 1.9K;
- two-layers coil with differently sized conductors;
- twin-apertures in a common force-retaining structure (collars, iron yoke and cryostat) which works also for magnetic flux return (iron yoke);
- coil inner diameter: 56 mm;
- distance between the axes of the aperture: 194 mm;

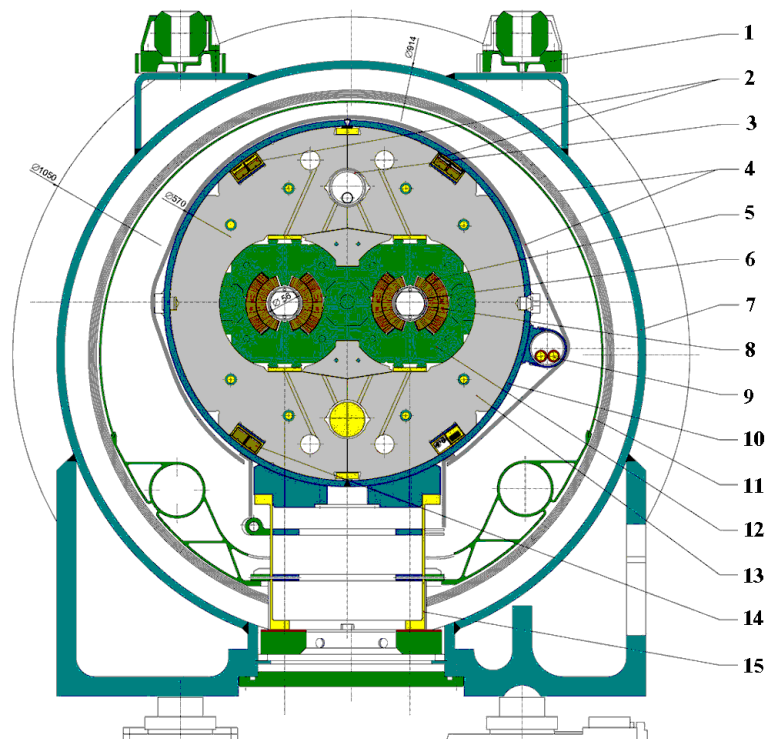


Figure 2.1 Twin aperture LHC dipole magnet cross-section: 1- alignment target; 2- main quadrupole bus-bars; 3- heat exchanger pipe, 4- superinsulation; 5- superconducting coils; 6- beam pipe; 7- vacuum vessel; 8- beam screen; 9- auxiliary bus-bars; 10- shrinking cylinder / He I-vessel; 11- thermal shield (55 to 75K); 12- non magnetic collars; 13- iron yoke (cold mass, 1.9K); 14 -dipole bus bars; 15- support post.

The cross section of the cryo-dipole is shown in Figure 2.1. It consists of two superconducting coils (inner and outer layer (5)) clamped by laminated collars (12) providing two apertures for the *cold bore tubes* (6) (i.e. the tubes where the particle beams will circulate). This sub-set of components is assembled in the so-called *collared coil*. When the iron yoke (13) is assembled to the collared coil and a shrinking cylinder (10) is welded on it, a *cold mass* is obtained. It contains all the components cooled by liquid helium and it is surrounded by the equipment needed to form a cryostat (1, 7, 11, 14, 15).

Table 2.1 Main parameters and characteristics of the LHC dipole

Parameter	Value	Unit
Injection field (0.45 TeV beam energy)	0.54	T
Nominal field (7TeV beam energy)	8.4	T
Ultimate operational field	9.0	T
Nominal current	11.8	kA
Operating temperature	1.9	K
Coil aperture	56	mm
Magnetic length at 1.9 K	~14300	mm
Structure		
Distance between aperture axes at 1.9 K	194	mm
Collar height	192	mm
Collar width	396	mm
Yoke outer diameter	550	mm
Shrinking cylinder outer diameter	570	mm
Length of cold mass	~15000	mm
Outer diameter of cryostat	914	mm

2.2 Main components

The LHC dipole is manufactured by assembling a large number of components. Here, the main components are presented briefly, with particular interest in components which constitute the cold mass assembly. Referring to Figure 2.2, the cold mass is made of:

- superconducting coils (1);
- collars (2);
- ferromagnetic inserts (3);
- iron yoke (4);
- shrinking cylinder (5).

In the last part of the assembly procedure, the cold mass is inserted into the cryostat, together with other components (spool pieces, corrector magnets, etc... See [4], [24]).

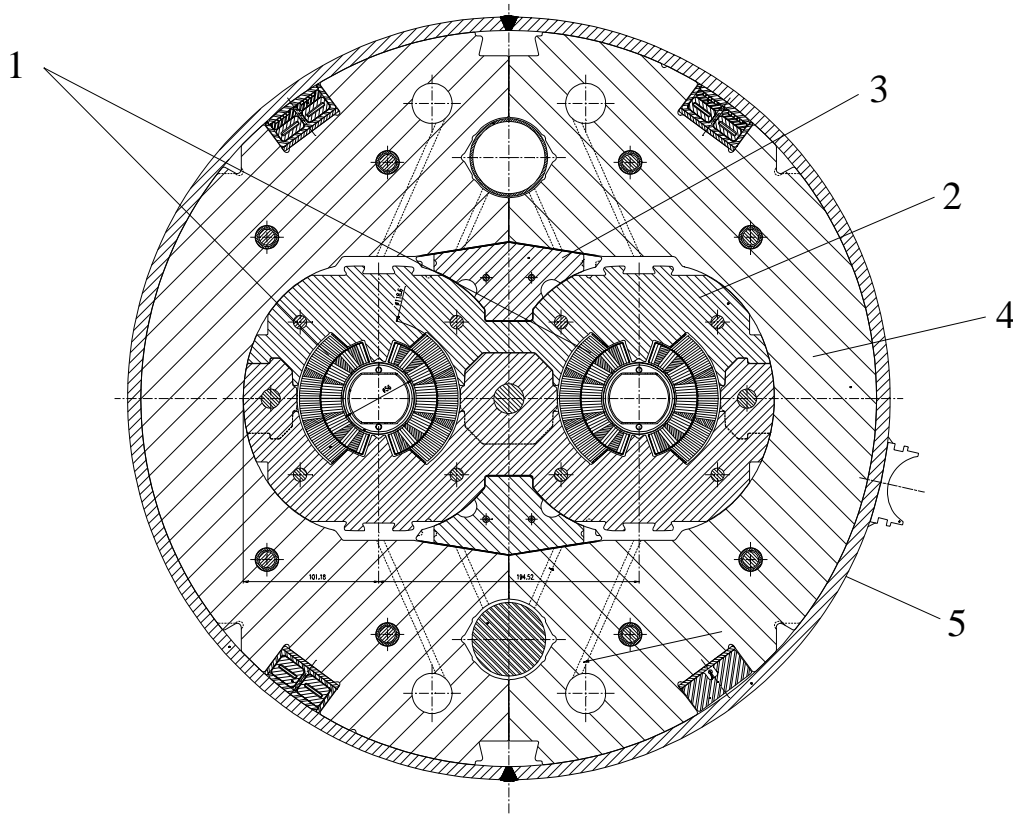


Figure 2.2 Dipole cold mass cross section: 1 - superconducting coils; 2 - austenitic stainless steel collars; 3 - ferromagnetic insert; 4 - iron yoke; 5 - shrinking cylinder.

2.2.1 Superconducting coils

The dipole coils consist of two layers of different superconducting cables distributed in six blocks over a coil quadrant (see Figure 2.3). Each aperture is fed by the same operating current, so as to originate two vertical uniform magnetic fields of opposite sign. Here we only present some general features; coil design issues are discussed in the next chapter.

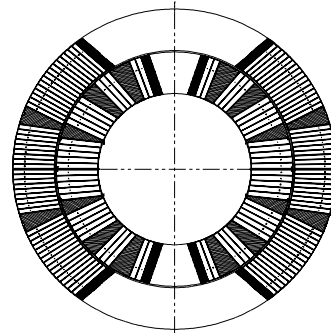


Figure 2.3 Single aperture cross-section the LHC dipole superconducting coil. 6-bloc

2.2.1.1 Superconductivity

Superconductivity was discovered in 1911 by the Dutch physicist H. Kamerlingh Onnes, only three years after he had succeeded in liquefying helium. During his investigations on the conductivity of metals at low temperature, he found that the electrical resistance of mercury dropped to an unmeasurably small value just at the boiling temperature of liquid helium. This was indeed a great discovery: when an electric current is made to go through a normal conductor there is an energy loss due to the electric current converting in heat proportional to the conductor electric resistance; if the electric resistance vanishes, also the electric losses do. Onnes called this phenomenon *superconductivity* and his name has been retained since. The temperature at which the transition took place was called the *critical temperature* T_c .

Superconductivity is a quantistic effect strictly bound to the electronic reorganization which a particular material undergo reaching its critical temperature. A complete description of the state-of-the-art knowledge about superconductivity (see for instance [7], [8] for references), obviously goes beyond the aim of this work. It is enough to say that the cables used for LHC magnets are made of NbTi. This material maintains the superconducting state if its values of temperature T , magnetic field B and current density J are below the so-called *critical surface*, see Figure 2.4. For NbTi the critical values of

temperature and magnetic field at zero current density are:

$$B_c = 14.5 \text{ T}$$

$$T_c = 9.2 \text{ K}$$

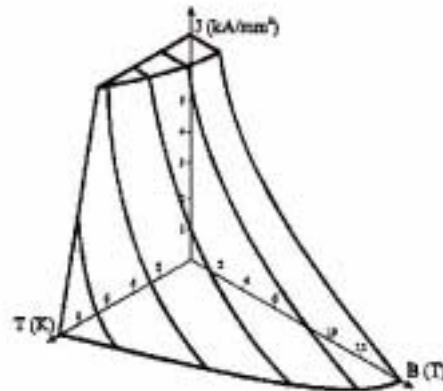


Figure 2.4 Critical surface for a superconductor: depending on the values of temperature T , magnetic field B and current density J at its interior, the conductor change to the normal state if the three value localize a position outside the critical surface.

The transition of a superconductor to its normal state is called *quench* and it can happen for a variation of one of the three parameters. For the LHC and the cables used in its design is rather improbable that a quench will be provoked by the magnetic field or by the current density going over their design values. Instead, the main cause of quenches in the LHC magnets is the thermal energy release after whatever conductor displacement. In fact, there is a release of energy due to friction and to the variation of the total magnetic energy stored when a conductor move even by some microns. Such a conductor displacement is enough to rise the conductor temperature above its critical value at operational magnetic field and current density, so that the magnets involved undergo a quench. Since NbTi in its normal state has little conductivity, when a NbTi superconductor quenches, the huge amount of current passing through it is converted in heat (according to Ohm law, [7]) and the conductor is burnt if no protection devices are present.

2.2.1.2 The cables

The transverse cross-section of the coils for the LHC 56 mm aperture dipole magnet shows two layers of different cables distributed in 6 blocks (Figure 2.3).

The cables used in the dipole coils are of the Rutherford type, see Figure 2.5, and they are composed by strands arranged in trapezoidal shape. Their insulation is designed to provide simultaneously the required electrical insulation level, allow for heat transfer (achieved by allowing superfluid helium to permeate the insulation and wet the conductors) and maintain the coil turns in their position.

The Rutherford cables used in the LHC dipole coil has 28 strands in the inner layer, each of 1.065 mm diameter, and 36 strands in the outer layer, each of 0.825 mm diameter. Each strand is made by a large number of NbTi filaments embedded in copper which provide a bypass to the electric current flowing in the superconducting filaments when they undergo a quench. Figure 2.6 shows an example of strand used for the LHC magnets.

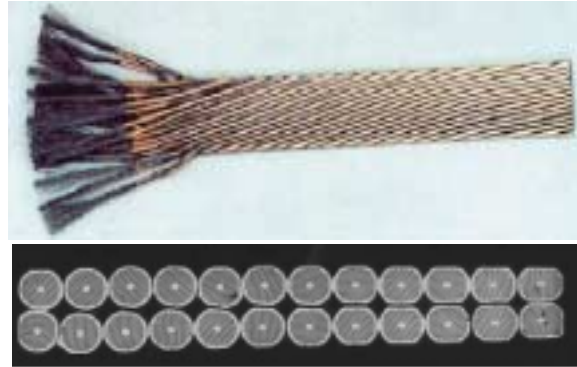


Figure 2.5 Rutherford type cable: (Top) conductor windings; (bottom) keystone cross section (the left side is thicker).

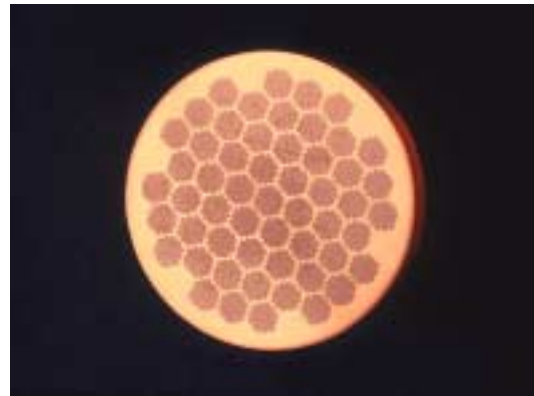


Figure 2.6 LHC superconducting strand made of around 8000 NbTi filaments embedded in copper.

2.2.2 Mechanical structure

The structure of the dipole is designed to withstand the high forces generated in the magnet and limit as much as possible the coil deformation over the range of operation. The materials used for the most highly stressed components have, therefore, a high load-bearing capacity, high elastic moduli, good fatigue endurance and a good behavior at cryogenic temperatures down to 1.9 K.

2.2.2.1 Collars

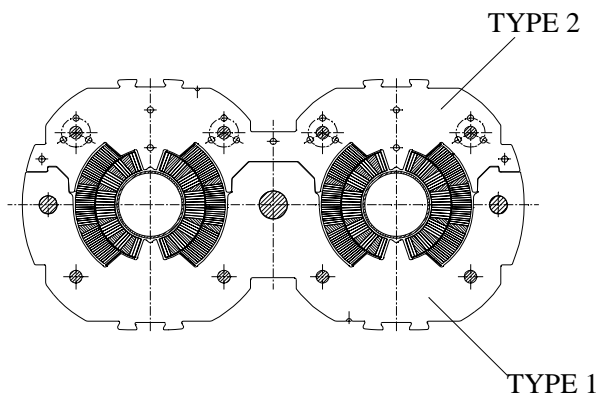


Figure 2.7 Collared coil assembly straight part cross-section: type 1 and type 2 collars mounted on coils are shown.

The collars are austenitic stainless steel laminations which represent a non magnetic, force retaining structure common to both aperture. They confine and pre-stress the coils to maintain their geometry in presence of very high electromagnetic forces that would make the coils repulse each other. The required high quality of the field calls for high precision and tight tolerances on the

collars, so they are precision-fine-blanked from high-strength austenitic steel sheets 3 mm thick. Since they have to be assembled on the coil, collars are of two kind in the straight part of the magnet: type 1 and type 2, [9] (see Figure 2.7). During operation, the superconducting coils must be under compressive stress. So collars are mounted on the coils under interference with the help of locking rods in a collaring press. After that, the collared coil is ready for the cold mass assembly.

2.2.2.2 Iron yoke

Referring to Figure 2.2, the iron yoke (3) is made of 6 mm thick low-carbon-steel laminations split into two at the vertical symmetry plane of the twin-aperture magnet. Between the two halves, a gap is present to compensate for the difference in thermal contraction of the iron yoke and the coil/collar assembly during cooling from room temperature to 1.9 K. [9]

The iron yoke is needed as a magnetic flux return circuit and a force retaining component. The pressure with which this component is mounted on the collared coil is transmitted to collars by ferromagnetic inserts ((1) in Figure 2.2), which are used also to channel the magnetic flux in the region between the two apertures, where saturation effects are present at high field.

2.2.2.3 Shrinking cylinder

When the iron yoke laminations are mounted on the collared coil, a stainless steel cylinder is welded around the assembly. In effect, this part is welded with interference around the iron yoke in such a way that the required pre-stress is obtained. The shells are made up of austenitic stainless steel, grade 316LN. They have a length of 15350 mm, a 275 mm inside radius and a thickness of 10mm. Furthermore, they are bent in opposite directions, so that one is concave and the other convex in order to achieve, after longitudinal welding around the yoke, the specified horizontal curvature of the dipole cold mass.

The shrinking cylinder gives to the cold mass assembly the stiffness necessary to contain the electromagnetic forces during magnet operation, and the inertia necessary to keep the self-weight induced deflection within the specified limits. It is also the main part of the helium containment vessel, which has to be leak tight at 300 K with respect to gaseous helium at a test pressure of 26 bar, and at 1.9 K with respect to superfluid helium at an operating absolute pressure of 1.3 bar. [24]

2.2.3 Cryostat

The so-called cryo-magnet consists of a dipole cold mass assembled inside its cryostat, comprising a support system, cryogenic pumping, radiative insulation and thermal shield, all contained within a vacuum vessel. The cryostat provides a stable mechanical support for the inner cold mass whilst limiting heat inleak to a level matching the strict heat-load budget of the LHC, determined to keep cables temperature in the range needed for NbTi to be in the superconducting state.

In the cross-section of the dipole cryomagnet shown in Figure 2.1, the cryostat and the dipole thermal shields are visible. The dipole cryostat runs at three temperature levels, 1.9 K for the cold mass, and at 5-20 K and 50-70 K for the two intermediate heat intercept levels. The vacuum vessel contains insulation vacuum at a pressure below 10^{-6} mbar [9] and is made of construction steel to reduce costs and shield stray magnetic flux. Two alignment target are mounted on it and works as outer reference to the inner magnetic axis to properly align the LHC components.

2.3 Magnet assembly

In previous sections, the LHC dipole main components have been presented. Since the LHC machine is designed to have 1232 dipoles, series production has been the only option to be taken into account for the manufacture of this item. Components will be manufactured by different firms, that will have to follow CERN specifications in the production steps. Once components have been manufactured, they are assembled in the following sub-assemblies:

- Coils;
- Collared coils;
- Cold mass.

After the cold mass has been assembled, it is inserted into the cryostat at CERN.

2.3.1 Coils

A twin-aperture dipole consists of two single dipoles, each around a beam channel. Each dipole has an upper and a lower pole which are identical. Each pole consists of a coil wound in two layers, called inner layer and outer layer (see Figure 2.3), wound with two different cables (see Section 2.2.1.2). The six sets of adjacent coil turns within the limits of the various copper wedges are defined as cable *blocks*.

The two layers are wound and cured on different dedicated mandrels. The objectives of curing are three-fold:

- to polymerize the epoxy of the cable insulation (see Figure 2.8) in order to make the coil rigid and thus easier to manipulate;
- to form the coil into the correct shape and correct dimensions;
- to make the coil as uniform as possible along its length.

Correctness of coil dimensions is important for the magnetic field quality. Uniformity of the coil is also required to achieve uniform pre-compression after collaring. [25]

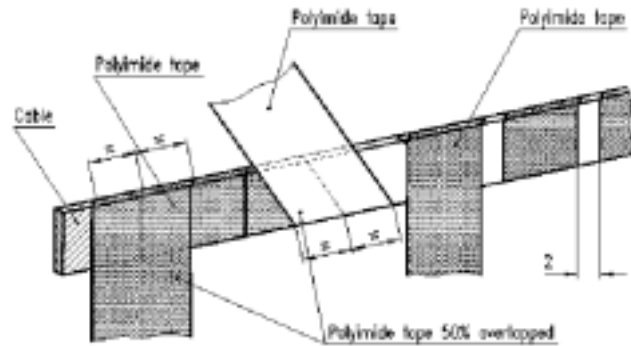


Figure 2.8 Conductor insulation with wraps of overlapping polyimide tape.

During pressing and curing operation, the cable temperature must never exceed the threshold of 200°C. Before increasing the temperature to the curing level, a phase of pressure and thermal cycles takes place in order to settle the coils. The pressure in the coil is increased from 10 to 80/100 MPa and then sizing is performed at temperatures between 100 and 135 °C. After curing has been brought at an end, poles are assembled and the coils can undergo the collaring procedure.

2.3.2 Collared coil

To obtain the collared coil sub-assembly, the four poles are assembled in couples around the cold bore tubes in order to obtain two dipole apertures. Pre-assembled packs of collars or pairs of collars are placed around the two insulated single coils. During these operations, collaring shims are inserted in the inner and outer coil layer in order to fine tune both magnetic field quality (see next chapter) and coil pre-stress.

The coil/collar assembly is then introduced into a collaring press. Starting with a pre-stress phase when the collars are only partially closed and increasing up to a pressure where temporary locking rods of reduced diameter can be inserted into the stack, pressure cycles are performed until the introduction of the final nominal rods (see Figure 2.7).

2.3.3 Cold mass

Assembling the cold mass begins with a set of collared coils, half yokes, yoke insert packs and austenitic stainless steel half-cylinders, as shown in Figure 2.2. After the assembly is obtained, it is transferred to a welding press. The half cylinders have to be longitudinally welded around the yoke so that the final average circumferential pre-stress is at least 150 MPa (see [9]). To obtain such a level of pre-stress, the two shells are welded under pressure. The desired pre-stress level gives the assembly the correct stiffness to withstand its own weight and to be manipulated without affecting the coils.

Before welding, the active part (collared coil, half yokes and magnetic inserts) is pushed against a curved jig, so that the nominal horizontal curvature and sagitta are obtained. Then all the ancillary parts and components (not mentioned in this work, for reference see [9]) are fixed on the shrinking cylinder, which has to be leak and pressure tested, and then inserted into the cryostat.

Chapter 3

Magnetic design of the dipole coil

LHC dipole magnets must exhibit a highly uniform magnetic field inside the apertures. Through a careful design of the coil, one can approximate a theoretical distribution of currents giving an ideal field. In this chapter the theory on which coil design is based is first presented, and then applied in a geometrical model that computes magnetic field errors arising from a non nominal conductors arrangement.

3.1 Coil design

In standard iron-dominated normal conducting magnets, the field strength and quality are determined by the gap width and the shape of the magnetic steel poles. However, because of iron yoke saturation already below 2.0 T, the use of these magnets is rather limited. For higher fields, magnets could be designed without iron yoke, but they are usually not economical due to their big volume and high energy consumption [8], [10]. In a superconducting coil, the field pattern is governed by the arrangement of the current conductors and a precise coil geometry is of utmost importance. The multipolar expansion for magnetic field computation is at the basis of the coil design. From the theory applied to a single current-carrying wire, it will be shown how the coil design influence the field quality in an accelerator magnet.

3.1.1 Definition of field harmonics

In a region in space which is free of any currents and magnetized materials, the magnetic field fulfils the two following simplified Maxwell equations:

$$\vec{\nabla} \cdot \vec{B} = 0 \quad \vec{\nabla} \wedge \vec{B} = 0 \quad (3.1)$$

If a 2D magnetic field is present (with only two non zero cartesian components B_x and B_y), the following equations can be derived from equation (3.1):

$$\frac{\partial B_x}{\partial x} = -\frac{\partial B_y}{\partial y} \quad (3.2)$$

$$\frac{\partial B_x}{\partial y} = \frac{\partial B_y}{\partial x} \quad (3.3)$$

Referring to the reference system in the Gaussian plane of Figure 3.1 where $\zeta=x+iy$, if the total magnetic field B is defined in complex notation as:

$$B(x, y) \equiv B_y(x, y) + iB_x(x, y) \quad (3.4)$$

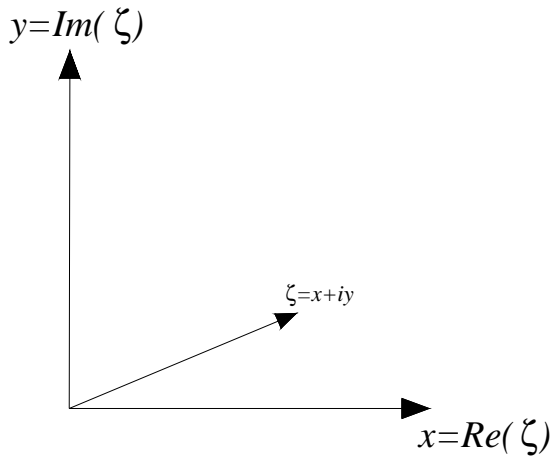


Figure 3.1 Reference system of the Gaussian plane used to expand the magnetic field in a Taylor's series.

equation (3.3) corresponds to the Cauchy-Riemann conditions, which provide a necessary and sufficient condition for the complex function $B(x, y)$ to be analytic in ζ . So, we can expand the magnetic field as a Taylor series of the following kind:

$$B(x, y) = \sum_{n=1}^{\infty} C_n (x + iy)^{n-1} = \sum_{n=1}^{\infty} C_n \zeta^{n-1} \quad (3.5)$$

where the complex coefficients of the series C_n can be written as:

$$C_n = B_n + iA_n \quad (3.6)$$

where B_n and A_n are the field harmonics (called *multipoles*). Usually, the field expansion is normalized with respect to a reference field B_{ref} at a reference radius R_{ref} . So one can write the following equation:

$$B(x, y) = B_{ref} \sum_{n=1}^{\infty} (b_n + ia_n) \frac{\zeta^{n-1}}{R_{ref}^{n-1}}, \quad (3.7)$$

where b_n and a_n are called normalized *normal* and *skew* multipoles, respectively.

3.1.2 Field harmonics of a current line

In the reference system of Figure 3.2, if an electric direct current (DC) is made to pass through an infinitely long conductor parallel to the z -axis, in the xy -plane a magnetic field arises according to the Biot Savart law (see Figure 3.2):

$$\vec{B}(x, y) = \frac{\mu_0 I}{2\pi r^*} \left(\frac{\vec{I}}{|\vec{I}|} \wedge \frac{\vec{r}^*}{|\vec{r}^*|} \right) \quad (3.8)$$

where:

- \vec{I} is a vector with modulus I equal to the DC intensity and direction parallel to the z axis;
- \vec{r}^* is the position vector for (x, y) in the local conductor reference system;
- μ_0 is the magnetic permeability of free space;
- \vec{B} is the magnetic field vector due to the electric current \vec{I} : since \vec{I} is parallel to the z axis, B_z is null.

The magnetic field components along the x and y axis (which direction are determined by \hat{i} and \hat{j}) and the resultant field can be expressed as follows:

$$B_x = \left(-\frac{\mu_0 I}{2\pi r} \right) \sin(\alpha) \quad (3.9)$$

$$B_y = \left(\frac{\mu_0 I}{2\pi r} \right) \cos(\alpha) \quad (3.10)$$

$$\vec{B}(x, y) = B_x \hat{i} + B_y \hat{j}, \quad (3.11)$$

where α is the (x, y) positioning angle in the current line relative reference system (see Figure 3.2). In the absolute reference coordinate system, the magnetic field vector can be described by the following equation:

$$\vec{B} = \frac{\mu_0 I}{2\pi |\vec{r} - \vec{r}_c|} \left(\frac{\vec{I}}{|\vec{I}|} \wedge \frac{\vec{r} - \vec{r}_c}{|\vec{r} - \vec{r}_c|} \right). \quad (3.12)$$

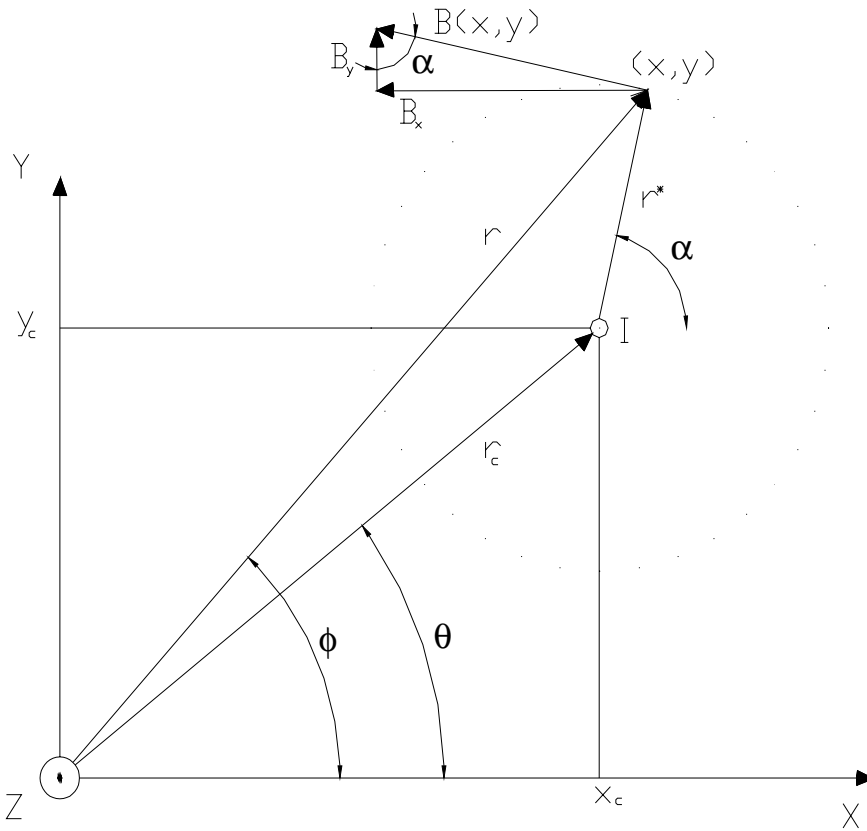


Figure 3.2 An electric current I going through a line conductor origins a 2D magnetic field B described by Biot Savart law with $B_z = 0$.

Using the complex notation, position vectors can be defined as follows:

$$\zeta_c = x_c + iy_c \quad (3.13)$$

$$\zeta = x + iy, \quad (3.14)$$

and the magnetic field can be written using Euler notation as:

$$\vec{B}(x, y) = |B|e^{-i\alpha} = B_y + iB_x = \frac{\mu_0 I}{2\pi} \frac{1}{(\zeta - \zeta_c)} \quad (3.15)$$

Since the region around the line current is free of any currents and magnetized materials, B fulfils the simplified Maxwell equations (see equation (3.1)) and it can be series ex-

panded. One can write:

$$\frac{1}{(\zeta - \zeta_c)} = -\frac{1}{\zeta_c \left(1 - \frac{\zeta}{\zeta_c}\right)} = -\frac{1}{\zeta_c} \sum_{n=1}^{\infty} \left(\frac{\zeta}{\zeta_c}\right)^{n-1} = -\sum_{n=1}^{\infty} \frac{\zeta^{n-1}}{\zeta_c^n}, \quad (3.16)$$

which converges for $\left|\frac{\zeta}{\zeta_c}\right| < 1$. Equation (3.15) can be re-written as:

$$= B_y + iB_x = -\frac{\mu_0 I}{2\pi} \sum_{n=1}^{\infty} \frac{\zeta^{n-1}}{\zeta_c^n} = \sum_{n=1}^{\infty} C_n \zeta^{n-1}, \quad (3.17)$$

where recalling equation (3.6):

$$C_n = B_n + iA_n \quad (3.18)$$

$$B_n = -\frac{\mu_0 I}{2\pi r_c^n} \cos(n\theta) \quad A_n = -\frac{\mu_0 I}{2\pi r_c^n} \sin(n\theta), \quad (3.19)$$

where θ is conductor position angle in the line current relative reference system, r_c is the conductor distance from the absolute reference system origin (see Figure 3.2), A_n and B_n are the field harmonics as defined in Section 3.1.1.[10],[11] As it can be seen from equation (3.19), the skew and normal coefficients decay with r_c^n . So with increasing order n , coefficients are smaller and are less affected by variations of r_c , i.e. conductors positioning: a conductor displacement mainly affects low order coefficients.

The multipole expansion for magnetic field calculation is a powerful instrument to design magnet coils featuring a desired magnetic field. From equation (3.17) it can be seen that a current line origins a highly not uniform magnetic field. Accelerator magnets featuring a vertical uniform magnetic field are needed to bend particles: if the only non-zero coefficient is the normal coefficient B_1 , a uniform vertical field is obtained (i.e. a dipolar field). This is the principle to obtain a desired multipolar content of a magnetic field and it will be presented in the next paragraph.

3.1.3 Generation of pure multipole fields

From equation (3.17), it is evident that a single current line produces multipole fields of any order n . To find out how one can generate a useful field, an arrangement of current conductors which are mounted on a cylinder of radius r_c parallel to the z direction, must be considered (see Figure 3.3). Using the orthogonality of the trigonometric functions, it can be proved (for reference see [7]) that a pure multipole field, containing just the single order $n = m$, is obtained inside the cylinder if the current distribution as a function of the azimuthal angle θ is given by:

$$I(\theta) = I_0 \cos(m\theta). \quad (3.20)$$

In the case of a $\cos(m\theta)$ -like current distribution, the magnetic field inside the region delimited by conductors can be expressed as the following:

$$B(z) = \frac{\mu_0 I_0}{2r_c^m} \zeta^{m-1} \quad (3.21)$$

For $m=1, 2, 3$ one can obtain dipole, quadrupole and sextupole fields, respectively. These are shown in Figure 3.4, together with the iron pole shoes of the corresponding normal

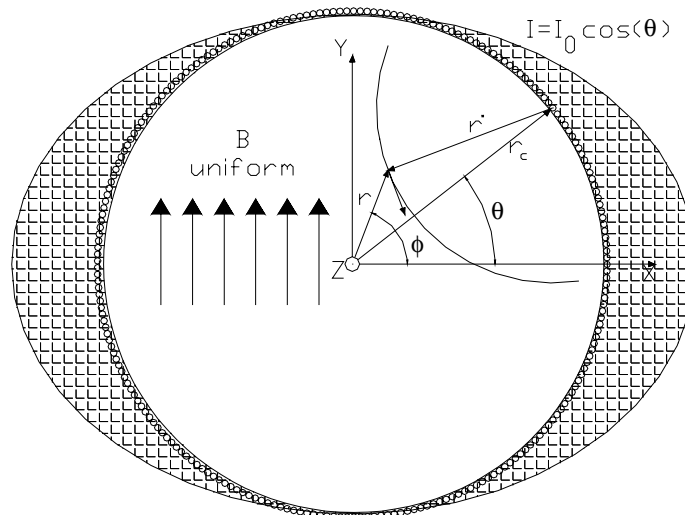


Figure 3.3 In order to obtain a useful field, an arrangement of conductors mounted on a cylinder of radius r_c must be provided: the magnetic field in any position inside the cylinder is given by the superimposition of any conductor contribution to the total magnetic field. If a DC with a cosine shape is made to go through the conductors, a dipolar field inside the cylinder is originated.

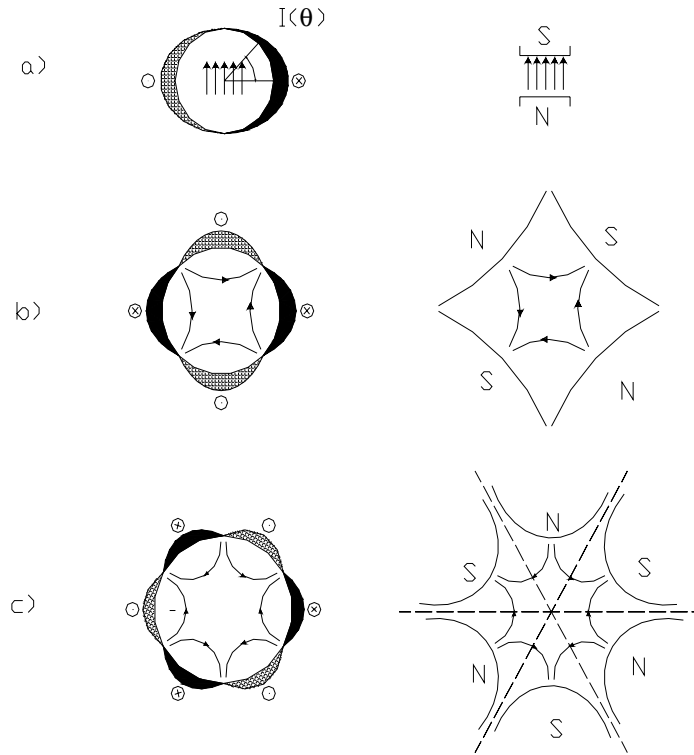


Figure 3.4 Generation of pure multipole fields by $\cos(m\theta)$ current distributions and by conventional magnets with iron pole shoes: a) dipole field ($m=1$); b) quadrupole field ($m=2$); sextupole field ($m=3$).

magnets. Recalling equation (3.17) and equation (3.18), one can write equation (3.21) as:

$$(z) = \frac{\mu_0 I_0}{2r_c^m} \zeta^{m-1} = (B_m + iA_m) \zeta^{m-1} \quad (3.22)$$

from which is derived that for pure $\cos(m\theta)$ -like current distribution, one get $A_m = 0$ while $B_m = \frac{\mu_0 I_0}{2r_c^m}$: fields of this kind are called *normal-multipole* fields, while if $A_m \neq 0$, one gets also a *skew-multipole* field. A pure skew dipole (for instance) has a horizontal field.

Current distributions with a $\cos(m\theta)$ dependence are difficult to fabricate with a superconducting cable of constant cross section. They can be approximated instead by current shells or by current blocks or both. The quality of the approximation to a desired

current distribution can be directly judged from the series expansion written using the normalized multipoles as in equation (3.7), which we repeat here:

$$B = B_{ref} \sum_{n=1}^{\infty} (b_n + ia_n) \left(\frac{\zeta}{R_{ref}} \right)^{n-1}. \quad (3.23)$$

In fact, for a dipole magnet usually it is chosen:

$$B_{ref} \equiv B_1, \quad (3.24)$$

which implies:

$$b_1 = 1, \quad (3.25)$$

and the field quality is determined by the other normalized harmonics. Since in the case of accelerator magnets the desired uniformity is of the order of 10^{-4} , multipoles a_n and b_n are given in *units of 10^{-4}* . [8], [9]

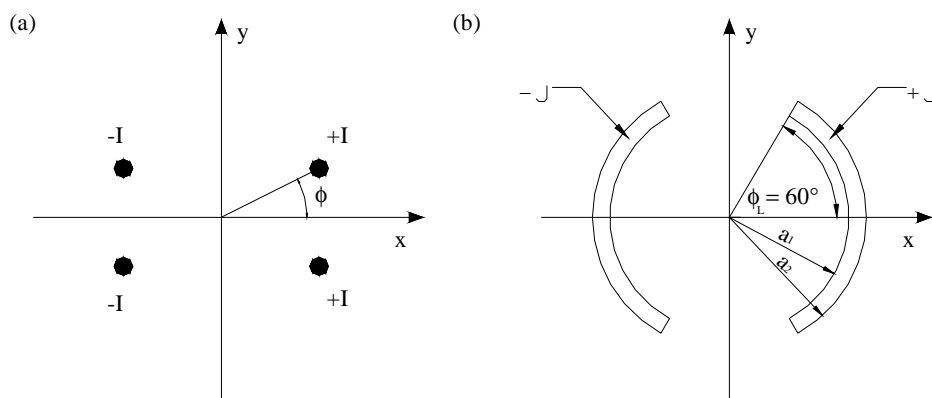


Figure 3.5 (a) Four line currents with dipole symmetry. (b) Simplest current shell arrangement for a dipole coil. ϕ_L (layer limiting angle) is chosen for b_3 to vanish.

The ideal multipole coils of Figure 3.4 have well defined symmetries. In a dipole coil, for any line current $+I$ at an angle ϕ , there exist three more currents: $+I$ at $-\phi$ and $-I$ at $\pi-\phi$ and $\pi+\phi$ (see Figure 3.5 (a)). Applying equation (3.23), it can be seen (see [7]) that for a symmetric coil featuring a magnetic field with a desired multipole structure of order m (e.g. for a dipole it would be $m = 1$), only the multipoles of order $n = (2k + 1)m$ with $k = 0, 1, 2, 3, \dots$ are present. The current shell approximation takes into account these symmetry features to generate magnetic fields of desired shapes. Furthermore from the multipole expansion of the magnetic field it can be proven (see [7]) that if a current shell with dipole symmetry (see Figure 3.5 (b)) is made with limiting angles of 60° , the sextupole normal coefficient (i.e. b_3 , the first non vanishing term in a coil with dipolar symmetry) is made to vanish.

A single layer current shell arrangement with constant current density often is not a desired approximation for a dipole coil, because even if the sextupole is made to vanish there is still a too strong b_5 (for reference see [7], [11]). With two current shells, b_3 and b_5 can both be made to vanish by choosing a limiting angle of about 72° in the inner and 36° in the outer layer. [7]

3.2 The LHC dipole coil

The theory for magnetic field quality computations presented in the previous section can be applied to the design of the LHC dipole coils. As previously stated, the length of an accelerator magnet is much larger than its aperture and the current conductors run parallel to the beam over the longest part of the magnet (see Figure 3.6). The multipolar

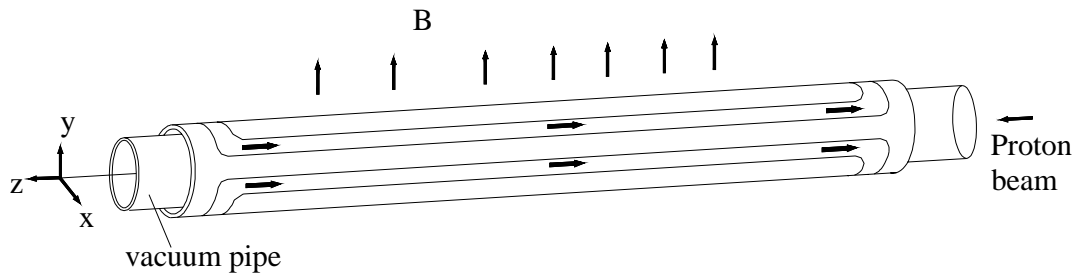


Figure 3.6 Schematic view of a superconducting dipole coil

expansion theory can be applied in the straight part of a magnet and in any region $[z_1, z_2]$ where

$$\left. \frac{\partial B}{\partial z} \right|_{z = z_1, z_2} = 0 . \quad (3.26)$$

In that case the multipolar expansion can be applied to the integral between z_1 and z_2 . This approach can be used to evaluate the contribution of heads to field shape. In Table 3.1 the overall dimensions and features for each aperture of LHC dipole coils are presented.

Table 3.1 Dipole coil parameters

Parameter	Value	Unit
Coil inner diameter	56	mm
Coil outer diameter (incl. insulation to ground)	120.5	mm
Coil length (incl. end pieces)	14467	mm
Inner layer		
Turns per beam channel	30	
Cable width	15.1	mm
Thickness	1.72/2.06	mm
No of strands	28	

Table 3.1 Dipole coil parameters

Parameter	Value	Unit
Strand diameter	1.065	mm
Filament diameter	7	μm
Copper to superconductor ratio	1.6	
Outer layer		
Turns per beam channel	52	
Cable width	15.1	mm
Thickness	1.34/1.6	mm
No of strands	36	
Strand diameter	0.825	mm
Filament diameter	6	μm
Copper to superconductor ratio	1.9	

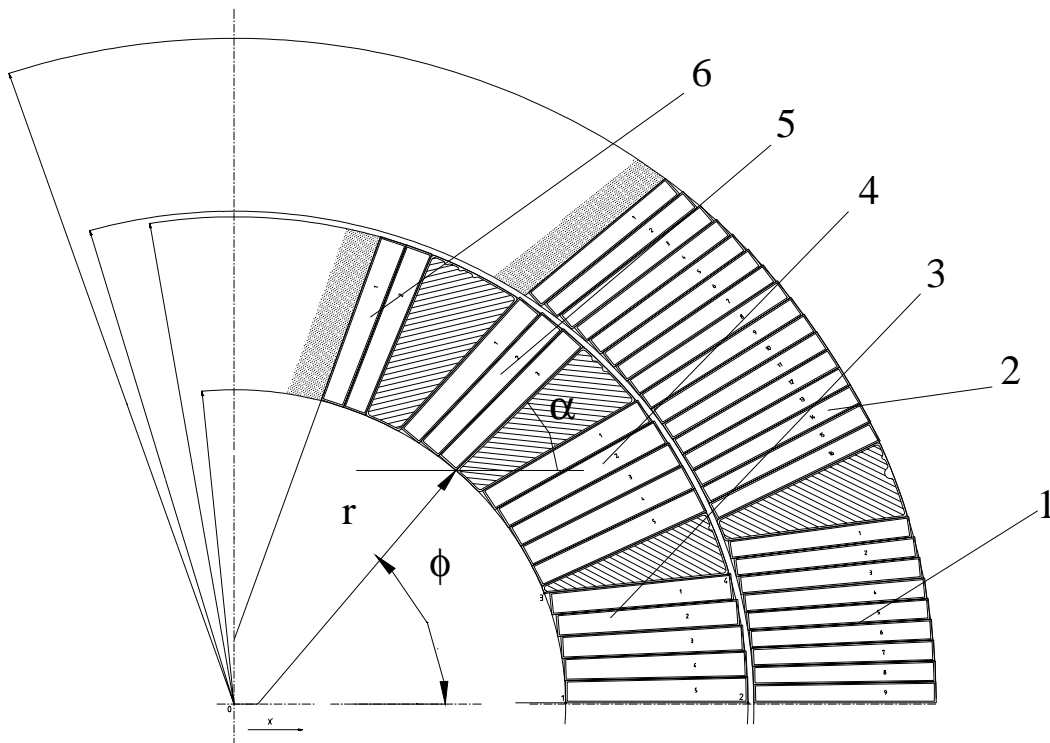


Figure 3.7 6- block symmetric quarter of an LHC dipole aperture: N is the block number (from 1 -bottom right- to 6 -top left). r , α and ϕ are used as a reference system for block naming and position.

3.2.1 Coil straight part design

The conductor distribution in one coil quadrant is shown in Figure 3.7 for the straight part of the dipole. This is the so-called 6-block design, where *block* define the set of adjacent coil turns within the limits of the various copper wedges, and shows also the naming convention used to refer to each block in the coil design.

Block	Nc	r (mm)	ϕ (°)	α (°)	Width (mm)	Thick 1 (mm)	Thick 2 (mm)	N 1	N 2
1	9	43.900	0.157	0.000	15.400	1.620	1.860	2	18
2	16	43.900	21.900	27.000	15.400	1.620	1.860	2	18
3	5	28.000	0.246	0.000	15.400	1.973	2.307	2	14
4	5	28.000	22.020	24.080	15.400	1.973	2.307	2	14
5	3	28.000	47.710	48.000	15.400	1.973	2.307	2	14
6	2	28.000	66.710	68.500	15.400	1.973	2.307	2	14

Table 3.2 Parameters for conductor dimensions and distribution in the coil quadrant of Figure 3.7: Block -block number; Nc- number of conductor in the block; r, α and ϕ - block positioning coordinates; Width - block cable width; Thick 1 - minimum thickness of Rutherford cable; Thick 2 - maximum thickness of Rutherford cable; N1 - number of strands along cable vertical dimension, N2 - number of strands along cable horizontal dimension.

Main dimensions of interest and main parameters of conductor positioning are given in Table 3.2 for each block in one coil quadrant. Conductor movements of any kind with respect to the aperture center correspond to a change in the parameters given in Table 3.2. The reference system of Figure 3.7 will be used further on to compute conductor positioning after coil deformation.

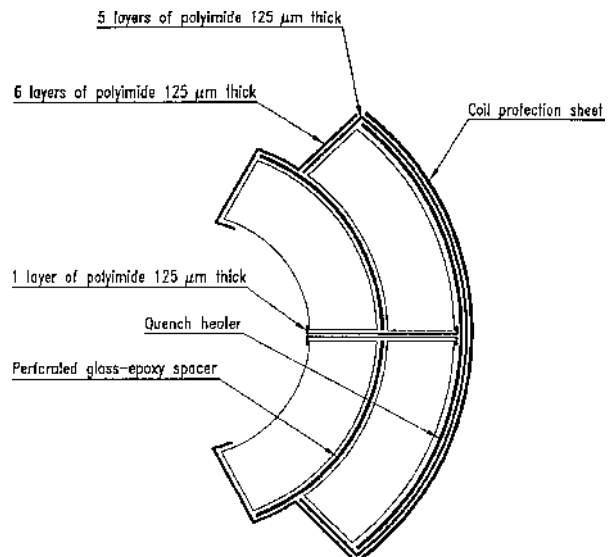


Figure 3.8 Ground insulation

The coil structure is completed by insulating material between coil layers, between poles and for ground insulation. Figure 3.8 shows the overall insulation structure around half an aperture. Stainless steel

protection sheets and collaring shim retainers (the coil protection sheet itself may work as a shim retainer) prevent damage due to contact with the serrated edges of collars. They make also possible a fine tuning of conductor positioning inside the coil for field quality or coil pre-stress purposes by mean of stainless steel shims to be inserted in the coil assembly.

3.2.2 Coil heads design

In the straight part of a magnet, conductors run parallel to the magnet axis and they feature a magnetic field that can be considered two-dimensional. Referring to Figure 3.6, there is no magnetic field component parallel to the z -axis. The regions where conductors are no more parallel to the magnetic axis are called coil *heads*, because they are at the magnet extremities. Here, cables are made to pass from one to the other side of magnet and from one to the other coil layer. The two heads are different and they are referred to

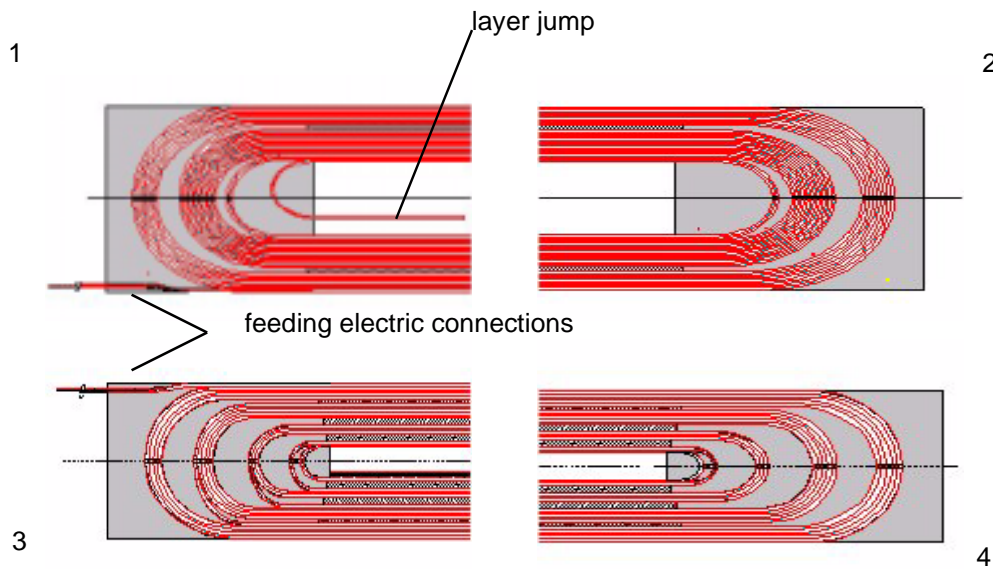


Figure 3.9 Developed longitudinal section of the inner and outer layers in the coil heads: 1 - outer layer in non connection side head (NCSH); 2 - outer layer in connection side head (CSH); 3 - inner layer NCSH; 4 - inner layer CSH

as Non Connection Side (NCS) and Connection Side (CS). Figure 3.9 shows a developed longitudinal section of coil windings in the outer and inner layer for NCS and CS. The NCS is totally right - left symmetric and there are 3 blocks in the outer layer (Figure 3.9

- 2) and 5 in the inner layer (Figure 3.9 - 4).

The CS features several asymmetries. In the inner layer (Figure 3.9 - 3) the last winding of a conductor block is the starting point of the next one (bringing a strong right - left asymmetry). In the CS outer layer (Figure 3.9-1), the cable is soldered to the most interior cable of the inner layer in the so- called *layer jump*. The last winding coming from the straight part of the magnet is not curved and exit the coil CS and is used as the electric feeding connection of the dipole coil.

These parts of the magnet are designed usually with 3D Finite Element Models, because the curved windings features a non-planar magnetic field. The structural complexity of the magnet heads and the magnetic non uniformity induce to consider these regions as the limiting parts for the magnet performance. In fact, cables undergo quench in the heads more often than those of the magnet straight part. Particular attention must be paid for the electro-mechanical design of coil heads: cables are curved and particularly difficult to immobilize with respect to the electro-magnetic forces arising during coil excitation. So, in coil heads the magnetic field magnitude is limited to a fraction of that of the straight part, in order to assure a larger margin for superconductors not undergoing a quench, and the mechanic structure is fitted to the particular condition of the coil extremities. This is possible since the coil heads are rather short (nearly 200 mm) if compared to the magnet straight section (nearly 14000 mm), and the beam behavior is little affected by the short coil heads.

Chapter 4

Modelling of magnetic field quality

In this chapter, magnetic measurements are briefly presented, focusing on the set of parameters which are used to characterize the field quality of a magnet. Then, we present methods to analyze measurement data and to trace multipolar variations to coil non-nominalities; in the final part of this chapter we describe a geometrical code implemented to model such non-nominalities.

4.1 Magnetic measurements at room temperature

Once a magnetic coil has been designed and manufactured, its field quality can be analyzed by magnetic measurements. The magnetic field in the straight part of a dipole as shown in Figure 3.6 can be considered two-dimensional and to evaluate the field quality inside the beam channel, the multipolar expansion can be written as in equation (3.7), which we repeat here:

$$B(x, y) = B_{ref} \sum_{n=1}^{\infty} (b_n + ia_n) \frac{\zeta^{n-1}}{R_{ref}^{n-1}}. \quad (4.1)$$

For superconducting accelerator magnets, usually it is needed a field uniformity corresponding to multipoles b_n, a_n of the order of 10^{-4} (with the exception of b_1 which is set to one by definition). The field quality for the LHC dipole magnets must be controlled up to 10^{-5} for some components. [26]

The magnetic measurements performed on superconducting accelerator magnets can be divided into two families depending on the temperature at which they are carried out: at room temperature and at cryogenic temperature. During magnetic measurements at cryogenic temperature, the field quality featured by a superconducting coil in its operational conditions of temperature (for LHC dipoles, 1.9 K) and electric current (for LHC dipoles, from 760 A to 11.8 kA) is measured. This kind of magnetic measurements imply, therefore, that the magnet must be assembled in its cryostat and that a cryogenic test bench is available. The probe used for measurements is usually anti-cryostatized to avoid the time needed for thermalization. Measurements are carried out at different values of the current (the so-called *load line*) to test the magnet in all operational conditions.

Magnetic measurements can be also performed at room temperature (around 300 K) by exciting a magnet coil in its normal conducting state with a low current (of the order of 10 A). In such way, measurements can be performed during industrial series produc-

tion, even if the magnet is still far from the final cryostatized assembly. The LHC dipoles undergo two measurements at room temperature during their assembly procedures:

- one on the collared coils;
- one on the cold mass.

These measurements are a powerful tool to detect assembly errors or faulty components at an early stage of production. Moreover, they give a relevant indication of the field quality in operational conditions. The magnetic content differs from collared coil to cold mass due to the presence of the yoke. Here some issues related with the measurements of the collared coil are discussed, but the same can be repeated for the cold mass, since the two measurements are similar and the equipment is the same.

4.1.1 Equipment and procedure

A precise measurement of the low magnetic field (~ 0.01 T) induced by an electric current of about 10 A in the collared coils is made using the technique of rotating search coils and harmonic analysis. [14], [15] These rotating coils are mounted in a so-called *magnetic mole* which is inserted in the cold bore tube. For the LHC dipoles, coils within the probe are 750 mm long. In order to cover the whole length of the collared coil, a full set of measurements is performed on 20 positions along the coil axis. The main components of the field-measuring probe, whose diameter is 50

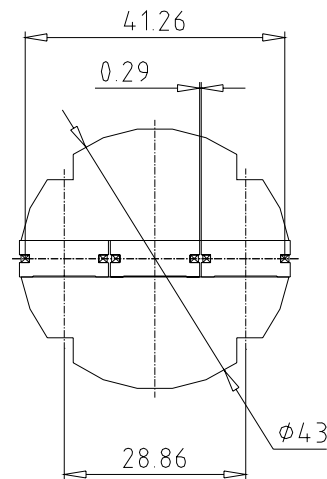


Figure 4.1 Rotating search coils

mm, are three rotating *search coils* (see Figure 4.1), an incremental *encoder*, an electronic *gravity sensor* and a pneumatic *brake* (see Figure 4.2). The encoder, mounted on the coils rotation axis, determines their angular position with an accuracy of the main field direction better than 0.1 mrad. The reference axis of the coils is adjusted by rotating the whole mole according to the electronic gravity sensor. The mole is held in position during the measurement by a pneumatic brake.

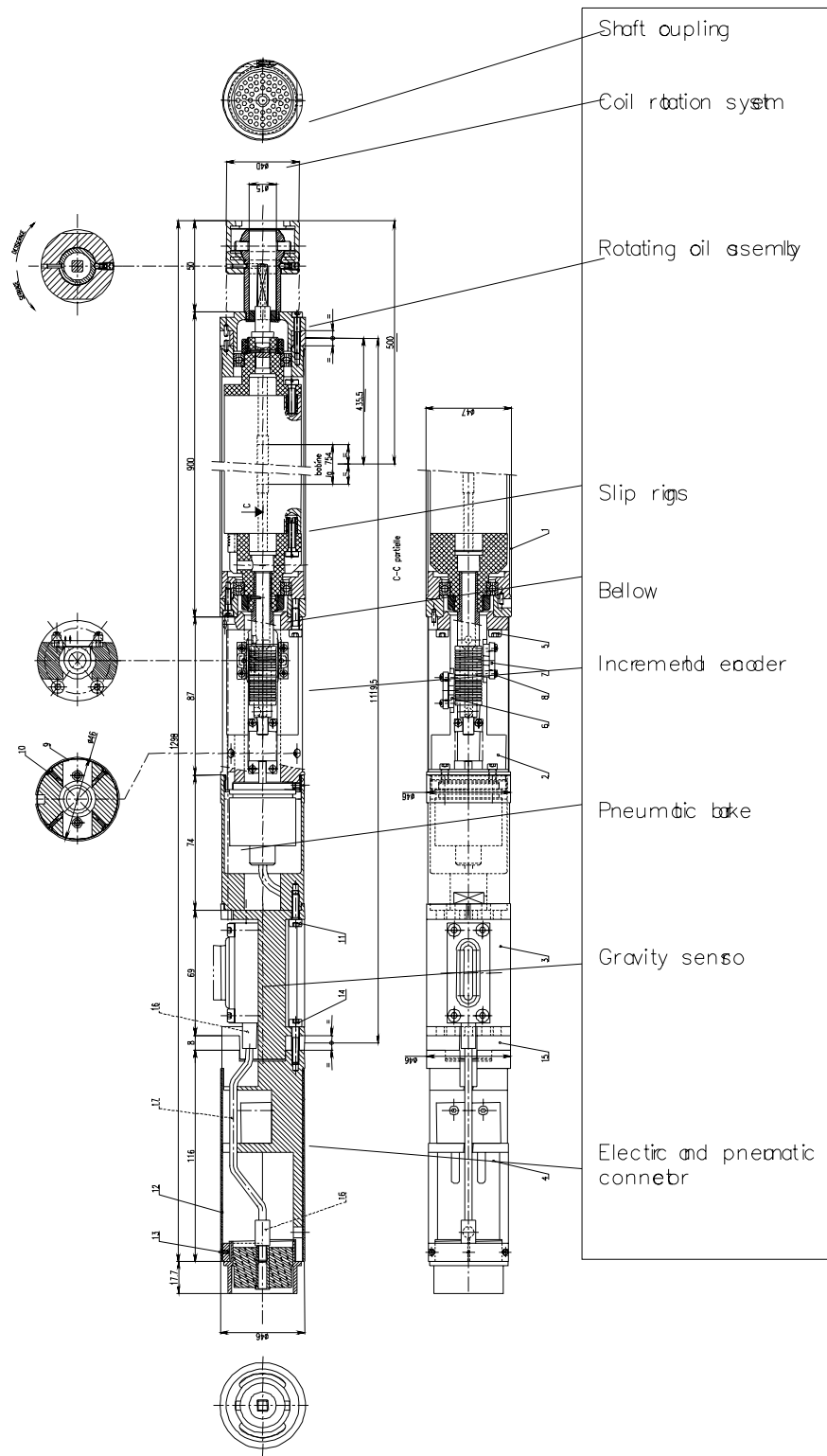


Figure 4.2 Magnetic probe (mole) assembly

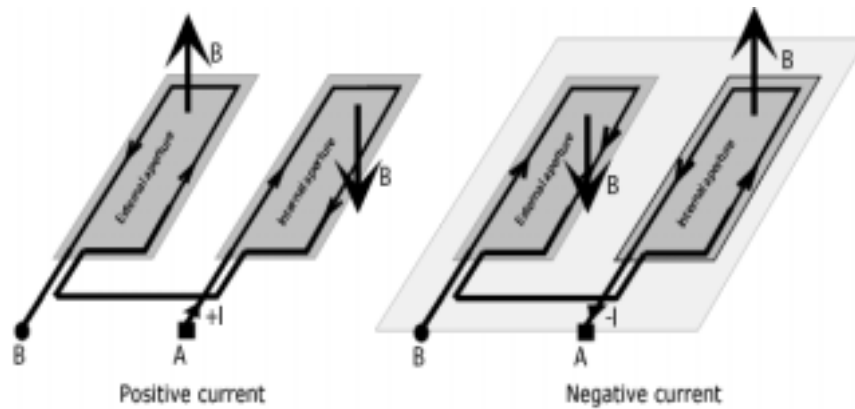


Figure 4.3 Electrical connections used for magnetic measurements.

Search coils are made of three identical coils, mounted side by side, the central one being centred on the rotating axis. They are made of 20-wire flat cable wound onto a fiberglass reinforced epoxy core. When inside a magnetic field, coils rotate to produce a voltage proportional to the flux and to the speed of rotation. Series of ten measurements are carried out at each longitudinal position, five at positive current and five at negative current (see Figure 4.3) in order to cancel iron magnetization and earth field effect. [14] The signal from the outward coil (absolute signal) is used to determine the main component. On the other hand, the field harmonics are calculated from a combination of signals coming from different coils. The system includes also two *motors* (one for rotating the coil and one for levelling the mole with respect to gravity) and an *acquisition system*.

4.1.2 Warm magnetic measurement data

Once a magnetic measurement has been carried on, the output signal has to be analyzed. The harmonic coefficients (i.e. multipoles) can be reconstructed from the Discrete Fourier Transform [14] and results can be given for each aperture as shown in Figure 4.4.

A data sheet of the kind of Figure 4.4 contains several parameters for each of the 20 positions in which measurements are taken along each collared coil aperture axis:

- C_1 , main field component in [T];

File	Aperture 1 - Cellated coils																	Integrals		
CT (T)	0.001	0.005	0.010	0.020	0.040	0.080	0.160	0.320	0.640	1.280	2.560	5.120	10.240	20.480	40.960	81.920	163.840	0.000	0.000	
Angle (rad)	0.000	0.000	0.000	0.000	0.000	0.000	0.000	0.000	0.000	0.000	0.000	0.000	0.000	0.000	0.000	0.000	0.000	0.000	0.000	0.000
Integration	Position 1	Position 2	Position 3	Position 4	Position 5	Position 6	Position 7	Position 8	Position 9	Position 10	Position 11	Position 12	Position 13	Position 14	Position 15	Position 16	Position 17	Position 18	Position 19	Position 20
a1	18300	10000	10000	10000	10000	10000	10000	10000	10000	10000	10000	10000	10000	10000	10000	10000	10000	10000	10000	10000
a2	-2.072	-0.415	-0.033	1.429	1.078	0.074	0.901	0.032	0.425	0.801	0.071	1.248	0.174	1.215	0.940	0.050	1.000	18300	10000	10000
a3	45.481	5.214	4.152	4.445	2.894	4.828	4.828	4.670	3.982	4.412	4.485	4.328	4.482	4.359	4.023	4.454	4.332	4.730	5.903	-0.912
a4	-0.087	0.136	0.291	0.276	0.415	-0.072	1.089	1.980	1.880	1.990	1.795	1.604	1.570	1.822	1.841	1.483	1.723	1.854	1.704	-0.193
a5	-1.870	1.897	1.843	1.420	1.711	1.882	1.889	1.980	1.880	1.820	1.866	1.828	1.107	1.822	1.814	1.166	1.680	1.528	0.002	0.229
a6	-0.073	0.820	0.041	-0.006	-0.178	0.084	-0.818	0.032	-0.827	-0.866	-0.610	-0.628	-0.180	-0.814	0.166	-0.680	-0.762	0.387	0.003	0.229
a7	2.447	0.820	0.041	0.007	0.760	0.394	0.756	0.760	0.767	0.826	0.654	0.773	0.172	0.804	0.769	0.742	0.767	0.787	0.769	0.501
a8	0.055	-0.334	-0.003	0.045	0.018	0.065	0.008	0.095	0.022	0.001	-0.009	0.000	0.054	0.033	0.028	0.000	0.003	0.000	0.023	0.014
a9	0.286	0.358	0.344	0.395	0.338	0.340	0.358	0.382	0.368	0.364	0.381	0.364	0.381	0.371	0.382	0.381	0.383	0.371	0.364	0.277
a10	-0.040	-0.817	-0.095	0.000	-0.035	0.082	-0.818	0.037	-0.807	-0.843	-0.690	-0.802	0.049	-0.808	0.043	-0.816	0.032	-0.802	-0.801	0.040
a11	0.680	0.742	0.734	0.739	0.738	0.748	0.736	0.736	0.736	0.733	0.737	0.742	0.736	0.743	0.738	0.727	0.738	0.738	0.738	0.699
a12	0.000	0.002	0.005	0.011	0.004	0.004	-0.003	0.002	0.002	-0.004	-0.002	0.004	0.000	0.000	0.004	-0.005	0.000	0.005	0.005	0.014
a13	0.000	0.000	0.000	0.000	0.000	0.000	0.000	0.000	0.000	0.000	0.000	0.000	0.000	0.000	0.000	0.000	0.000	0.000	0.000	0.000
a14	-0.003	-0.002	-0.001	-0.001	-0.004	0.000	-0.003	-0.003	-0.003	-0.005	-0.005	-0.003	-0.003	0.001	-0.004	-0.002	-0.005	-0.003	-0.002	0.007
a15	-0.007	0.031	0.031	0.030	0.033	0.030	0.038	0.035	0.034	0.033	0.035	0.037	0.030	0.034	0.035	0.036	0.034	0.035	0.036	0.016
a16	0.000	0.000	0.000	0.000	0.000	0.000	0.000	0.000	0.000	0.000	0.000	0.000	0.000	0.000	0.000	0.000	0.000	0.000	0.000	0.000
a17	-0.000	-0.000	-0.000	-0.000	-0.000	-0.000	-0.000	-0.000	-0.000	-0.000	-0.000	-0.000	-0.000	-0.000	-0.000	-0.000	-0.000	-0.000	-0.000	-0.000
a18	0.000	0.000	0.000	0.000	0.000	0.000	0.000	0.000	0.000	0.000	0.000	0.000	0.000	0.000	0.000	0.000	0.000	0.000	0.000	0.000
a19	0.000	0.000	0.000	0.000	0.000	0.000	0.000	0.000	0.000	0.000	0.000	0.000	0.000	0.000	0.000	0.000	0.000	0.000	0.000	0.000
a20	0.000	0.000	0.000	0.000	0.000	0.000	0.000	0.000	0.000	0.000	0.000	0.000	0.000	0.000	0.000	0.000	0.000	0.000	0.000	0.000
a21	0.000	0.000	0.000	0.000	0.000	0.000	0.000	0.000	0.000	0.000	0.000	0.000	0.000	0.000	0.000	0.000	0.000	0.000	0.000	0.000
a22	0.000	0.000	0.000	0.000	0.000	0.000	0.000	0.000	0.000	0.000	0.000	0.000	0.000	0.000	0.000	0.000	0.000	0.000	0.000	0.000
a23	0.000	0.000	0.000	0.000	0.000	0.000	0.000	0.000	0.000	0.000	0.000	0.000	0.000	0.000	0.000	0.000	0.000	0.000	0.000	0.000
a24	0.000	0.000	0.000	0.000	0.000	0.000	0.000	0.000	0.000	0.000	0.000	0.000	0.000	0.000	0.000	0.000	0.000	0.000	0.000	0.000
a25	0.000	0.000	0.000	0.000	0.000	0.000	0.000	0.000	0.000	0.000	0.000	0.000	0.000	0.000	0.000	0.000	0.000	0.000	0.000	0.000
a26	0.000	0.000	0.000	0.000	0.000	0.000	0.000	0.000	0.000	0.000	0.000	0.000	0.000	0.000	0.000	0.000	0.000	0.000	0.000	0.000
a27	0.000	0.000	0.000	0.000	0.000	0.000	0.000	0.000	0.000	0.000	0.000	0.000	0.000	0.000	0.000	0.000	0.000	0.000	0.000	0.000
a28	0.000	0.000	0.000	0.000	0.000	0.000	0.000	0.000	0.000	0.000	0.000	0.000	0.000	0.000	0.000	0.000	0.000	0.000	0.000	0.000
a29	0.000	0.000	0.000	0.000	0.000	0.000	0.000	0.000	0.000	0.000	0.000	0.000	0.000	0.000	0.000	0.000	0.000	0.000	0.000	0.000
a30	0.000	0.000	0.000	0.000	0.000	0.000	0.000	0.000	0.000	0.000	0.000	0.000	0.000	0.000	0.000	0.000	0.000	0.000	0.000	0.000
a31	0.000	0.000	0.000	0.000	0.000	0.000	0.000	0.000	0.000	0.000	0.000	0.000	0.000	0.000	0.000	0.000	0.000	0.000	0.000	0.000
a32	0.000	0.000	0.000	0.000	0.000	0.000	0.000	0.000	0.000	0.000	0.000	0.000	0.000	0.000	0.000	0.000	0.000	0.000	0.000	0.000
a33	0.000	0.000	0.000	0.000	0.000	0.000	0.000	0.000	0.000	0.000	0.000	0.000	0.000	0.000	0.000	0.000	0.000	0.000	0.000	0.000
a34	0.000	0.000	0.000	0.000	0.000	0.000	0.000	0.000	0.000	0.000	0.000	0.000	0.000	0.000	0.000	0.000	0.000	0.000	0.000	0.000
a35	0.000	0.000	0.000	0.000	0.000	0.000	0.000	0.000	0.000	0.000	0.000	0.000	0.000	0.000	0.000	0.000	0.000	0.000	0.000	0.000
a36	0.000	0.000	0.000	0.000	0.000	0.000	0.000	0.000	0.000	0.000	0.000	0.000	0.000	0.000	0.000	0.000	0.000	0.000	0.000	0.000
a37	0.000	0.000	0.000	0.000	0.000	0.000	0.000	0.000	0.000	0.000	0.000	0.000	0.000	0.000	0.000	0.000	0.000	0.000	0.000	0.000

Figure 4.4 Template used to store warm magnetic measurement data for one aperture of the dipole coil.

- *Angle*, main field component direction with respect to the gravity in [mrad];
- b_i and a_i , normal and skew multipoles up to the order 15th in units of 10^{-4} (multipoles are dimensionless);
- D_x and D_y , coordinates of the magnetic axis with respect to the mechanical one of the measured aperture in [mm]. They are determined by assuming that the not-allowed harmonics a_{10} and b_{10} are only due to first order feed down of b_n harmonics (see [27] for further reading).

When a particle beam crosses a dipolar field nearly at the speed of light, its motion is mainly affected by the mean magnetic field in the magnet straight part, if there are no strong multipolar variations, and the short magnet heads have limited influence on the field quality. For the LHC dipole, measurement position 1 and 20 are in the magnet heads. Measurement positions 2 to 19 are along the so-called straight part (see Figure 4.5). Accelerator physicists are therefore interested in values integrated along the magnet straight part to qualify the overall LHC machine performance. Magnetic measurements at room temperature provide such values, which can be used to characterize the aperture as a whole:

- *Magnetic Length*: it is defined by the following equation:

$$M_L = \frac{\int_{-\infty}^{\infty} C_1 dl}{\langle C_1 \rangle}, \quad (4.2)$$

where $\langle C_1 \rangle$ is the average of the main field component along the so-called straight part. It is computed along the whole aperture axis and it is shown in Figure 4.5.

- *Transfer Function (TF)*: it is the average transfer function in the straight part (in $\frac{T}{A}$), defined by the following equation:

$$TF = \frac{\langle C_1 \rangle}{I}, \quad (4.3)$$

where I is the DC current used for measurements (usually 8.5 A at room temperature).

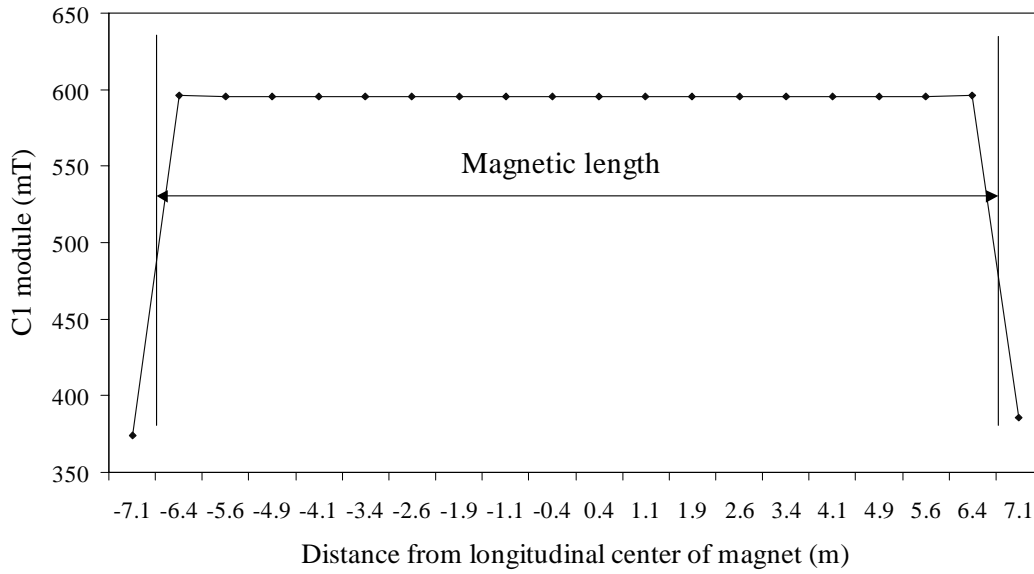


Figure 4.5 C_1 module of aperture 1 of collared coil HCMBB_A001-01000001 measured at room temperature in 20 position along collared coil axis with corresponding magnetic length.

- *Integrated multipoles*: for a generic multipole b_n , its integrated value is defined by the following equation:

$$\langle b_n \rangle = \frac{\int_{-\infty}^{\infty} C_1 b_n dl}{\int_{-\infty}^{\infty} C_1 dl} . \quad (4.4)$$

A similar equation holds for the skew multipoles a_n .

- *Coil waviness*: it is a parameter meant to take into account for the multipolar variations affecting the collared coil aperture along its longitudinal axis. Random conductor displacements with a rms amplitude d generate b_n and a_n distributions with standard deviation values that can be fitted according to

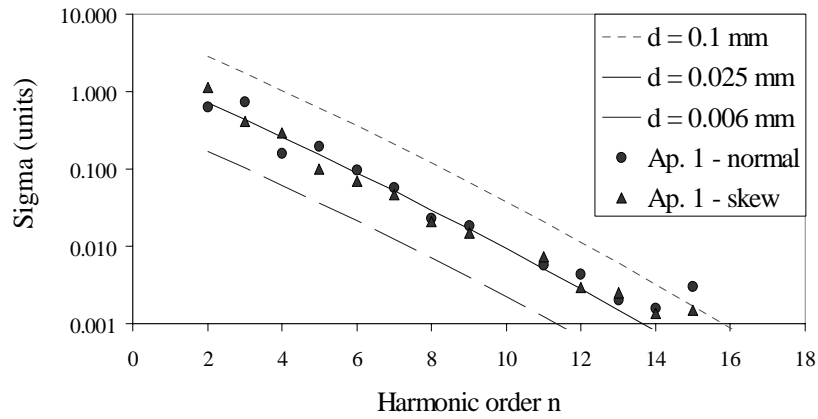


Figure 4.6 Measured multipoles sigma (markers) and parabolic fit (lines) for a collared coil aperture. Its *coil waviness* value is obtained as the fitting parameter d of the parabolic curves.

the following law:

$$\sigma_n(d) = d\alpha\beta^n\gamma^{n^2}, \quad (4.5)$$

where α , β and γ are scaling law constants worked out through simulations (see [13] for references) and n is the multipole order (see Figure 4.6). The coil waviness is the value of the parameter d that best fits the measured values of the multipole sigma. This gives an indication of the variation of the block positions along the axis.

The data sheet reports also the DC current I in [A] used to excite the collared coil during the magnetic measurement at room temperature.

4.1.3 Monitoring magnet construction through field quality

Superconducting magnets feature tight manufacture tolerances, of the order of 0.05 mm. The final magnet is obtained through a series of assembly steps, as previously mentioned. After each sub-assembly is obtained, measurements and tests of various kind

have been arranged in order to detect errors or faulty components at an early stage of production. By magnetic measurement at room temperature of collared coils, the field quality achieved by magnets can be evaluated according to equation (4.1) and assembly errors or drifts of the dimensions of the magnet components can be detected and corrected. [26]

During design phase, accelerator physicists and magnet builders interact to determine the final nominal cross-section according to the needed magnet performance and to the industrial feasibility. A feedback is engaged among them in order to define a field quality that is both reachable within manufacturing tolerances and tolerable for beam dynamics. [17][28] At this stage few modifications of the design are envisaged to fine tune some parameters during the production and when the overall design is complete a pre-series can start. The industrial production must be monitored to control its homogeneity. Data coming from the pre-series industrial production can be used to evaluate acceptance criteria for the industrial process which are more stringent than the beam dynamics specifications, since the latter have to be applied only on the magnet performance averages on all the production, while the former can be given for the different parts of a magnet and for the several parameters which characterize the performance of a single magnet.

Data coming from measurements carried on collared coils and cold mass can be used then to monitor magnet production and even to determine what counteractions can be taken on the measured assembly to recover its multipolar content. [17],[18],[19],[22],[26] Such production feedback is needed to compensate for the field errors arising from [19]:

- manufacturing errors;
- use of faulty components;
- manufacturing tools wear.

Magnetic measurements at room temperature performed at different stages of production can be considered a fast and effective way to have indications on the quality of industrial production. This method can be considered also a reliable tool to steer the industrial production towards specifications, but only if good correlations exist among

multipoles measured at room temperature and multipoles measured at cryogenic temperature (the so-called *warm-cold correlations*). If they exist, two fast feedback loops can be engaged on the magnet production, as shown in Figure 4.7. They can be used to monitor the production homogeneity and to verify the magnetic effect of possible design modifications needed to steer the production towards the specifications. Even if magnetic measurements at cryogenic temperature are performed on the cryodipole at the end of manufacturing line, they can hardly be used for monitoring the industrial production since the feedback loop with the field quality analysis is slow.

For several accelerator magnets (see for reference [29]) adjustable epoxy fiber-glass spacers (*shims*) have been used both for mechanical and field quality purposes. During pre-series production non-nominal shims are usually used to tune coil pre-stress. In the next section, we will describe a first-order approximation geometric model used to compute the magnetic effect which non-nominal shims and coil dimensions have on the LHC dipoles field quality.

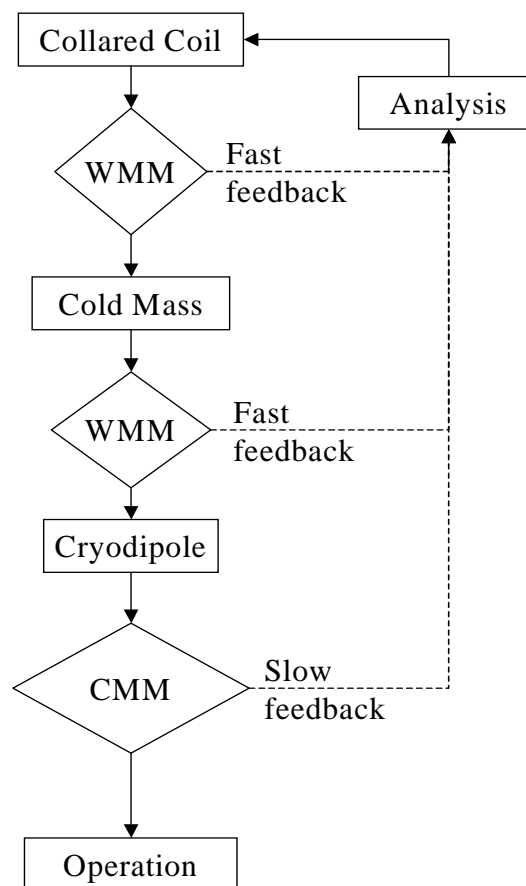


Figure 4.7 Magnetic measurements are taken at room temperature for a fast feedback at an early stage of production. Measurements at cryogenic temperature are the last magnetic test brought on the industrial production and very slow as a feedback on the design. WMM: Warm Magnetic Measurement (at 300K); CMM: Cold Magnetic Measurement (at 1.9K).

4.2 Field quality analysis methods

To monitor the homogeneity of the collared coil industrial production, each magnetic measurement performed on a new assembly is compared to the expected multipolar content coming from the statistical analysis performed on measurements data presented in the next chapter. Once a discrepancy has been found in a measurement, it must be localized along the axis and analyzed to understand what has caused it. The possible causes for a departure of measurements from what is expected can be the following:

- wrong measurement;
- wrong assembly (both due to human and tooling errors);
- the use of faulty components;
- tooling wear.

There is no straight method to single out a wrong measurement of a good magnet from a reliable measurement of a bad magnet. Only the analyst own experience can mark out the difference; in cases of anomalous results the measurement is always repeated. If the same anomalies still affect the new measurement, then the collared coil may contain a manufacturing or assembly error. In such cases the analyst must localize the possible collared coil defects along its axis and inside the coil. From the localization of the defect, the measurement discrepancy can be traced back to its cause and counteractions can be taken on the assembly to recover its wrong multipolar structure. There are many methods to analyze a bad field quality and correlate it to conductor displacements affecting the coil. Among them, the present work has been focused on models for construction errors and on the multipolar decay approach.

4.2.1 Models for construction errors

In principle, a careful measurement of the magnetic structure of the field allows to reconstruct the current distribution (the so-called *inverse problem*, see [22] for references). However, the limited accuracy of the measurements and the non-uniqueness of the

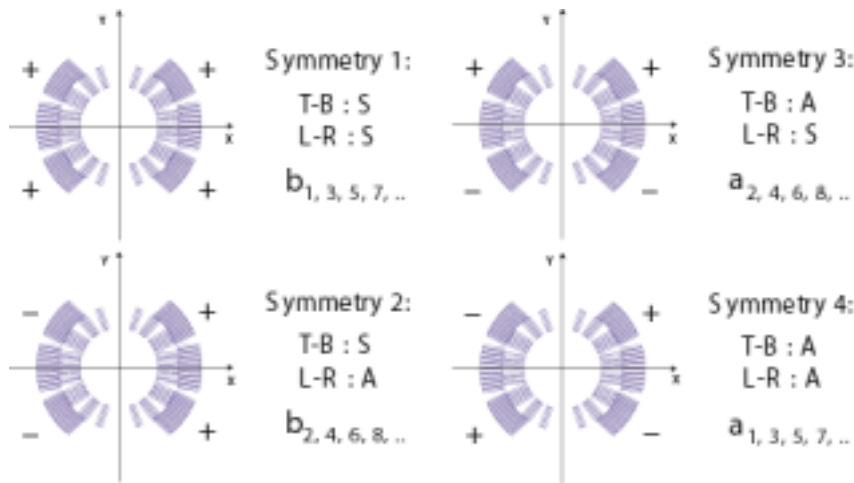


Figure 4.8 Conductors displacements can be given in terms of four set of movements constituting orthogonal families since excite four different set of multipoles. T-B: top-bottom; L-R: left-right; S: symmetric; A: anti-symmetric (courtesy of S.Redaeli, [30]).

solution makes the inverse problem very difficult (see [17] for references). An approach to the inverse problem, widely used in literature, is to study the most likely manufacturing errors. [7],[17],[30] To do so, it is better to refer to symmetries which characterize the magnet coil and to decompose errors in symmetric or anti-symmetric deformations. As introduced in Section 3.1.3, in fact, the Taylor's expansion coefficients b_n and a_n are differently excited according to the conductor arrangement patterns. Possible symmetries inside the coil can be referred to as top-bottom (T-B) or left-right (L-R) symmetries according to the aperture reference system centered on the coil axis, and conductors movements can be described according to symmetric (S) or anti-symmetric (A) displacements of Figure 4.8. According to the possible combinations of symmetries, one has that:

- odd normal multipoles b_{2k+1} ($k=0,1,2,\dots$) are excited by conductor displacements that follow the T-B and L-R symmetries;
- even normal multipoles b_{2k} ($k=0,1,2,\dots$) are excited by conductor displacements that follow the T-B symmetry and the L-R anti-symmetry;
- even normal multipoles a_{2k} ($k=0,1,2,\dots$) are excited by conductor displacements that follow the T-B anti-symmetry and the L-R symmetry;
- odd normal multipoles a_{2k+1} ($k=0,1,2,\dots$) are excited by conductor displacements that follow the T-B and L-R anti-symmetry;

Hence, any movement of conductors inside the coil can be decomposed in four set of symmetrical or anti-symmetrical coil movements and deformations which let only a set of multipoles be non-zero. They are four *orthogonal families* of deformation (see Figure 4.8, [30]) and can be used to describe the following cases, which have been assumed to be likely for the industrial production of the LHC collared coil:

- non-nominal polar shim thickness;
- non-nominal isolation thickness in the coil midplane;
- non-nominal azimuthal size of upper or lower coil layers;
- non-nominal coil radial dimensions.

In order to compute the field quality featured by a coil affected by such manufacturing errors, a geometrical model for the straight part cross-section is needed. A finite element model has been already implemented for the field quality computations of the LHC dipoles. [31] Indeed, it can only compute the field quality of a T-B symmetric coil, since it has been implemented for a coil half only. Therefore, we have developed models and codes to evaluate the impact of assumed non-nominalities of any asymmetry based on an existing magnetostatic code. [32]

4.2.2 Multipoles decay

Among the different attempts to obtain some indications on manufacturing errors affecting a measured collared coil, a method can be derived directly from the multipolar expansion theory. In Section 3.1.2 we have shown that the magnetic field featured by a single current line can be expanded in the following way:

$$B_y + iB_x = B_1 \sum_{n=1}^{\infty} c_n \frac{\zeta^{n-1}}{R_{ref}^{n-1}}, \quad (4.6)$$

where c_n is the complex multipole according to the following:

$$c_n = b_n + ia_n = -\frac{\mu_0 I}{B_1 R_{ref}^{1-n}} \frac{1}{2\pi \zeta_c^n}. \quad (4.7)$$

B_l is the main field magnitude at the reference radius R_{ref} and $\zeta=x+iy$ is the complex coordinate. If we group all terms not depending on the multipole order n in a constant A , then we obtain:

$$c_n = -A \left(\frac{R_{ref}}{\zeta_c} \right)^n. \quad (4.8)$$

From equation (4.7), it can be seen that multipoles magnitude *decay* naturally, because the bigger is n , the smaller becomes the term $\left(\frac{R_{ref}}{\zeta_c} \right)^n$, since R_{ref} is 17 mm and ζ_c is greater than 28 mm. A small variation of the conductor position $\Delta\zeta_c$ leads to a variation in c_n as following:

$$\Delta c_n = \frac{nA\Delta\zeta_c}{R_{ref}} \left(\frac{R_{ref}}{|\zeta_c|} \right)^{n+1}. \quad (4.9)$$

If we compute the logarithm of equation (4.9) absolute value, we find:

$$\ln(|\Delta c_n|) = \ln(n) + n \ln \left(\frac{R_{ref}}{|\zeta_c|} \right) + \ln \left(A \frac{|\Delta\zeta_c|}{|\zeta_c|} \right), \quad (4.10)$$

where $|\zeta_c|$ is the conductor distance R_c from the aperture center. We can write also the following relation:

$$f(n) = \ln(|\Delta c_n|) - \ln(n) = n \ln \left(\frac{R_{ref}}{R_c} \right) + const, \quad (4.11)$$

where *const* is a constant independent of n . For a given position of a magnetic measurement the function $f(n)$ can be evaluated for each multipole deviation from straight part average and plotted versus n . It can be then linearly fitted and from the fitting line slope Q , one can try to localize at which radius the conductors have been displaced, applying the following formula:

$$R_c = R_{ref} \exp(-Q), \quad (4.12)$$

and from its intercept:

$$const = \ln\left(A \frac{|\Delta \zeta_c|}{|\zeta_c|}\right), \quad (4.13)$$

some indication of the displacement magnitude can be derived.

In such a way magnetic field quality analysts can have some indications on the distance from the aperture center at which manufacturing errors are located, i.e. inner or outer layer. We tried then to analyze the multipolar decay trend according to the four orthogonal families of deformations and to localize defects inside the coil according to symmetry patterns. To understand the reliability of this method, we performed some simulations. We first considered multipoles variations featured by a collared coil with a 0.3 mm thick polar shim in the coil first quadrant inner layer (the nominal dimension is 0.2 mm) and then those of a collared coil with a 0.9 mm thick polar shim in the coil first quadrant outer layer (the nominal dimension is 0.8 mm). In Figure 4.9, the function $f(n)$ computed out of odd normal multipole variations are plotted together with the fitting line for both cases, while Figure 4.10 reports even normal multipoles. In both figures, the fitting line slope in the inner layer case is smaller (in absolute value) than those computed for the outer layer case, which means that the method gives some indications on the error position. Moreover, in each case the multipole decay trend is the same for odd and even

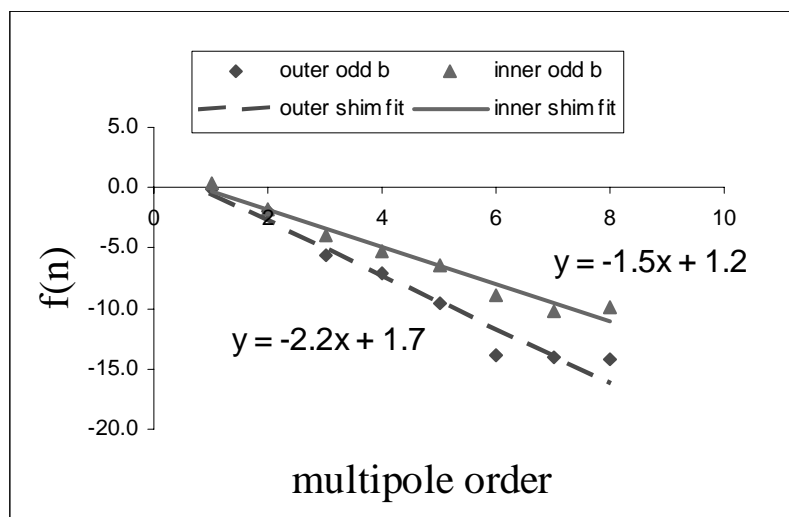


Figure 4.9 Odd normal multipole decay extrapolation for an asymmetrical polar shim insertion in the inner layer and in the outer layer. The fitting equation is also reported.

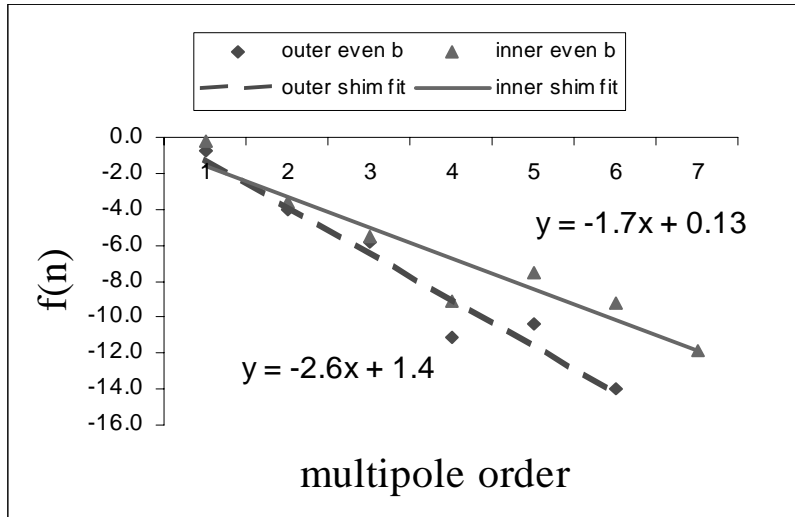


Figure 4.10 Even normal multipole decay extrapolation for an asymmetrical polar shim insertion in the inner layer and in the outer layer. The fitting equation is also reported.

normal multipoles (and it is also for the skew coefficients, not reported for brevity), which positively point out that all symmetries have been excited. In Table 4.1 the computed *error radius* which have been extrapolated from the multipolar decay featured for the polar shim insertion in the outer and in the inner layer are reported. Since the inner layer is localized between 28 and 43 mm from the aperture center, while the outer layer extends from 43 to 59 mm, the indications on the error position that can be derived from Table 4.1 are good. It must be observed, anyway, that the estimated radii of the manufacturing error position are affected by large errors.

Table 4.1 Error radii extrapolated from measured multipoles decay for odd and even normal multipoles. For each radius, the error estimate (1σ) is reported. Values are given in mm.

	Polar shim in the inner layer		Polar shim in the outer layer	
	R_c (mm)	Err (1σ)	R_c (mm)	Err (1σ)
odd b_n	36	4	52	10
even b_n	40	10	62	20

4.3 Geometrical models for the coil straight part

In this section we develop a geometrical model to understand and quantify the magnetic influence of non-nominalities affecting components of the dipole coil which are in direct contact with conductors and which have strong effects on the field quality (see Section 3.2.1). One of the difficulties which affect the computation of conductors displacements is the fact that the coil has non-homogenous physical proprieties. During collaring, for example, coil conductors should be pushed in their nominal position if a nominal shim is used. But if used shims are not nominal, then conductors are positioned inside the coil according to the way in which the coil is squeezed with respect to the nominal case, strongly dependant on its mechanical structure and properties. The coil is made by copper wedges and insulated superconducting cables. The measured values of the azimuthal elastic modulus at room temperature for copper wedges and for conductor blocks are the following:

- copper wedges: 120000 MPa;
- coil blocks: 6000-10000 Mpa.

In order to implement a simplified model, one has to choose between two extreme approximations:

- *Copper wedges have the same properties of the cables.* This approximation implies that the coil has an homogenous structure (see for instance [33]).
- *Copper wedges are infinitely rigid if compared to the properties of cables:* This approximation assumes that the whole deformation is taken by cables.

We implemented both approximations in a L-R, T-B symmetric model to find out discrepancies between the two approaches in terms of field quality in the case of a non-nominal polar shim insertion. The results of the two models have then been compared with an approach based on realistic material properties of coil blocks and copper wedges analyzed through a finite element model [31] (see Appendix B). We have found that the difference between the two approximations are not negligible (the largest difference is around 25% on b_3) and that the hard copper wedge approximation is more realistic, fea-

turing a better agreement with the FEM (the largest difference is 10% on b_5) than the soft copper wedge approximation (the largest difference is around 20% on b_3).

4.3.1 Symmetric model

In order to properly describe the geometric model in which we implemented the hard copper wedges approximation and which can be only used to compute conductor positions after a non-nominal polar shim insertion in a T-B, L-R symmetric coil, we will refer only to the outer layer of a coil quadrant of Figure 4.11. It consists in two conductor blocks interspaced by a copper wedge and delimited by the median plane insulation polyimide sheet and the polar shim. Nevertheless, all formulas that will be given can apply to the coil inner layer.

If the elastic modulus of copper wedges is much larger than that of cables, conductors are squeezed uniformly while copper wedges dimensions remain unchanged. From the design position of conductors given as in Table 3.2 for nominal shims, one has to compute the new positions of conductors after the insertion of a non-nominal shim in the polar region, according to the reference system given in Figure 3.7. To compute cables thickness, we assumed that the block angle α is not modified by the non-nominal shim insertion (for coil blocks reference system see Section 3.2.1). This assumption is justified by the rectangular shape of the tuning shims to be inserted which is different from the trapezoidal one of the Rutherford type cables and it implies that cables are squeezed by the same amount both on the inner and on the outer side ($\delta th_i = \delta th_e$). Cables squeeze of an amount which can be written (for the reference block 2) as:

$$\delta th_i(2) = \delta th_e(2) = \frac{\delta_{shim,polar}}{nc(1) + nc(2)}, \quad (4.14)$$

where $nc(2)$ and $th_i(2)$ corresponds to the number and the inner thickness of conductors

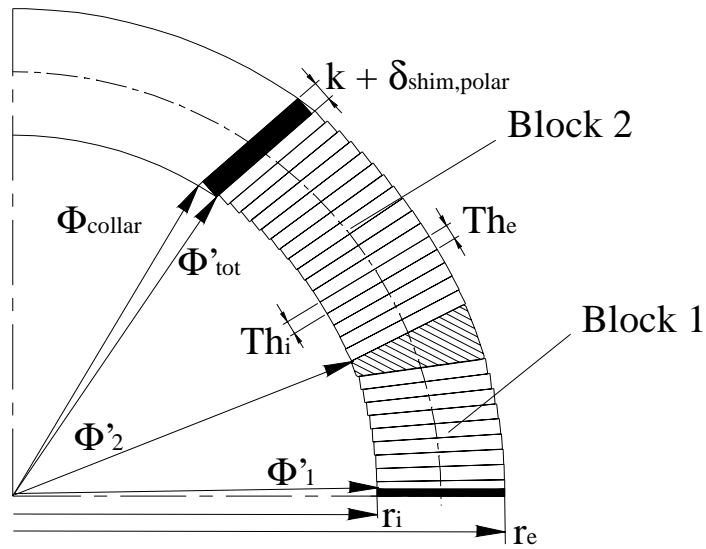


Figure 4.11 Notation used to compute conductor displacement in the outer layer of a coil quadrant after the insertion of a polar shim.

belonging to block 2. We can then write for the angular coordinates of block 2:

$$\Phi'_2 = \Phi_2 - nc(1) \frac{\delta th_i(2)}{r_i} \frac{180}{\pi}. \quad (4.15)$$

For the other coil blocks, one has to substitute $nc(1)$ in equation (4.15) with the number of conductors belonging to the blocks on which it is piled up, e.g. for block 6 one has to write $(nc(3)+nc(4)+nc(5))$. These formulas have been implemented into a Fortran code (see Appendix C) which compute conductor positions to perform magnetostatic computations with an available code (see [32]).

4.3.2 Asymmetric model

The hard copper wedge approximation has been also implemented into a code for the analysis of the field quality in a completely asymmetric case, for which the position of conductors in all 24 blocks (see Figure 4.12) must be given as input. The model computes cables displacements due to the following non-nominalities (both for inner and outer layer):

- azimuthal coil size variation;
- non-nominal polar shim thickness;
- polyimide sheet insertion in the coil median plane;

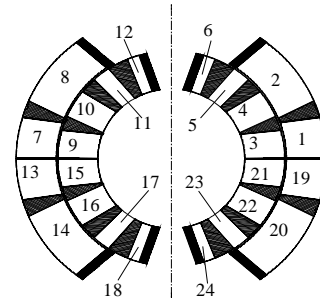


Figure 4.12 Coil blocks numbering convention used in the asymmetric geometric code

The implemented Fortran code (reported in Appendix C) compute conductor positions needed by the magnetostatic model.[32]

4.3.2.1 Azimuthal coil size variations

In the curing mould, cables are assembled in layers. A pole is formed by assembling inner and outer layers and two poles are then assembled into one coil. If two facing poles have different azimuthal size, the median plane is shifted from the nominal position when they are assembled. In fact, the only reference positions are the collar edges. Here, we evaluate the position of the median plane by taking into account the effective azimuthal coil size of all the 8 layers assigned as input to the code. Figure 4.13 shows the outer layer used as a reference to present the equations implemented into the code. Equations written for the outer layer have been generalized to the other layers in order to compute the complete conductor distribution inside the coil.

If upper and lower pole have different azimuthal size, the median plane is shifted by an amount proportional to the size difference. Each half layer is characterized by its azimuthal size which can be written as $L_{azim} + \delta_{l,sup}$, being L_{azim} the nominal azimuthal size. The coil median plane is shifted downward of an angle expressed in degrees by the fol-

lowing equation:

$$\delta_{\varphi} = \frac{\delta_{l, sup} - \delta_{l, inf} 180}{r_i \pi}. \quad (4.16)$$

If the corresponding half layers have the same azimuthal size (even if not nominal), the median plane is obviously kept at its nominal position.

When upper and lower pole azimuthal sizes are different, conductors are squeezed and each block is shifted by an amount which depends on the position inside the coil (see Figure 4.12):

$$\Phi'_1 = \Phi_1 - \delta_{\varphi}, \quad (4.17)$$

$$\Phi'_2 = \Phi_2 - \delta_{\varphi} \frac{nc(2)}{nc(1) + nc(2)}, \quad (4.18)$$

$$\Phi'_{19} = \Phi_{19} + \delta_{\varphi}, \quad (4.19)$$

$$\Phi'_{20} = \Phi_{20} + \delta_{\varphi} \frac{nc(20)}{nc(19) + nc(20)}. \quad (4.20)$$

Being squeezed, conductors thickness changes according to the following:

$$th'_i(1) = th'_i(2) = th_i(1) + \frac{\delta_{\varphi} r_i}{nc(1) + nc(2)}, \quad (4.21)$$

$$th'_i(19) = th'_i(20) = th_i(19) + \frac{\delta_{\varphi} r_i}{nc(19) + nc(20)}. \quad (4.22)$$

As for the symmetric model, α is assumed to be unchanged by conductor displacements. This implies that each cable is squeezed by the same amount both on its inner and outer side ($\delta th_i = \delta th_e$).

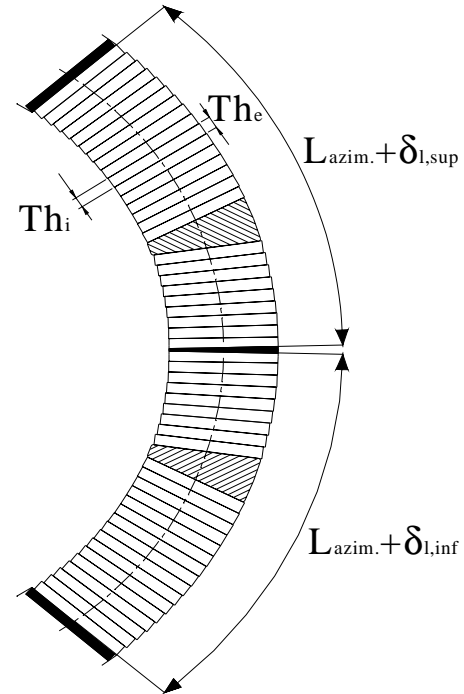


Figure 4.13 Complete outer layer (upper and lower pole) assembly: the median plane is centered only if upper and lower half layer have the same azimuthal size. Naming convention used for non-nominalities is shown.

4.3.2.2 Non-nominal polar shims and polyimide sheet insertion in the coil midplane

Once the position of the median plane has been computed, the geometrical code can calculate cable block positions corresponding to the real size of polar shims and of the insulation on the coil median plane. For the asymmetric model, it has been chosen to compute blocks movements proportional the real angular dimension of each block as being proportional to the ratio of the angular amplitude of the coil occupied by conductors after the shim insertion and the angular amplitude of the coil occupied by conductors in the nominal condition.

The angular amplitude of the coil suitable for conductor positioning is equal to the total angular aperture of the collar minus the copper wedge angular amplitude. For the LHC dipole coil, the total nominal angular amplitude of the collar is different for inner and outer layer:

$$\Phi_{tot, inner} = 150.89^\circ, \quad (4.23)$$

$$\Phi_{tot, outer} = 113.29^\circ. \quad (4.24)$$

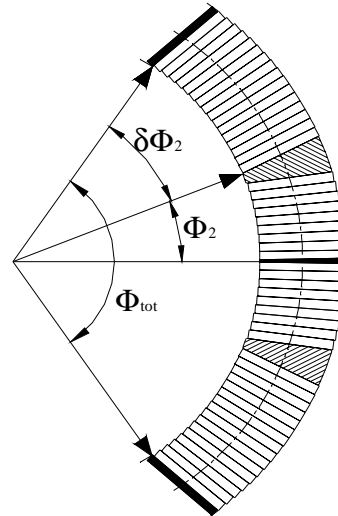


Figure 4.14 Naming convention used for conductor position calculations after the azimuthal coil size variations have been taken into account.

Referring to Figure 4.14, for the outer coil it can be written:

$$\Phi_{occ} = \Phi_{tot} - 2cw(1) - \Phi_1 - \Phi_{19}, \quad (4.25)$$

where Φ_{occ} is the angular amplitude suitable for conductor positioning and $cw(i)$ (with $i = 1, 2, 3, 4$) is the angular amplitude of each of the four possible copper wedges (considered infinitely rigid), corresponding to the following:

$$cw(1) = 2.71^\circ; \quad cw(2) = 1.84^\circ; \quad (4.26)$$

$$cw(1) = 5.63^\circ; cw(2) = 6.96^\circ. \quad (4.27)$$

When non-nominal shims are inserted in the coil plane region or a polyimide sheet is inserted into the median plane, the angular amplitude suitable for conductor positioning is changed, according to the following:

$$\Phi'_{occ} = \Phi_{occ} - \left(\frac{\delta_{pol,up}}{r_i} + \frac{\delta_{pol,dw}}{r_i} + \frac{\delta_{med,up}}{r_i} + \frac{\delta_{med,dw}}{r_i} \right) \frac{180}{\pi}, \quad (4.28)$$

where $\delta_{pol,up}$ and $\delta_{pol,dw}$ refers to the difference from the nominal value of polar shim in the upper and lower half layers, while $\delta_{med,up}$ and $\delta_{med,dw}$ is the corresponding notation for polyimide sheets inserted into the median plane.

Finally, new block positions can be computed by considering that the angular amplitude of each block is changed proportionally to the change of the total angular amplitude of the coil suitable for conductor placement. After the azimuthal coil size variation have been considered, the code computes the angular amplitude of each block in a way similar to that used for Φ_{tot} . The final angular amplitude of each block after shim insertion can be written in analogy to what can be written for block 2 in the reference layer of Figure 4.14:

$$\delta\Phi'_2 = \delta\Phi_2 \frac{\Phi'_{occ}}{\Phi_{occ}}. \quad (4.29)$$

Final cable inner and outer thicknesses are computed multiplying the values computed for the azimuthal coil size variation by the same ratio $\frac{\Phi'_{occ}}{\Phi_{occ}}$. Block coordinates given in the usual reference system of Figure 3.7 can then be reconstructed from the lower or upper edge of the collar. The geometrical Fortran code (reported in Appendix C) outputs block positions and cable thicknesses for the magnetostatic computations. [32]

4.3.2.3 Non-nominal coil radial dimension

The radial variations have been modelled according to which layer they affect:

- *for the inner layer:* the inner radius of the inner layer is kept constant, while its outer radius is reduced of the radial variation δr_e . The outer layer is rigidly displaced towards the aperture center of the amount δr_e ;
- *for the outer layer:* the inner radius of the outer layer is kept constant, while its outer radius is reduced of the radial variation δr_e . The inner layer is not displaced or deformed;

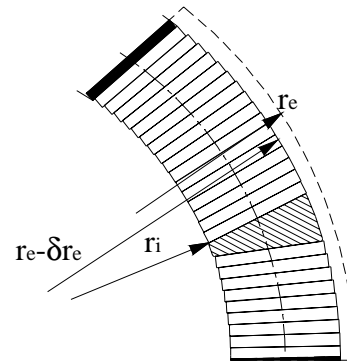


Figure 4.15 When coil layers are squeezed, the outer radius has a dimension inferior to the nominal one ($r_e - \delta r_e$), while the inner radius (r_i) is fixed by the winding mandrel of the curing mould.

The non-nominal coil radial dimension has been modelled in this way to follow the features of coil manufacturing during and after curing (see Figure 4.15). In fact, the coil layers inner radius is kept constant by the mandrel on which they are winded and then cured, and it appears more probable a manufacturing error due to the curing mould rather than due to the mandrel.

4.3.3 Sensitivity results

Sensitivity data are reported in Table 4.2 for odd and even normal multipoles, in Table 4.3 for odd and even skew multipoles. Computations have been carried by decoupling coil deformations according to the four orthogonal families described in Section 4.2.1. According to data presented in Table 4.2 and Table 4.3, the azimuthal coil size variation excites skew multipoles only, while the shim insertion in the coil midplane excites only normal multipoles. This is partly due to the symmetry pattern which the coil assumes after it has undergone such deformations. In fact, on one side the shim insertion in the coil midplane does not affect the T-B symmetry, because the coil midplane position

remains unchanged if the azimuthal coil size of two facing half layer is the same, and consequently does not excite skew multipoles. On the other hand, even if the azimuthal coil size variation affects T-B and L-R symmetries, the normal multipole sensitivity to this kind of coil defect is negligible

Table 4.2 Computed odd and even normal multipoles sensitivity to the three following manufacturing errors: non-nominal shim insertion in the coil polar region; non-nominal shim insertion in the midplane insulation; non nominal coil radial dimension. They have been computed for non-nominality of 0.1 mm according to the orthogonal families of coil deformations. For even multipoles, positive non-nominallities affect the righth side and negative non-nominallities affect the left side (see Figure 4.8). Values are expressed in units of 10^{-4} .

Multipole	Polar shim		Midplane insulation		Coil squeeze	
	Inner	Outer	Inner	Outer	Inner	Outer
C_1	5.71	3.79	-2.88	-2.00	-6.56	-4.78
b_3	2.21	1.60	-3.68	-1.38	1.05	0.35
b_5	-0.39	-0.076	-1.10	-0.198	-0.043	0.084
b_7	0.155	-0.0217	-0.30	-0.017	0.043	-0.016
b_9	-0.055	0.0025	-0.083	-0.0026	0.011	-0.0010
b_{11}	0.0078	0.0000	-0.027	-0.0004	-0.012	0.0010
b_2	6.52	3.79	-4.57	-2.31	-1.90	-1.11
b_4	-0.37	0.28	-2.14	-0.58	0.74	0.32
b_6	0.108	-0.070	-0.56	-0.058	-0.13	-0.0090
b_8	-0.0012	-0.0004	-0.16	-0.0059	0.076	-0.0060
b_{10}	-0.0196	0.0012	-0.044	-0.0012	-0.023	0
b_{12}	0.0059	0.0000	-0.018	-0.0002	0	0

Reported sensitivity data have been computed by magnetic simulations performed for non-nominallities of 0.1 mm, since for small deformations multipole variations can be considered linearly dependent on the difference from the nominal dimensions (see for instance [31]). A non-nominallity of δ [mm] gives a magnetic effect $\delta(b_n)$ on the multipole b_n which can be computed from the coefficients $C(b_n)$ of Table 4.2 and Table 4.3 according to:

$$\delta(b_n) = C(b_n) \frac{\delta}{0.1}. \quad (4.30)$$

Values reported in Table 4.2 corresponding to the polar shim insertion sensitivity data (2nd and 3rd columns) can be used to normalize magnetic measurements at room temperature to nominal shims. It is then possible to compare magnetic measurements performed on collared coils manufactured by the three different firms using non-nominal polar shims with the other consistent available data. Moreover, any deviation from the expected multipolar content pointed out by such comparison can be analyzed in terms of manufacturing errors using computed sensitivity data..

Table 4.3 Computed odd and even skew multipoles sensitivity to the three following manufacturing errors: non-nominal shim insertion in the coil polar region; non-nominal azimuthal coil size; non-nominal coil radial dimension. They have been computed for non-nominality of 0.1 mm according to the orthogonal families of coil deformations. For even multipoles, positive non-nominalities affect the upper part and negative non-nominalities affect the lower part (see Figure 4.8). For odd multipoles, positive non-nominalities affect the upper-right and lower-left parts, and negative non-nominalities affect the lower-right and upper-left parts (see Figure 4.8). Values are expressed in units of 10^{-4} .

Multipole	Polar shim		Azimutal coil dimension		Coil squeeze	
	Inner	Outer	Inner	Outer	Inner	Outer
a_1	12.79	11.05	7.34	6.00	-12.38	-3.32
a_3	-0.52	0.298	2.34	1.02	-4.81	1.13
a_5	0.254	-0.186	0.28	0.035	-0.24	-0.030
a_7	-0.0200	0.018	0.066	0.0048	-0.12	0
a_9	-0.0070	0.0039	0.0178	0.0017	-0.011	-0.0015
a_{11}	0.0239	-0.0002	0.0115	0.0002	-0.0070	0
a_2	4.89	4.17	5.28	3.14	-11.20	-2.74
a_4	-0.61	-0.386	0.80	0.229	-1.18	-0.28
a_6	0.267	-0.022	0.13	0.0067	-0.16	0.0037
a_8	-0.087	0.0124	0.032	0.0034	-0.045	-0.0020
a_{10}	0.037	0.0005	0.014	0.0006	-0.0070	0
a_{12}	0.0057	0.0001	0.0078	0.0000	-0.0040	0

Chapter 5

A tool to monitor collared coil industrial series production

Magnetic measurements reflect the inner structure of the collared coil assemblies. In order to monitor production homogeneity, measured data have been statistically analyzed. Control bounds have been derived on the basis of available measurements to detect deviations in the multipolar content featured by new collared coils and a field quality monitoring tool has been implemented in a macro embedded into the template used for magnetic measurement at room temperature.

5.1 Statistical analysis of magnetic measurements at room temperature

LHC beam dynamics imposes a set of tolerances on multipoles featured by the whole accelerator machine. They are given in terms of averages and standard deviations of the multipoles of all the magnets which compose the accelerating ring. [12] But having been defined for a set of magnets, beam dynamics constraints cannot be imposed to multipoles featured by a single magnet. Furthermore such constraints would be too loose to detect production drifts or manufacturing errors. Instead, since magnetic measurements at room temperature are an economic and fast way to figure out the harmonics which characterize the magnetic performance of a magnet and since multipoles are a reflection of the magnet geometry, then the magnetic measurements at room temperature can be analyzed to monitor magnet production. A large departure of a collared coil from the multipolar content usually encountered during production may indicate, in fact, an unacceptable component or assembly of that particular magnet. [16], [19]

In September 2000, the industrial pre-series production of the LHC dipole magnets has started and magnetic measurements at room temperature have been performed on each manufactured collared coil. From available data (around 20 measurements), the expected multipolar structure of a collared coil can be computed in terms of mean value and standard deviation of the previous production. In this way, a comparison between the field quality featured by a single magnet with what measured in the previous production is possible and the homogeneity of production and its reproducibility can be monitored to point out deviations due to trend in the manufacturing processes. In the following sections, the statistical approach used to analyze available data is presented and constraints to assure the homogeneity of the industrial production of the LHC dipole magnet after the collared coil stage of assembly are derived. The same approach will be used in the future to derive a monitoring tool for the cold mass assembly (for which pre-series data are too few at the moment this work is being written).

Table 5.1 Available data of magnetic measurements used for statistical analysis of the field quality featured by collared coils. *HCMBB_A001*- is the component name; two digits refer to the manufacturer (01- Firm1, 02- Firm2; 03- Firm3), and 000001 is the collared coil serial number for each firm.

Firm1	Firm2	Firm3
HCMBB_A001-01000001	HCMBB_A001-02000001	HCMBB_A001-03000001
HCMBB_A001-01000002	HCMBB_A001-02000002	HCMBB_A001-03000002
HCMBB_A001-01000003	HCMBB_A001-02000003	HCMBB_A001-03000003
HCMBB_A001-01000004	HCMBB_A001-02000004	HCMBB_A001-03000004
HCMBB_A001-01000005	HCMBB_A001-02000005	HCMBB_A001-03000005
HCMBB_A001-01000006	HCMBB_A001-02000008	HCMBB_A001-03000006
HCMBB_A001-01000007		HCMBB_A001-03000007
HCMBB_A001-01000008		HCMBB_A001-03000008
HCMBB_A001-01000009		HCMBB_A001-03000009
HCMBB_A001-01000010		
HCMBB_A001-01000011		
HCMBB_A001-01000012		

5.1.1 Available data

Magnetic measurements at room temperature have been performed on each collared coil manufactured by one of the three firms in charge of the dipole production for the pre-series. Table 5.1 shows the set of measurements available for statistical analysis. Each measurement has been reported in a data sheet (like the one in Figure 4.4) and it is referred to by the name of the corresponding collared coil. The collared coil sub-assembly is referred to with the acronym *HCMBB_A001-00000000*. The first two digits refer to the firm number while the remaining ones to the progressive number of the magnet. As an example:

- *HCMBB_A001-01000001*: first (000001) collared coil (*HCMBB_A001*) produced at Firm1 (01);
- *HCMBB_A001-02000003*: third (000003) collared coil (*HCMBB_A001*) produced at Firm2 (02);
- *HCMBB_A001-03000002*: second (000002) collared coil (*HCMBB_A001*)

produced at Firm3 (03).

The above naming convention is used to refer to measurements. But herein after we will refer to each collared coil with the manufacturer number, its serial number and the aperture number (Firm1 1-1 and 1-2, Firm2 3-1 and 3-2 and Firm3 2-1 and 2-2, respectively for the given examples).

5.1.2 Measurement data subdivision

For each collared coil, magnetic measurements for each aperture are available. A statistical analysis have been carried on single-value parameters which characterize each aperture (the magnetic length M_L and the coil waviness) and on the parameters measured on 20 positions along each aperture axis (see Section 4.1.2). Measurement data have been subdivided for analysis purposes. In fact, not all of the data are homogenous because the coil straight section extends from position 2 to position 19, while positions 1 and 20 are in the coil short heads. Straight part positions have been analyzed by separating aperture average (1 value for each aperture) and local variations from the aperture straight part average (18 values for each aperture), which then form two separate set of data.

Heads feature multipole values different from those of the straight part, and they have been analyzed separately. Since measurements in the CS are different from those in

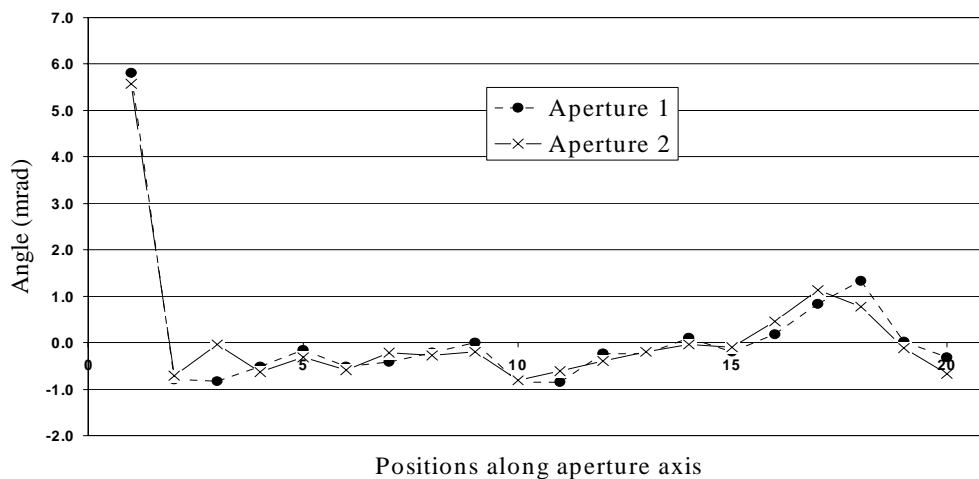


Figure 5.1 Plot of main field direction along the Firm3-3 collared coil. At CS the value is completely different from that of NCS and it can be used to distinguish CS from NCS.

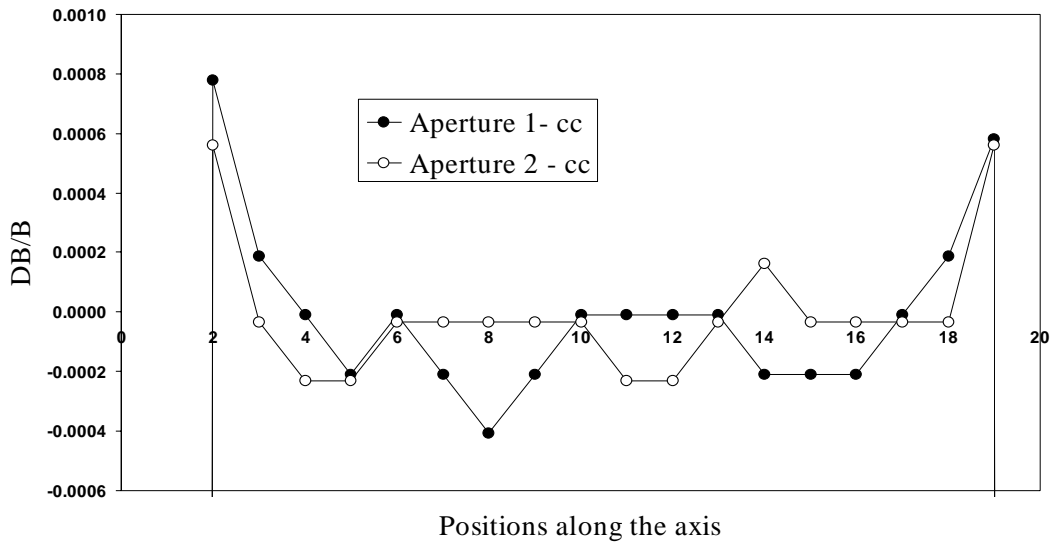


Figure 5.2 Main field relative module along Firm3-3 collared coil (cc). Measuring positions 2 and 19 feature non-homogenous values with respect to the positions 3 to 18. CS and NCS values are out of scale.

NCS (see Section 3.2.2 for naming convention, see [34] for references), also data taken in the coil heads have been separated. In fact, the CS multipoles are affected by the non symmetrical structure of its cross-section, which is different from that of NCS. In Figure 5.1, the main field direction has been plotted for all the measuring positions, and it can be seen that the CS features a main field value different from that of NCS. Such difference is due to the presence of dipole connections and of the layer-jump and it provides a fast and reliable way to check the sign of odd skew multipoles and to distinguish CS from NCS measurement data.

Another important feature is that C_I values at measurement positions 2 and 19 are around $5 \cdot 10^{-4}$ higher than the values in the straight part positions (see Figure 5.2). This main field increase is due to the presence of magnet heads. Therefore, position 2 and 19 have been then separately analyzed for what concerns this parameter. Since the C_I values encountered at these measuring positions do not appear when the corresponding cold mass is measured, they can be used as a reference to distinguish collared coil measurements from those performed on a cold mass (see Figure 5.2). Finally, the measurement of the magnetic axis position (D_x and D_y) has not been taken into consideration for the analysis. Table 5.2 shows the available statistics which we have considered sufficient to compute acceptance criteria for all measured quantities and Table 5.3 shows the whole

statistics which will be available at the end of the LHC dipole magnet industrial series production.

Table 5.2 Number of data available at present from the magnetic measurement at room temperature performed on collared coils. Data are subdivided as they have been statistically analyzed.

Collared coils	27			
Apertures	54			
Magnetic length	54			
Coil waviness	54			
	CS	NSC	Positions 2 to 19	
Multipole b_n or a_n	54	54	972	
	CS	NCS	Positions 2 and 19	Positions 3 to 18
Main component C_I	54	54	108	864

Table 5.3 Number of data available at the end of industrial series production from the magnetic measurement at room temperature performed on collared coils. Data are subdivided as those used for statistical analysis.

Collared coils	1232			
Apertures	2464			
Magnetic length	2464			
Coil waviness	2464			
	CS	NSC	Positions 2 to 19	
Multipole b_n or a_n	2464	2464	44352	
	CS	NCS	Positions 2 and 19	Positions 3 to 18
Main component C_I	2464	2464	4928	39424

5.1.3 Normality test and considerations on variability among the manufacturers

Available data of Table 5.1 have been subdivided according to the criteria described in Section 5.1.2 and they have been statistically analyzed. In order to settle proper constraints on the magnetic measurements performed on the collared coils, it is necessary

to assess if data belong to a normal distribution. It is not the aim of this work to introduce the statistical analysis and only some hints will be given in the text. In Appendix E some basic statistical notions applied during this work are introduced, but the reader can address himself to [21], [35], [36] and [37] for further reading.

A normality test has been used in order to assess if measurement data can be considered as following a Gaussian distribution. The test has been performed on multipole data measured along the straight section of the collared coils. By mean of the normality test, furthermore, some collared coil measurements have been found to be not consistent with the main part of magnetic measurements. This was due either to problems related to the use of two different measuring systems or to collared coils that did not feature a careful control of the coil geometry (see Chapter 6). Some measurements, then, have been discarded from the analysis.

Table 5.4 lists measurement data used in the statistical analysis. A $\tilde{\chi}^2$ -normality test has been carried on these data (see Section D.1). Such test can compute the confidence level at which the hypothesis that the sample is consistent with a normal distribution can be rejected for a given data sample. This means that if the computed confidence level is

Table 5.4 Data of magnetic measurements effectively used for statistical analysis of the field quality featured by collared coils. Some measurements have been discarded because they were affected by anomalous variation of data, mainly due to the manufacturing process not yet stabilized. A.1 and A.2 stay for aperture 1 and 2 respectively.

Firm1	Firm2	Firm3
HCMBB_A001-01000001	HCMBB_A001-02000001-A.2	HCMBB_A001-03000001
HCMBB_A001-01000002-A.2	HCMBB_A001-02000002-A.2	HCMBB_A001-03000003-A.1
HCMBB_A001-01000003-A.1	HCMBB_A001-02000003	HCMBB_A001-03000004
HCMBB_A001-01000004-A.1	HCMBB_A001-02000004	HCMBB_A001-03000005
HCMBB_A001-01000007	HCMBB_A001-02000005	HCMBB_A001-03000006-A.2
HCMBB_A001-01000009-A.1	HCMBB_A001-02000008-A.1	HCMBB_A001-03000007
HCMBB_A001-01000010		HCMBB_A001-03000008
HCMBB_A001-01000011-A.2		

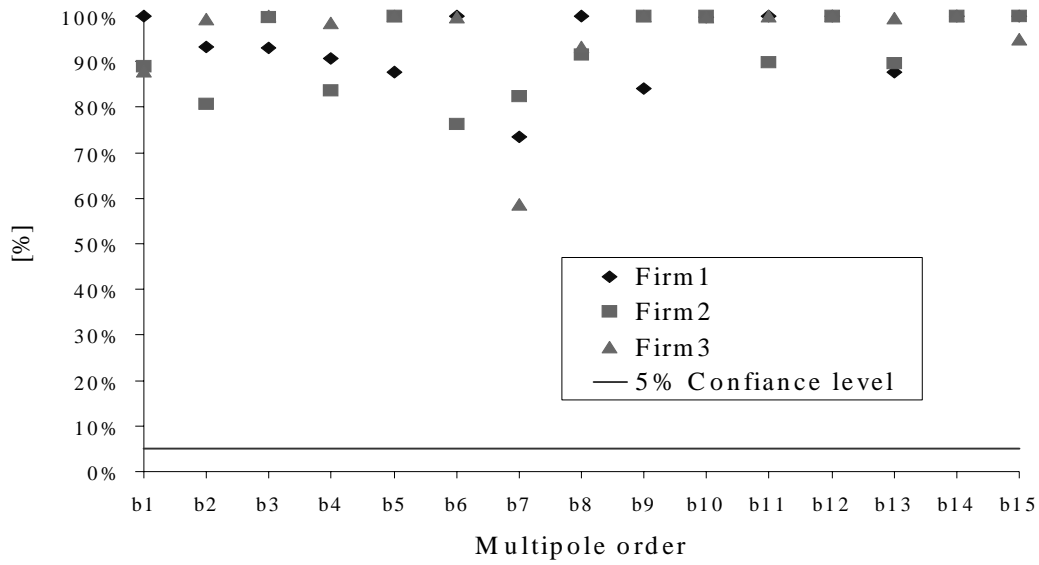


Figure 5.3 Computed confidence level for the normality test carried on normal multipoles measured at the straight part positions of considered measurements. All values in [%].

bigger than that assumed to be significant (usually 5%), the sample cannot be said not to be taken from a normal distribution. Test results are reported for normal multipoles and for skew multipoles featured by collared coils listed in Table 5.4 in Appendix D. Figure 5.3 and Figure 5.4 shows the computed and the chosen confidence level at which the normality hypothesis can be rejected for normal and skew multipoles. From both fig-

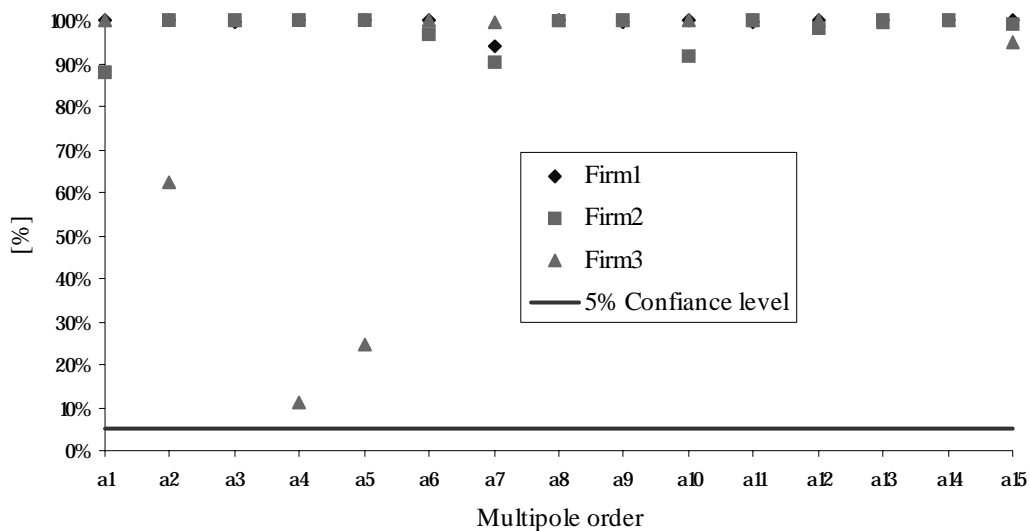


Figure 5.4 Computed confidence level for the normality test carried on skew multipoles measured at the straight part positions of considered measurements. All values in [%].

ures, it can be derived that the hypotesys that tested data are taken from a normal distribution cannot be rejected at the confiance level of 5%. This means that sample data can be described by a Gaussian distribution, i.e. that the occurrence frequencies of multipoles in the magnetic measurements of collared coils have comparable values of those arising if data were taken from ideal normal distributions with the mean and standard deviation values of samples. In fact, if the following relation is fulfilled:

$$P(\tilde{\chi}^2 > \tilde{\chi}_0^2) > 5\% , \tag{5.1}$$

data belong to a probability distribution compatible with the Gaussian one.

As it can be seen from Figure 5.5 for the case of Firm3-3 a_4 for which the computed confiance level is 11%, the $\tilde{\chi}^2$ -test is particularly sensitive to the presence of outliers in the tails, i.e. the distribution regions far from the average, which are rather critical in the monitoring of an industrial production. Tails, in fact, are rather difficult to be taken into consideration during a statistical analysis for quality control purposes, because even

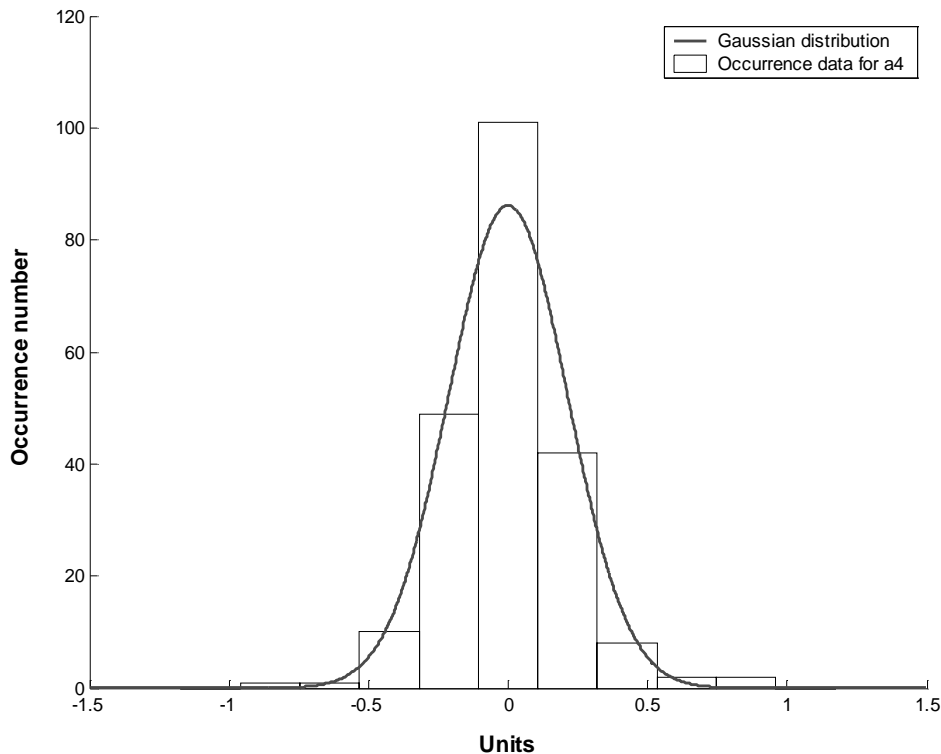


Figure 5.5 The histogram of skew multipole a_4 of collared coils manufactured at Firm3 differs from the computed Gaussian distribution mainly for the presence of outliers in tails.

if they may contain many elements of a large population, control bounds could simply cut them. We think that the chosen test is then more appropriate than others, like, for example, the Kolmogorov-Smirnov test, which analyze the cumulative probability more than the distribution tails.[37]

As already stated, the production of the LHC dipoles has been assigned to three different manufacturers. In order to assess the feasibility of applying common process bounds to multipoles featured by magnets assembled by different firms, a test ANOVA (ANalysis Of VAriance) has been carried on available data. The test did not give significant results, and it has been chosen to separate the statistical analysis of data coming from measurements carried on collared coils manufactured at different firms. The test will be redone when the available statistics is larger.

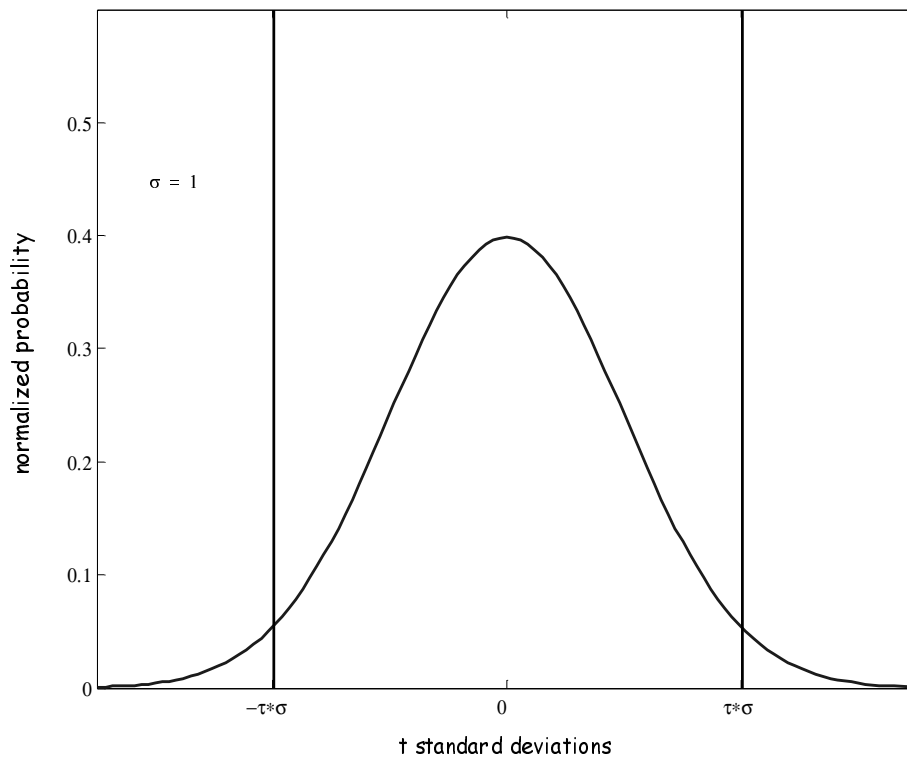
5.1.4 Control bounds and test choice

We have shown that magnetic measurements at room temperature performed on collared coils feature values that can be considered to follow a Gaussian distribution. Average and standard deviation values can be computed out of available samples to derive control bounds for the industrial production. Since a normal distribution is a probability distribution, limits can be chosen to hedge magnetic measurement data that will occur during the whole production. An automatic tool can be implemented in order to clearly mark out deviations of the production from the expected trend and to monitor collared coil production homogeneity. Table 5.5 shows the probability for a measurement x taken from a sample following a normal distribution to occur in an interval given by a multiple of the sample standard deviation ($-t\sigma < x < t\sigma$), as it is shown in Figure 5.6. Last column in Table 5.5 shows the dimension of the sample N for which one value of the sample falls outside the interval $[-\tau\sigma, +\tau\sigma]$. This means that if we have, e.g., a population of 20000

Table 5.5 Occurrence probabilities according to Figure 5.6 for bounds given in terms of standard deviation of a normal distribution. Each occurrence percentual probability corresponds to a statistical non-occurrence expressed in the third column.

t	% probability for $-\tau\sigma < x < \tau\sigma$	1 value outside $[-\tau\sigma, +\tau\sigma]$ over:
1	68.27	3
2	95.45	22
3	99.73	370
3.5	99.95	2000
4	99.994	16666
4.5	99.9993	142857
5	99.99994	1666666

data belonging to a normal distribution with average $\langle x \rangle$ and standard deviation σ and we assign the interval $[\langle x \rangle - 3.5\sigma, \langle x \rangle + 3.5\sigma]$ as control bound, then from Table 5.5 is derived that 10 data belonging to the population will be discarded simply because tails have not been taken properly into account. Tails, in fact, are the extreme regions of the considered distribution for which the occurrence probability is very low (e.g. one each 10^6). But



if the sample is large (e.g. 10^6), then some element in the sample will have a value in the tails (e.g. at least one). Therefore, control bounds based on sample average and standard deviation values have to be decided according to the size of the population of the parameter to be monitored which is settled when tests to be performed on measurement data have been designed. To monitor collared coils homogeneity measured parameters have been compared to the previous production by mean of the following tests:

- on the magnetic length of the aperture: measured value;
- on the main component module: average in the straight section, local variations with respect to the straight section average separately for CS, NCS, measurement positions 2 and 19 and measurement positions 3 to 18;
- on the main component direction: local variations with respect to the straight section average separately for CS, NCS and measurement position 2 to 19 and field parallelism between the two aperture;
- on multipoles: average in the straight section, local variations with respect to the straight section average separately for CS, NCS and measurement positions 2 to 19;
- on coil waviness: measured value.

Table 5.3 reports the population size of measured parameters at the end of the LHC dipole production. Control bounds can be decided with the help of Table 5.5 according to the parameter population size for each test. It has been decided to implement two levels of control bounds:

- *yellow alarm level*: the control bounds are directly derived from a statistical approach and are meant to point out each non-nominality affecting the assembly;
- *red alarm level*: control bounds are computed doubling the yellow alarm level control bounds and are meant to point out only very large multipolar deviations.

5.1.4.1 Control bounds for straight part averages

At the end of the LHC dipole production there will be 1232 dipoles. Each dipole is made of two magnetic apertures and there will be 2464 magnetic measurements. For each aperture the straight part average is computed for:

- C_I : values from position 3 to position 18 are averaged;
- b_n and a_n for $n = 2,3,\dots,15$: values from position 2 to position 19 are averaged;

The population for these measurement parameters will be made at the end of industrial production of 2464 elements. From Table 5.5, it can be derived that if control bounds are defined in terms of rms σ and average $\langle x \rangle$ by the interval $[\langle x \rangle - 3.5\sigma, \langle x \rangle + 3.5\sigma]$, then at the end of production one data is outside the control bounds. Then, a larger interval (e.g. $\pm 4\sigma$) would not be good for the quality analysis, while an interval too little (e.g. $\pm 3\sigma$) would be too much preservative and the analysis would be too much *alarmist*. Then the interval $[\langle x \rangle - 3.5\sigma, \langle x \rangle + 3.5\sigma]$ can be assigned as yellow bounds and the interval $[\langle x \rangle - 7\sigma, \langle x \rangle + 7\sigma]$ as red bounds. In Table 5.6 average and standard deviation values applied to compute control bounds are reported for the three firms and for C_I and b_n . Standard deviation values applied are the same for the three firms because for the pre-series it has been decided to apply the largest σ encountered among measurements coming from different manufacturer. For the computation of allowed normal multipoles and C_I , measurement data have been reduced to nominal polar shims according to the sensitivity table given in Table 4.2 applying equation (4.30). In Table 5.7

Table 5.6 Average and standard deviation values applied to set control bounds on the main component C_I and normal multipoles. C_I is given in mT/kA, while multipoles are reported in units.

Parameter	Straight part average			Standard deviation
	Firm1	Firm2	Firm3	
C_I/i [mT/kA]	595.85	595.85	595.85	0.36
b_2	0	0	0	0.64
b_3	0	0	0	2
b_4	0	0	0	0.14
b_5	1.34	1.43	0.74	0.5
b_6	0	0	0	0.054

Table 5.6 Average and standard deviation values applied to set control bounds on the main component C_1 and normal multipoles. C_1 is given in mT/kA, while multipoles are reported in units.

Parameter	Straight part average			Standard deviation
	Firm1	Firm2	Firm3	
b_7	0.73	0.54	0.7	0.09
b_8	0	0	0	0.02
b_9	0.33	0.28	0.26	0.03
b_{10}	0	0	0	0.0045
b_{11}	0.74	0.74	0.74	0.0110
b_{12}	0	0	0	0.0018
b_{13}	0.085	0.085	0.085	0.0083
b_{14}	0	0	0	0.006
b_{15}	0.034	0.043	0.032	0.007

Table 5.7 Average and standard deviation values applied to set control bounds on skew multipoles a_n given in units.

Parameter	Straight part average			Standard deviation
	Firm1	Firm2	Firm3	
a_2	0	0	0	1
a_3	-0.1	-0.5	0.1	0.35
a_4	0	0	0	0.27
a_5	0	0	0	0.14
a_6	0	0	0	0.12
a_7	0	0.04	0	0.03
a_8	-0.02	-0.02	-0.02	0.035
a_9	0.01	0.03	0.01	0.03
a_{10}	0.002	0.002	0.002	0.003
a_{11}	0.01	0.04	0	0.03
a_{12}	0	0	0	0.005
a_{13}	0	0	0	0.004
a_{14}	-0.012	-0.012	-0.012	0.006
a_{15}	0	0.006	0	0.005

average and standard deviation values used to set control bounds are reported for the three firms and skew multipoles a_n . No control bounds have been set neither for the multipole a_1 average value (because it is proportional to the main field direction), nor for b_1 (which is 10000 by definition, see Section 5.1.4.4).

5.1.4.2 Control bounds for variations along the straight part

All measurement positions in the straight part of the collared coils have been treated as being part of a same sample. The local variations of measured values with respect to the computed average are monitored for the following parameters:

- C_1 : the local relative variations $(\frac{\delta C_1}{\langle C_1 \rangle})$ are computed for positions 3 to 18;
- C_1 direction: local absolute variations with respect to the aperture average are computed for positions 2 to 19;
- Multipoles b_n and a_n for $n = 2, 3, \dots, 15$: local absolute variations with respect to the averages are computed from position 2 to position 19 for each multipoles.

For these parameters each collared coil magnetic measurements contains 16 (for C_1) or 18 data. The population at the end of industrial production will be made of 39424 or 44352 respectively. If the interval $[-4\sigma, +4\sigma]$ is assigned as the yellow bound, at the end of the production 2 or 3 measured values will be out of the yellow acceptance range, as it can be computed from Table 5.5. The red alarm is set at $[-8\sigma, +8\sigma]$. In Table 5.8 the

Table 5.8 Standard deviation values applied to all manufactured coils to compute control bounds to monitor local variations with respect to the aperture average. Values are given in units for multipoles, in mT/kA for C_1 and in mrad for C_1 direction.

Parameter	Standard deviation	Parameter	Standard deviation
C_1/i [mT/kA]	1.5	C_1 direction (mrad)	0.5
b_2	0.6	a_2	1.1
b_3	0.6	a_3	0.35
b_4	0.16	a_4	0.27
b_5	0.16	a_5	0.12
b_6	0.07	a_6	0.068

Table 5.8 Standard deviation values applied to all manufactured coils to compute control bounds to monitor local variations with respect to the aperture average. Values are given in units for multipoles, in mT/kA for C_1 and in mrad for C_1 direction.

Parameter	Standard deviation	Parameter	Standard deviation
b_7	0.054	a_7	0.056
b_8	0.034	a_8	0.025
b_9	0.02	a_9	0.021
b_{10}	0.04	a_{10}	0.034
b_{11}	0.0059	a_{11}	0.009
b_{12}	0.0061	a_{12}	0.0056
b_{13}	0.0025	a_{13}	0.0022
b_{14}	0.0034	a_{14}	0.003
b_{15}	0.0027	a_{15}	0.003

standard deviation values applied for all the three firms to compute control bounds are reported for C_1 , C_1 direction, b_n and a_n . The computed sigma have been plotted in logarithmic scale in order to evaluate the corresponding coil waviness (see Section 4.1.2). As it can be seen from Figure 5.7, the estimated coil waviness is about 25 μm which corresponds to the manufacturing tolerances. This proves that the measured field quality variations are in agreement with geometrical tolerances; this is a powerful tool to control

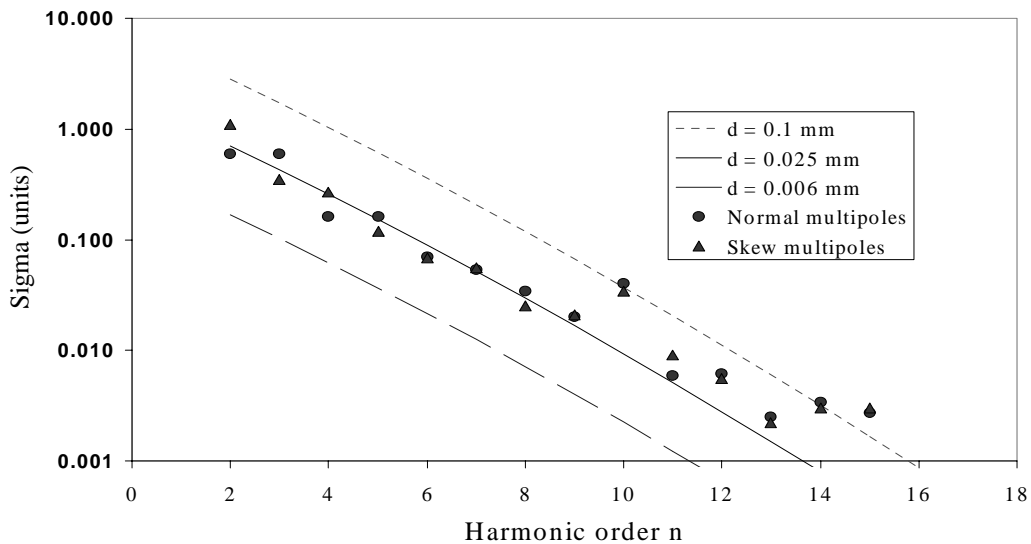


Figure 5.7 Coil waviness logarithmic plot corresponding to standard deviation values computed as control bounds of inner local multipolar variations from the straight part average.

actual tolerances in manufactured collared coils. Values at $n=10$ and $n=14$ and 15 are not on the same trendline because these multipoles are used for local feed-down (b_{10}) or because the measurement system is at its precision limit (b_{14} and b_{15}). This analysis shows that the measurement sensitivity is of the order of a few 10^{-3} units.

5.1.4.3 Control bounds for CS, NCS and C_1 in position 3 and 19

Measurement positions 1 (CS) and 20 (NCS) are in the short head regions where multipoles feature values that are totally different from those of the straight part. Positions 3 and 19 feature different values from the straight part only for C_1 . Control bounds for local variations have been so implemented for the following parameters:

- C_1 : local relative variations ($\delta C_1 / C_1$) with respect to the straight part average are monitored separately for CS, NCS and for position 2 and 19 considered as a unique sample;
- C_1 direction: local absolute variations from aperture average are computed separately for CS and NCS;
- Multipoles b_n and a_n for $n = 2,3,\dots,15$: absolute CS and NCS values are separately monitored

For these parameters each collared coil magnetic measurements contains 2 (for C_1 in position 2 and 19) or 1 data (for CS and NCS). The population at the end of industrial production will be made of 4928 or 2464 data respectively. If the mean value of each parameter is $\langle x \rangle$, the interval $[\langle x \rangle - 3.5\sigma, \langle x \rangle + 3.5\sigma]$ can be assigned as yellow bounds and the interval $[\langle x \rangle - 7\sigma, \langle x \rangle + 7\sigma]$ as red bounds, as it can be computed from Table 5.5. In Table 5.9, Table 5.10 and Table 5.11 the average and standard deviation values applied for all the three firms to compute control bounds of all the designed tests are reported respectively for CS, NCS and for measurement positions 2 and 19.

Table 5.9 Average and standard deviation values used to compute control bounds for the CS and for the three manufacturer.

Parameter	Firm1	Firm2	Firm3	Standard Deviation
C_1 (units)	-3850	-3850	-3850	151

Table 5.9 Average and standard deviation values used to compute control bounds for the CS and for the three manufacturer.

Parameter	Firm1	Firm2	Firm3	Standard Deviation
b_2	0	0	0	5
b_3	40	24	34	4.6
b_4	0	0	0	0.9
b_5	-2.4	-5.6	-4.4	1.3
b_6	0	0	0	0.34
b_7	2.6	1.6	2.5	0.3
b_8	0	0	0	0.1
b_9	0.26	0.15	0.3	0.05
b_{10}	0	0	0	0.1
b_{11}	0.61	0.55	0.6	0.03
b_{12}	0	0	0	0.015
b_{13}	0.09	0.08	0.11	0.01
b_{14}	0	0	0	0.006
b_{15}	-0.002	-0.005	-0.008	0.006
C_1 direction (mrad)	5	5	5	2
a_2	0	0	0	6
a_3	-1.7	-1.7	-1.7	2.1
a_4	-0.8	2	0.8	1.6
a_5	2.4	2.4	2.4	0.83
a_6	0	0	0	0.4
a_7	1.9	1.9	1.9	0.25
a_8	0	0	0	0.12
a_9	-0.11	-0.24	-0.23	0.05
a_{10}	0	0	0	0.085
a_{11}	0.2	0.2	0.2	0.025
a_{12}	0	0	0	0.015
a_{13}	0	0	0	0.01
a_{14}	0	0	0	0.006
a_{15}	0	0	0	0.01

Table 5.10 Average and standard deviation values used to compute control bounds for the NCS and for the three manufacturer.

Parameter	Firm1	Firm2	Firm3	Standard Deviation
C_1 (units)	-3650	-3650	-3650	284
b_2	0	0	0	2
b_3	-3.5	-6.6	2.4	2.5
b_4	0	0	0	0.38
b_5	-3	-3	-3	0.7
b_6	0	0	0	0.1
b_7	0.6	-0.05	0.4	0.2
b_8	0	0	0	0.05
b_9	0.23	0.23	0.23	0.06
b_{10}	0	0	0	0.075
b_{11}	0.65	0.65	0.65	0.018
b_{12}	0	0	0	0.01
b_{13}	0.059	0.059	0.059	0.009
b_{14}	0	0	0	0.0035
b_{15}	0.013	0.024	0.013	0.0068
C_1 direction (mrad)	-0.4	-0.4	-0.4	1
a_2	0	0	0	3
a_3	1.35	-0.1	1	0.7
a_4	0	0	0	0.7
a_5	-0.2	-0.2	-0.2	0.25
a_6	0	0	0	0.17
a_7	-0.01	0.11	-0.003	0.077
a_8	0	0	0	0.06
a_9	0	0	0	0.024
a_{10}	0	0	0	0.045
a_{11}	0	0	0	0.026
a_{12}	0	0	0	0.006
a_{13}	0	0	0	0.0037

Table 5.10 Average and standard deviation values used to compute control bounds for the NCS and for the three manufacturer.

Parameter	Firm1	Firm2	Firm3	Standard Deviation
a_{14}	-0.003	-0.003	-0.003	0.004
a_{15}	0	0	0	0.006

Table 5.11 Average and standard deviation values used to compute control bounds for the C_1 local variation in measurement positions 2 and 19 and for the three manufacturer.

Parameter	Firm1	Firm2	Firm3	Standard Deviation
C_1 (units)	8.2	8.2	8.2	2

5.1.4.4 Control bounds for magnetic length, coil waviness and field parallelism between coil apertures

Control bounds have been computed for the magnetic length and the field parallelism between the coil apertures. The field parallelism is computed as the difference between the averages of the main field direction in both aperture. It gives indication about the divergence between the direction of the main field in one aperture with respect to the direction of the main field in the other. Even if the collared coil is twisted along its axis, the main field in one aperture must be parallel to the main field in the other, otherwise a non-nominality is present. In fact, the main field direction in twin-apertures is determined by the coil layer positions, which are fixed by collar laminations and which cannot rotate in opposite directions if the coil has been properly assembled.

The population of these parameters at the end of industrial production will be made of 2464 elements for magnetic length and of 1232 elements for the field parallelism. If the mean value of each parameter is $\langle x \rangle$, the interval $[\langle x \rangle - 3.5\sigma, \langle x \rangle + 3.5\sigma]$ can be assigned as yellow bounds and the interval $[\langle x \rangle - 7\sigma, \langle x \rangle + 7\sigma]$ as red bounds, as it can be

Table 5.12 Average and standard deviation values for all the manufacturers used to compute control bounds for the magnetic length (given in [mm]) and field parallelism (given in [mrad]).

Parameter	Average	Standard deviation
Magnetic length (mm)	14450	10

Table 5.12 Average and standard deviation values for all the manufacturers used to compute control bounds for the magnetic length (given in [mm]) and field parallelism (given in [mrad]).

Parameter	Average	Standard deviation
Field parallelism (mrad)	0	0.32

computed from Table 5.5. In Table 5.12, the average and standard deviation values applied for all the three firms to compute control bounds for magnetic length and field parallelism are reported.

Control bounds have been computed with a different approach for the coil waviness, defined in Section 4.1.2. The yellow alarm level has been put to 30 μm and the red alarm level to 60 μm . This is directly correlated to the manufacturing tolerances. If a collared coil aperture features a coil waviness value of 30 μm , it means that it has been manufactured with the larger accepted tolerances. Its multipolar structure corresponds to that of a collared coil with geometrical dimensions which feature variations along the axis with a standard deviation value equal to that of coil waviness.

5.2 A macro to monitor the homogeneity of industrial production

Computed control bounds have been implemented into a software which can perform the presented tests directly on the magnetic measurements at the manufacturer, speeding up the field quality analysis. Magnetic measurement performed on a collared coil are loaded in a file that contains the monitoring macro (see Appendix E for the code), the measurement data and other worksheets.

5.2.1 Layout

The measurement file containing the macro implemented is made of several worksheets. An *Original data* worksheet contains all raw measurement data which are reported in the *Summary data* worksheet. After all the tests have been performed, the cells in *Summary data* containing parameters outside the control bounds range are colored in red or yellow. The *Alarm sheet* summarizes the test results by mean of cells colored in green if tested values agree with control bounds, in yellow or red if the tested values are out of the corresponding control bounds. The worksheet contains a table of alarms for each aperture of the collared coil as it is shown in Figure 5.8.

	Aperture 1			
Magnetic length	status ok			
	Average straight positions 2 to 19	Variation straight positions 2 to 19	Heads CS position 1	Heads NCS position 20
Main field Angle	status ok	status ok	status ok	status ok
b2	status ok	status ok	status ok	status ok
b3	status ok	yellow alarm	status ok	status ok
b4	status ok	yellow alarm	status ok	status ok
b5	status ok	status ok	status ok	status ok
b6	status ok	status ok	status ok	status ok
b7	status ok	yellow alarm	status ok	status ok
b8	status ok	status ok	status ok	status ok
b9	status ok	yellow alarm	status ok	status ok
b10	status ok	status ok	status ok	status ok
b11	status ok	status ok	status ok	status ok

Figure 5.8 Part of the *Alarm sheet* summary table of results. There is a summary table for tests performed on each collared coil. If a parameter is out of the control bounds range, a corresponding cell is colored in yellow or red according to deviation severity.

	Mean	Sigma	Ybound	Rbound
Magnetic Length (mm)	14.45	0.01	3.5	7
dB/B Heads CS+NCS (units)	-3.75E+03	130	3.5	7
	Mean Value (3:18) (mT/kA)			
	Mean	Sigma	Ybound	Rbound
Main Field Component	595.85	0.36	4	8
	Mean Value (2:19)			
	Mean	Sigma	Ybound	Rbound
Delta Angle (mrad)	0	0	3.5	7
b2 (units)	0	0.64	3.5	7
b3 (units)	-4	2	3.5	7
b4 (units)	0	0.14	3.5	7
b5 (units)	0.04	0.5	3.5	7
b6 (units)	0	0.054	3.5	7
b7 (units)	1.03	0.09	3.5	7
b8 (units)	0	0.02	3.5	7
b9 (units)	0.53	0.03	3.5	7
b10 (units)	0	0.0045	3.5	7

Figure 5.9 Upper part of the Firm1 bounds sheet where mean and standard deviation values can be input, together with the control bounds in terms of standard deviation (e.g. 3.5 and 7 σ are the bounds in figure for a3)

The Assembly Data worksheet mainly contains data about shims applied to adjust the collared coil pre-stress which must be taken into consideration to perform the desired tests on the measurement data. In Worksheet, computations necessary to the macro are performed and multipoles are compensated for the eventual use of non-nominal shims. In order to localize the position in which multipoles deviate from what expected, cells are colored also here at the end of tests. Finally the last three sheets named Firm1 bounds, Firm2 bounds and Firm3 bounds contains the average and standard deviation values (see

	Inf. Y limit	Sup. Y limit	Inf. R limit	Sup. R limit
Magnetic Length (mm)	14.415	14.485	14.38	14.52
dB/B Heads CS+NCS (units)	-4205	-3295	-4660	-2840
	Mean Value (3:18) (mT/kA)			
	Inf. Y limit	Sup. Y limit	Inf. R limit	Sup. R limit
Main Field Component	594.41	597.29	592.97	598.73
	Mean Value (2:19)			
	Inf. Y limit	Sup. Y limit	Inf. R limit	Sup. R limit
Delta Angle (mrad)	0	0	0	0
b2 (units)	-2.24	2.24	-4.48	4.48
b3 (units)	-11	3	-18	10
b4 (units)	-0.49	0.49	-0.98	0.98
b5 (units)	-1.71	1.79	-3.46	3.54
b6 (units)	-0.189	0.189	-0.378	0.378
b7 (units)	0.715	1.345	0.4	1.66
b8 (units)	-0.07	0.07	-0.14	0.14
b9 (units)	0.425	0.635	0.32	0.74
b10 (units)	-0.01575	0.01575	-0.0315	0.0315

Figure 5.10 Part of the lower part of Firm1 bounds sheet in which inferior and superior control limits can be read for both the control levels.

Figure 5.9) to compute the control limits for each manufacturer for all the tests performed by the macro (see Figure 5.10). In this way control bounds can be updated according to the needs, e.g. for a new cross-section design.

5.2.2 Macro test procedure

The implemented macro for the magnetic measurement analysis follows a simple procedure. Before starting to perform the analysis on measurement data, the code performs worksheet formatting, it subtracts the non-nominal shims contribution from the measured allowed normal multipoles, it evaluates which cross section measurements are referred to and which macro version must be used. In fact two versions have been imple-

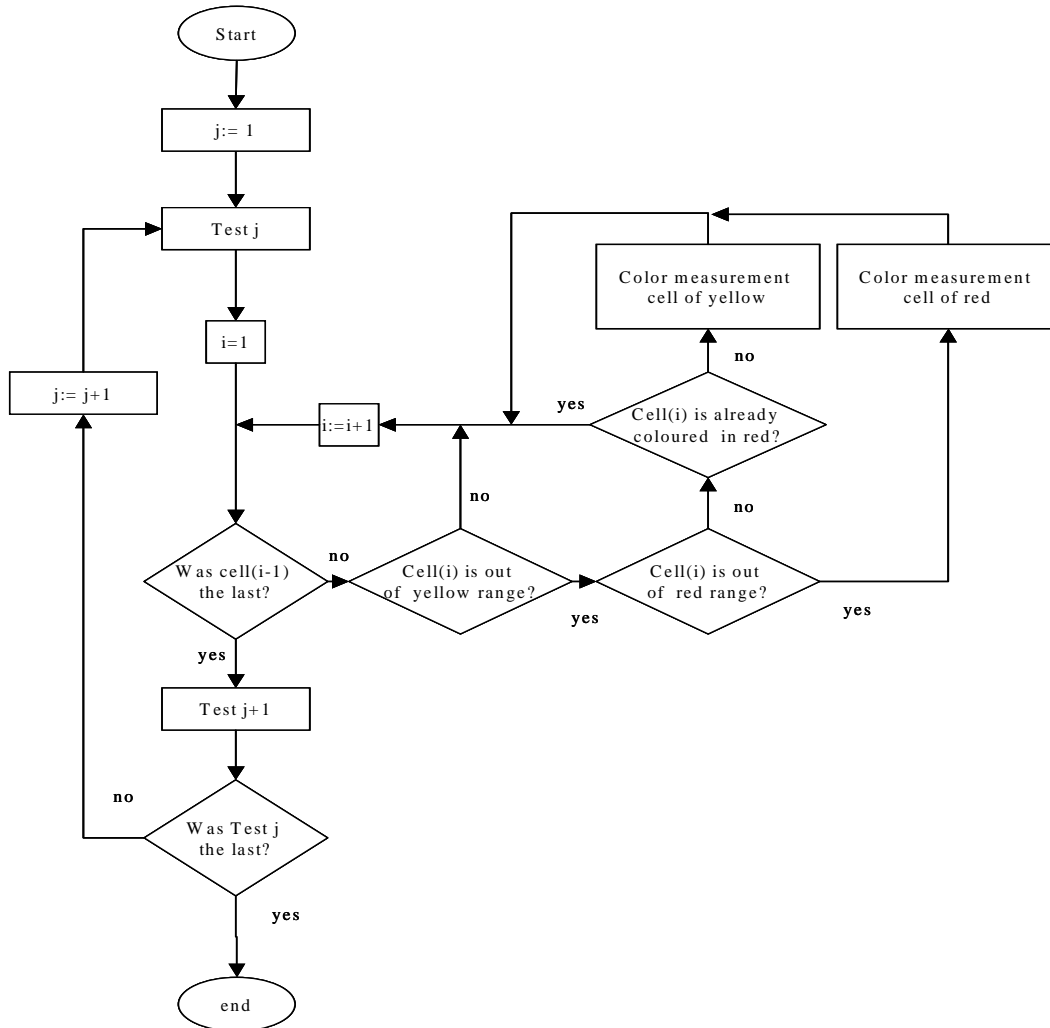


Figure 5.11 Sketch of the flow chart followed by the macro to perform each test and give the analysis results as colored cells.

mented: one to be used at CERN and one to be used at the manufacturer. The former performs test applying the two envisaged control bounds (yellow and red alarm bounds) while the latter compare the parameters with the red level control bounds only, in order to point out directly to the operators only those multipolar deviations for which a counteraction must be taken as soon as possible (e.g., the measurement must be repeated).

The macro performs designed tests according to the flow chart sketch shown in Figure 5.11. After each test, if a measured parameter is outside the corresponding control bounds, the cell containing it is colored in yellow or red. Finally it performs the last sheets formatting and visualize the *Alarm sheet* containing the analysis results.

5.2.3 Analysis results

Results for the test performed are given in *Alarm sheet* which is visualized at the end of a macro run (see Figure 5.8). In *Summary data* and *Worksheet* cells containing a value out of range are colored according to which level of control bounds has been overpassed (see Figure 5.12 and Figure 5.13). Therefore, deviations from the expected multipolar content are localized and they can be studied to trace back tooling degradation, assembly errors or use of faulty components which eventually affected that particular section of the collared coil.

a1	29.640	5.040	4.504	-7.510	-14.542
a2	-1900	-0.129	-0.421	-3.226	-4.362
a3	-5.396	-1.726	-1.921	-1.785	-0.919
a4	-0.956	-0.755	-1.566	-0.483	-0.200
a5	0.877	-0.358	-0.209	-0.389	-0.477
a6	-0.107	-0.007	-0.341	-0.461	-0.695
	Position1	Position2	Position3	Position4	Position5

Figure 5.12 Part of a *Summary data* sheet with red and yellow alarms for local deviations from control bounds.

da2	-0.439	-1.900	0.309	0.018	-2.788	-3.923
da3	-0.212	-5.396	-1.514	-1.709	-1.572	-0.707
da4	-0.472	-0.956	-0.284	-1.095	-0.012	0.271
da5	0.061	0.877	-0.419	-0.270	-0.450	-0.539
da6	-0.061	-0.107	0.055	-0.280	-0.399	-0.634
	mean 2:19	position 1	position 2	position 3	position 4	position 5

Figure 5.13 Part of a *Worksheet* sheet with red and yellow alarms for local deviations from control bounds. Cells contain post processed data used for the tests.

Chapter 6

Applications of field quality analysis to production cases

Anomalies in magnetic measurements of collared coils with respect to previous production must be interpreted to localize defects inside the assembly. Here, cases of collared coils featuring a wrong multipolar structure are analyzed and indications on possible sources of errors are given, based on simulations.

6.1 Wrong magnetic measurement

In the case of the collared coil named Firm3-2, its magnetic measurements featured large multipolar variations in both apertures. In Figure 6.1 a section of the magnetic measurement *Summary data* sheet relative to aperture 2 is reported, while Figure 6.2 shows the main field variations in both apertures. Such large variations in the main field component and in the main field direction cannot be coherently explained in terms of conductor displacements. In fact, to explain this magnetic content, conductors should have displaced by around 10 mm, which seems unrealistic. A further analysis showed that one of the 10 measurements which are performed at each position (see Section 4.1.1) was null due to a rotating coil defect and the averaged measure was affected. The defect has been recovered and the measuring system is now reliable. The same magnet measured with another apparatus and by different operators did not show any anomalous multipolar variation affecting the assembly, as Figure 6.3 shows.

Summary data - Aperture 2				
C₁/i (mT/KA)	596.471	596.471	567.647	596.824
Angle (mrad)	3.968	2.815	-63.579	3.367
Multipoles	Position 16	Position 17	Position 18	Position 19
b1	10000	10000	10000	10000
b2	0.183	1.296	0.370	1.454
b3	0.853	1.258	1.748	2.204
b4	0.129	-0.080	0.024	0.011
b5	1.274	1.104	0.700	0.733
b6	0.149	0.028	-0.050	0.023
b7	0.545	0.552	0.580	0.551
b8	-0.019	-0.016	-0.002	0.010
b9	0.325	0.321	0.320	0.317
b10	0.049	-0.003	-0.024	-0.034
b11	0.743	0.742	0.740	0.734
b12	0.006	0.002	-0.004	-0.001

Figure 6.1 Section of the Summary data sheet taken from the magnetic measurement of Firm3-2-Ap.2. In position 18 there is a localized C_1 magnitude variation so large to change the aperture straight part average. Since C_1 average is affected, all positions have values outside control bounds applied by the analysis macro. Values are reported in units.

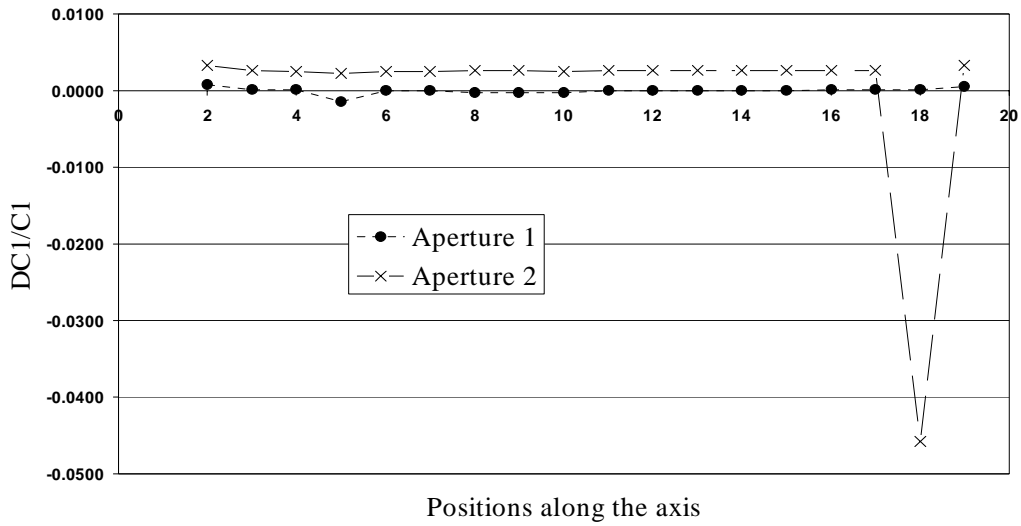


Figure 6.2 Plot of C_1 relative values along coil axis for both apertures of Firm3-2.

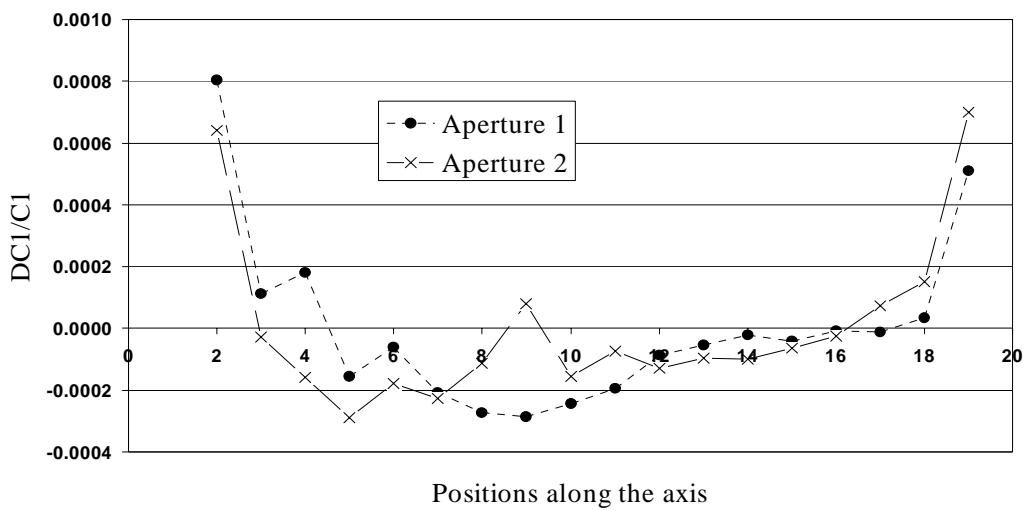


Figure 6.3 The same magnet of Figure 6.2 do not feature variations in C_1 relative module along coil axis when measured with a different apparatus. Note the different scale with respect to Figure 6.2.

6.2 Assembly error

Firm2-2 collared coil has been found to have large multipolar variations along the axis, as Figure 6.4 shows. C_1 (Figure 6.5) and b2 (Figure 6.6) presented large variations mainly at position 10 and 11. Aperture 1 featured a coil waviness value of $30 \mu\text{m}$, at the limit of

	Aperture 1			
Magnetic length	status ok			
	Average central positions 1 to 20	Central positions 2 to 19	Heads CS position 1	Heads NCS position 20
Main field Angle	status ok	red alarm	status ok	status ok
	yellow alarm	red alarm	status ok	status ok
b2	status ok	yellow alarm	status ok	status ok
b3	yellow alarm	yellow alarm	status ok	status ok
b11	status ok	yellow alarm	status ok	status ok
b12	status ok	red alarm	status ok	status ok
b13	yellow alarm	status ok	status ok	status ok
a15	yellow alarm			
Coil Positioning	yellow alarm			

Figure 6.4 Section of Alarm sheet relative to Firm2-2, aperture 1. Colors point out deviations in multipoles.

yellow control bounds, and minor but sensible variations were detected mainly for normal multipoles, as it can be seen from Table 6.1. The same results were obtained by repeating the measurement. Since skew multipoles were not excited beyond the normal stochastic variations, the deviations featured by C_1 and normal multipoles gave indications of a strong right-left asymmetry. When the coil has been de-collared, it has been found, in fact, that a double protection sheet (0.5 mm thick, 1 m long, see Figure 6.7) had been wrongly inserted around position 10 on the left outer layer of aperture 1.

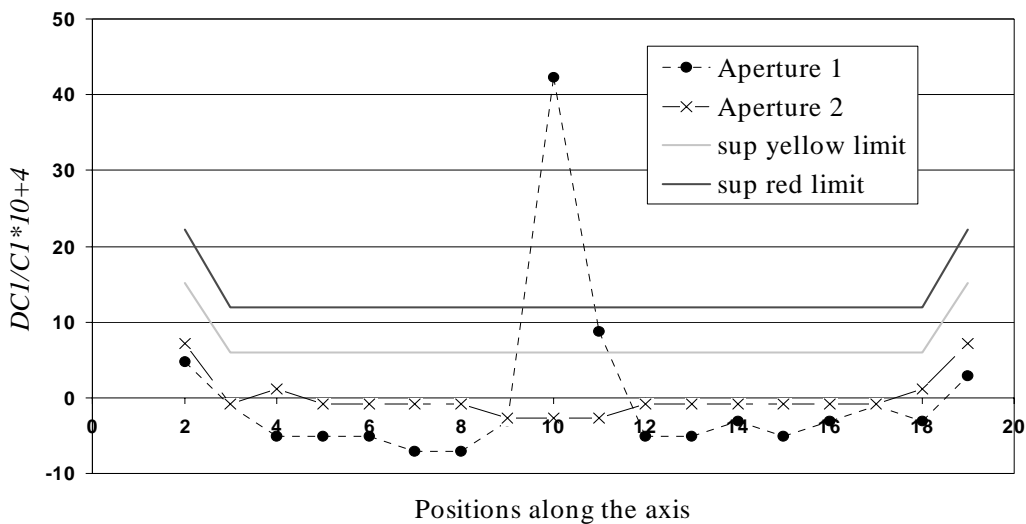


Figure 6.5 Plot of C_1 relative values along coil axis for both apertures. Only aperture 1 is affected by large variations (position 10 and 11) which are outside control bounds. Values are given in units of 10^{-4} .

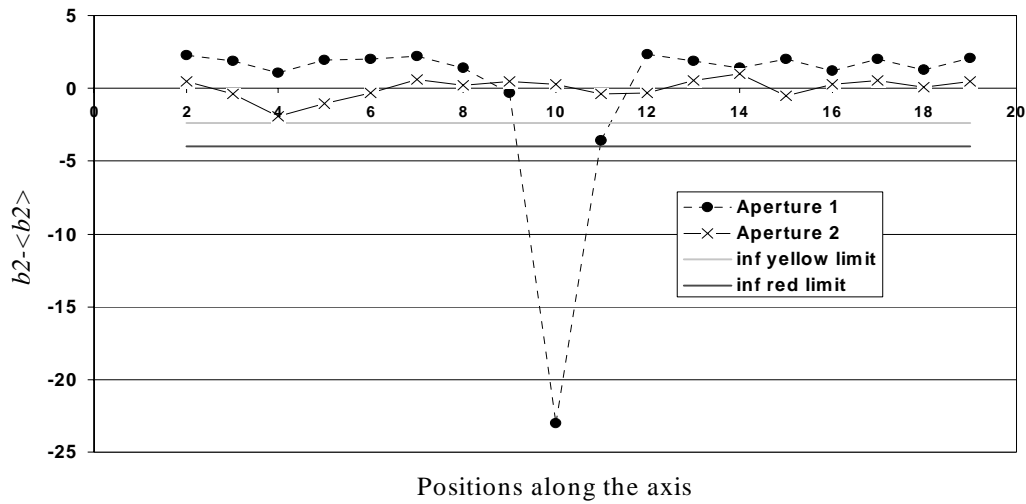


Figure 6.6 Plot of b_2 variations from straight part average along coil axis for both apertures. CS and NCS (positions 1 and 20) are not plotted because they would be out of scale. Only aperture 1 is affected by large variations (position 10 and 11) which are outside control bounds.

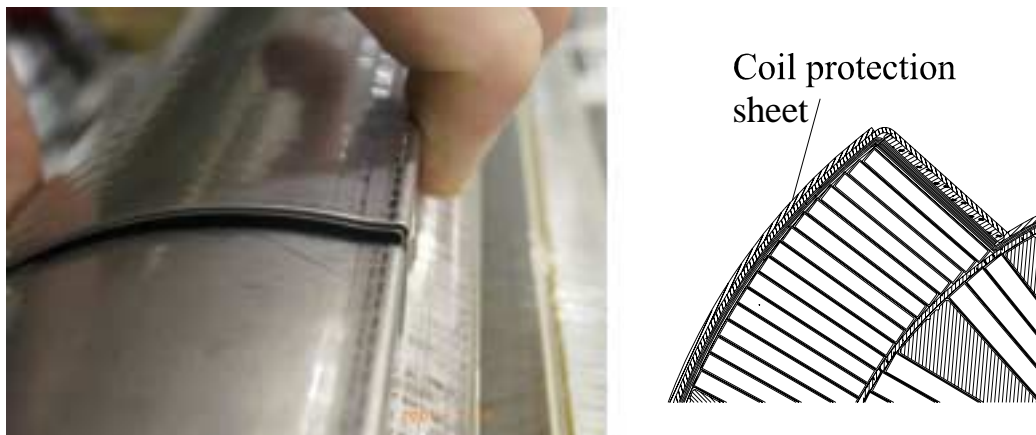


Figure 6.7 An assembly error affected the collared coil Firm2-2: a double coil protection sheet (0.5 mm thick and 1 m long) was wrongly inserted in the assembly.

Table 6.1 Variations from straight part average for main b and a multipoles of Firm2-2, aperture 1. Values for control bounds are also reported. All values are given in units of 10^{-4} .

Parameter	Position 10	Position 11	Yellow bounds	Red bounds
$DC_1/C_1 * 10^{-4}$	42.8	9.2	[-6.0,+6.0]	[-12.0,+12.0]
$b_2-<b_2>$	-23.0	-3.6	[-2.4,+2.4]	[-4.0,+4.0]
$b_3-<b_3>$	4.7	0.3	[-2.4,+2.4]	[-4.0,+4.0]
$a_1-<a_1>$	-13.7	-0.9	[-20.0,+20.0]	[-40.0,+40.0]
$a_2-<a_2>$	3.7	1.4	[-4.4,+4.4]	[-8.8,+8.8]
$a_3-<a_3>$	-0.6	-0.3	[-1.4,+1.4]	[-2.8,+2.8]

6.2.1 Simulations

Firm2-2-Ap1 featured a wrong multipolar structure because its superconducting coil was deformed with respect to the nominal design. The erroneously inserted double coil protection sheet deformed the coil during collaring procedures according to its Gamma shape (see Figure 6.8). Some computations have been made to reproduce the manufacturing error and the field quality featured by the collared coil in order to understand in which way the inner layer has moved. In fact, since it is in direct contact with the rigid collar, the outer layer is pushed inward by the inser-

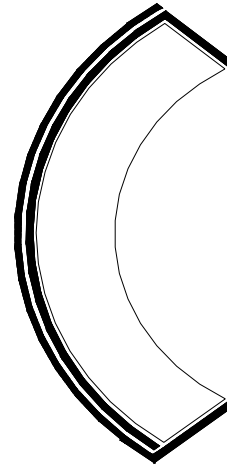


Figure 6.8 Sketch of position and shape of coil protection sheets.

tion of a double coil protection (which is a 0.5 mm thick stainless steel sheet), while nothing can be said a priori for the inner layer. The manufacturing error has been modelled by the insertion of a 0.5 mm thick polar shim on the outer layer and by blocks movements assigned according to the following assumptions:

- inner and outer layer are rigidly displaced towards the aperture center by 0.5 mm ($R_i=27.5$ mm for the inner and $R_i=43.4$ mm for the outer layer). In such way, it is assumed that layers are neither squeezed radially, nor ovalled;
- inner layer is rigidly displaced by 0.25 mm ($R_i=27.75$ mm), while the outer layer is rigidly displaced by 0.5mm ($R_i=43.4$ mm);
- inner and outer layer are deformed according to a FEM simulation [38]: outer and inner layers are deformed by the double coil protection sheet insertion more in the midplane than in the polar region (where the inner layer is not affected at all, see Figure 6.9).

Measured multipolar deviations from the straight part average are given in Table 6.2 together with simulation results. The rigid displacement model (third column) is partly in agreement with the sign trend of measured data (for C_1 , b_2 and with skew multipoles up to a_6), but not with measured values. The interlayer compression model (fourth column) has the same agreement than the previous model for the sign trend, while giving a better estimate on C_1 . Finally, the FEM (fifth column) features the best agreement with measured values, both for the sign trend (up to the 6th order of normal and skew multipoles) and for multipoles values. Layer deformations computed by the FEM have been implemented into the geometrical model by modifying

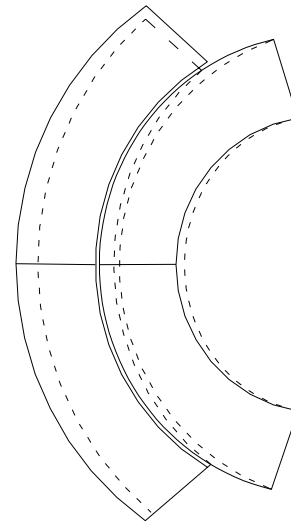


Figure 6.9 Sketch of the coil deformation undergone by Firm2-2-Ap.1 following a double protection sheet insertion on the outer layer derived by FEM computations [38] (dashed lines). Deformation magnitude is here enlarged of a factor 20.

block inner radii as it is reported in Table 6.3 for the deformed inner and outer layers according to the numbering convention of Figure 4.12: the outer coil layer is ovalled radially while the inner layer is pushed inward on its midplane, even if its polar regions remain fixed.

Table 6.2 Firm2-2 measured multipolar variation with respect to the straight section average and simulation results. Column I - Inner and outer layers are assumed to displace rigidly. Column II - Inner and outer layers are assumed to displace but the interlayer compresses. Column III - Layers displacements have been computed by a FEM simulation. Results are given as variations from nominal multipoles in units.

	Measured	Layer rigid displacement	Interlayer compression	FEM
C_1	46.3	58.8	40.9	44.5
b_2	-24.6	-18.5	-13.3	-23.1
b_3	5.1	-2.5	-0.2	5.7
b_4	0.3	3.7	2	0.89
b_5	-0.5	-0.3	-0.4	-1.3
b_6	0.1	-0.4	-0.1	0.5
b_7	0.1	-0.1	-0.1	-0.1

Table 6.2 Firm2-2 measured multipolar variation with respect to the straight section average and simulation results. Column I - Inner and outer layers are assumed to displace rigidly. Column II - Inner and outer layers are assumed to displace but the interlayer compresses. Column III - Layers displacements have been computed by a FEM simulation. Results are given as variations from nominal multipoles in units.

	Measured	Layer rigid displacement	Interlayer compression	FEM
a_1	-15.3	-13.8	-13.8	-14.6
a_2	4.1	5.3	5.3	5.2
a_3	-0.6	-0.4	-0.4	-0.4
a_4	-0.4	-0.5	-0.5	-0.4
a_5	0.1	0.2	0.2	0.2
a_6	-0.1	-0.1	-0.1	-0.1
a_7	0.1	-0.1	-0.1	-0.1

Table 6.3 Radial deformations of cable blocks due to a double coil protection sheet evaluated through the FEM [38].

Block number	Nominal inner radius	FEM inner radius	radial deformation
Outer layer			
8	43.900	43.600	-0.300
7	43.900	43.450	-0.450
13	43.900	43.450	-0.450
14	43.900	43.600	-0.300
Inner layer			
12	28.000	28.000	0.000
11	28.000	27.825	-0.175
10	28.000	27.600	-0.400
9	28.000	27.550	-0.450
15	28.000	27.550	-0.450
16	28.000	27.600	-0.400
17	28.000	27.825	-0.175
18	28.000	28.000	0.000

6.3 Anomalous multipole variations along the axis

For some magnetic measurements performed on collared coils manufactured at Firm1, strong multipolar variations have been detected along coil axis: Firm1-3, Firm1-4, Firm1-5 and Firm1-6. The field quality analysis has been focused on Firm1-5 and Firm1-6, since the other assemblies were less affected. In Appendix F all measurements relative to this set of magnets are reported. In Figure 6.10 and Figure 6.11, b_3 and b_5 variation from straight part average are shown for inner measuring positions as an example. As it can be seen, multipolar variations have a similar shape for the apertures of both magnets and the variability is always at its maximum around measuring positions 17, even if it affects all positions, particularly for Firm1-6. Moreover, the coil waviness values featured by these magnets are the largest encountered during the whole pre-series, as it can be seen from Figure 6.12. This can be considered an indication that the superconducting coil of these magnets have not been produced according to manufacturing tolerances.

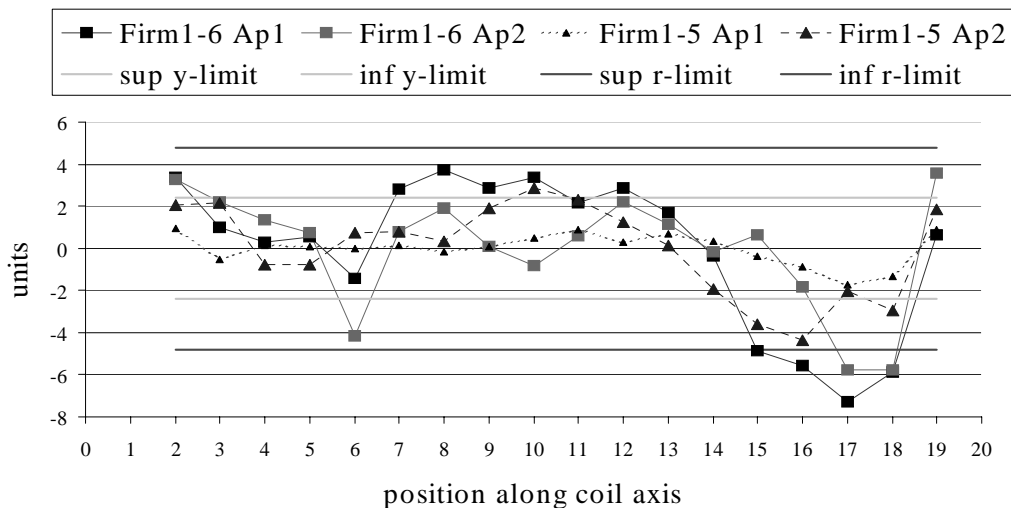


Figure 6.10 b_3 variations from the straight part average for Firm1-5 and Firm1-6 plotted for inner measuring positions. Applied control bounds are also plotted.

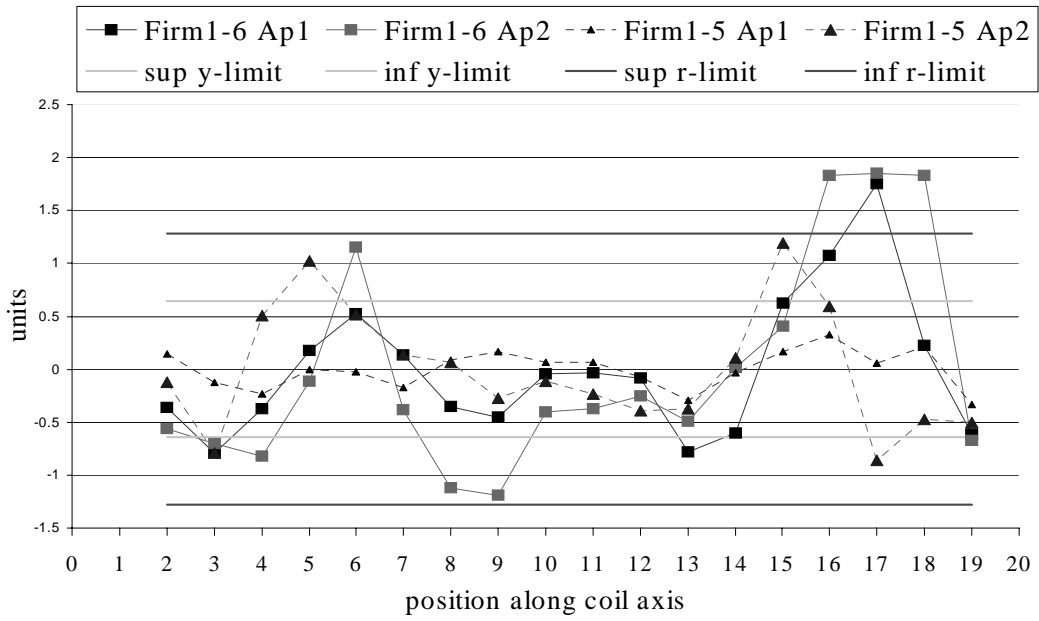


Figure 6.11 b_5 variations from the straight part average for Firm1-5 and Firm1-6 plotted for inner measuring positions. Control bounds are also plotted.

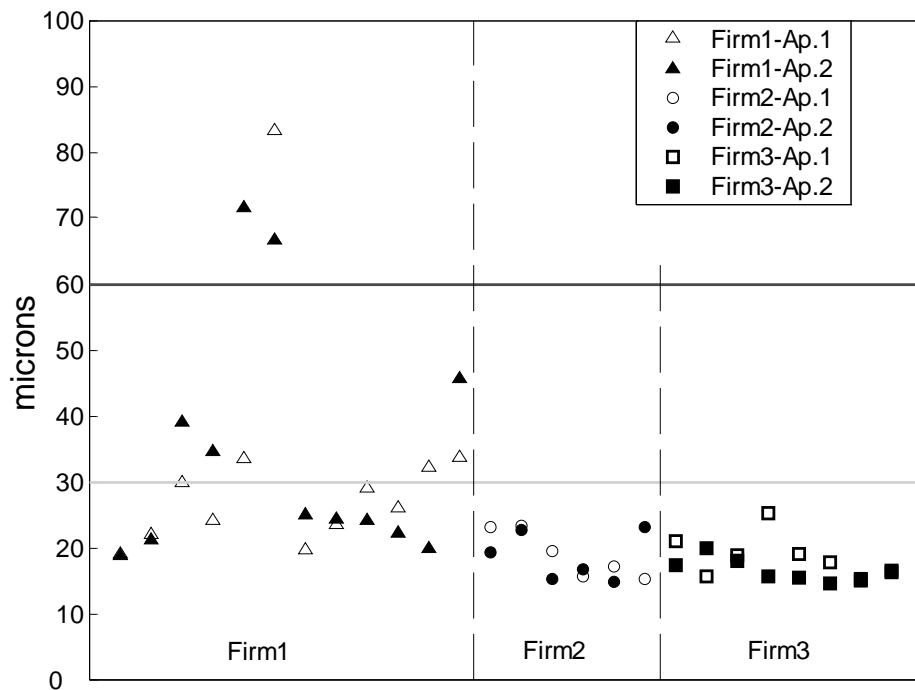


Figure 6.12 Coil waviness values for each manufactured aperture. Control bounds are also plotted.

Looking at the alarm sheet generated by our macro for Firm 1.6 ap1 in Figure 6.13 (and at the Firm1-5 and Firm1-6 Alarm sheet worksheets reported in Appendix F), the most excited multipoles have been found to be the odd normal and even skew ones. The magnitude of their variations are reported in Table 6.4 for aperture 2 of Firm1-6 at position 17 and 18. The excitation of odd normal multipoles is due to coil

	Aperture 1			
	status ok			
Magnetic length	Average central positions 1 to 20	Central positions positions 2 to 19	Heads CS position 1	Heads NCS position 20
Main field Angle	status ok	yellow alarm	status ok	status ok
b2	status ok	red alarm	status ok	status ok
b3	status ok	red alarm	status ok	status ok
b4	status ok	yellow alarm	status ok	status ok
b5	status ok	red alarm	status ok	status ok
b6	status ok	yellow alarm	yellow alarm	status ok
b7	status ok	red alarm	status ok	status ok
b8	status ok	status ok	status ok	status ok
b9	status ok	red alarm	status ok	status ok
b10	status ok	status ok	status ok	status ok
b11	status ok	red alarm	status ok	status ok
b12	status ok	status ok	status ok	status ok
b13	status ok	red alarm	status ok	status ok
b14	status ok	status ok	status ok	status ok
b15	status ok	yellow alarm	status ok	status ok
a2	status ok	red alarm	status ok	status ok
a3	status ok	status ok	status ok	status ok
a4	status ok	red alarm	status ok	status ok
a5	status ok	yellow alarm	status ok	status ok
a6	status ok	red alarm	status ok	status ok
a7	status ok	yellow alarm	status ok	status ok
a8	status ok	red alarm	status ok	status ok
a9	status ok	yellow alarm	status ok	status ok
a10	status ok	status ok	status ok	status ok
a11	status ok	yellow alarm	status ok	status ok
a12	status ok	yellow alarm	status ok	status ok
a13	status ok	status ok	status ok	status ok
a14	status ok	status ok	yellow alarm	status ok
a15	status ok	status ok	yellow alarm	status ok
Coil Positioning	red alarm			

Figure 6.13 Section of Firm1-6-Ap.1 Alarm sheet which points out variations mainly affecting odd normal and even skew multipoles.

variations respecting T-B and L-R symmetries. Since the outer shape of coil cannot vary along the axis

because it is determined by collars which have an elastic modulus much larger than the

Table 6.4 Measured multipolar variation with respect to the straight section average for measuring positions 17 and 18 of aperture 2 for Firm1-5 and Firm1-6. Values are reported in units.

Multipole	Fim1-6		Applied control bounds	
	Measuring position 17	Measuring position 18	Yellow	Red
b_3	-7.28	-5.85	[-2.40,+2.40]	[-4.80,4.80]
b_5	1.75	0.23	[-0.64,+0.64]	[-1.28,+1.28]
b_7	0.23	0.82	[-0.22,+0.22]	[-0.44,+0.44]
b_9	-0.13	-0.24	[-0.08,+0.08]	[-0.16,+0.16]
a_2	-3.77	5.02	[-4.40,+4.40]	[-8.80,+8.80]
a_4	3.96	2.12	[-1.08,+1.08]	[-2.16,+2.16]
a_6	-0.43	0.32	[-0.27,+0.27]	[-0.54,+0.54]
a_8	-0.30	-0.32	[-0.10,+0.10]	[-0.20,+0.20]

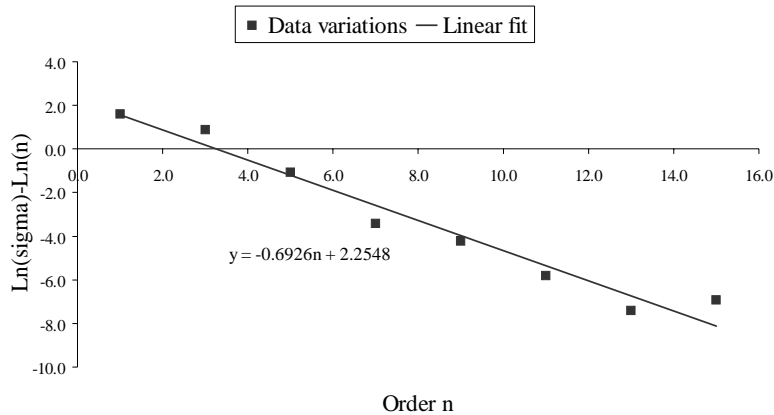


Figure 6.14 Linear fit of odd b_n variations from straight part average at position 17 of Firm1-6 aperture 2. The fitting line equation is reported.

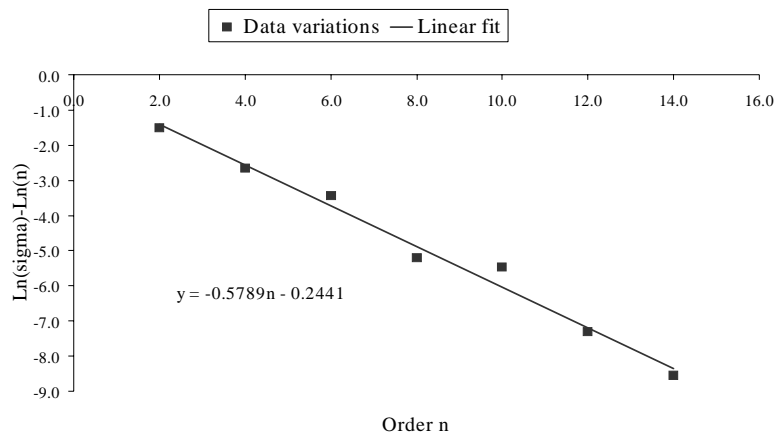


Figure 6.15 Linear fit of even b_n variations from straight part average at position 17 of Firm1-6 aperture 2. The fitting line equation is reported.

coil, odd b_n could have been excited by radial variations of inner coil dimension which respect T-B and L-R symmetries. On the other side, since even b_n have not been excited beyond the stochastic multipolar variability, the L-R symmetry has not been highly perturbed, while the existence of strong variations in even skew multipoles could mean that the T-B symmetry has been affected, probably by a shift of the coil median plane. This could have been due to a tooling imperfection, like a misalignment of the curing mould where poles are assembled. The coil median plane is in fact determined by poles azimuthal coil size.

In order to derive an indication of the distance from the aperture center of the coil

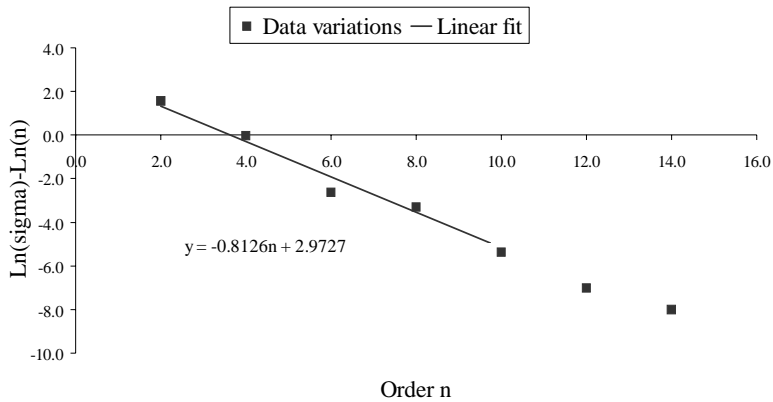


Figure 6.17 Linear fit of odd a_n variations from straight part average at position 17 of Firm1-6 aperture 2. The fitting line equation is reported.

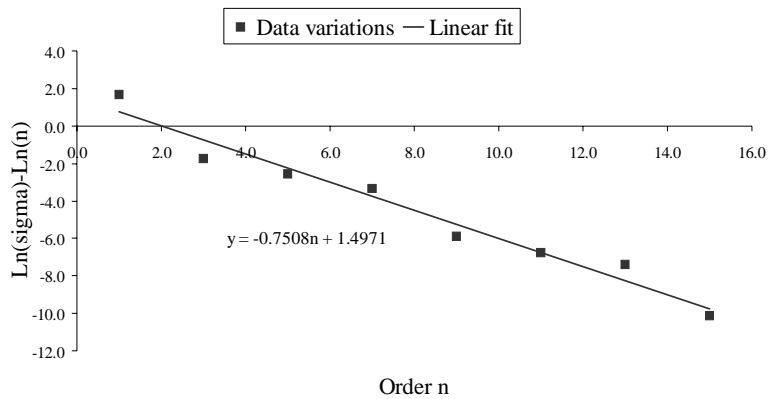


Figure 6.16 Linear fit of even a_n variations from straight part average at position 17 of Firm1-6 aperture 2. The fitting line equation is reported.

deformations, we analyzed the decay of multipoles at position 17 of aperture 1 of Firm1-6. The multipolar variations from the straight part average have been linearly fitted to estimate the error radius, as introduced in Section 4.2.2. Fitted data are given in Figure 6.14, Figure 6.15, Figure 6.16 and Figure 6.17 for odd b_n , even b_n , odd a_n and even a_n respectively, together with the fitting line equations. As it can be seen, the slope of lines which fit data are very similar for all the four orthogonal families of deformation. Furthermore if we look at error radius values in Table 6.5, all multipolar variations give similar indications, tracing the variation causes to the inner layer ($R_i=28$ mm, $R_e=43.4$ mm). But if we

Table 6.5 Error radii extrapolated from measured multipoles decay for odd and even normal multipoles. For each radius, the error estimate (1σ) is reported. Values are given in mm.

	Firm1-6-Ap.1 - Pos.17	
	R_c (mm)	Err (1σ)
odd b_n	32	3
even b_n	32	3
odd a_n	34	4
even a_n	35	26

look at the fitting line y-intercepts, the values for odd b_n and even a_n are larger than those computed for even b_n and odd a_n . From equation (4.10), that we report here written as following:

$$\ln(|\Delta c_n|) - \ln(n) = n \ln\left(\frac{R_{ref}}{|\zeta_c|}\right) + \ln\left(A \frac{|\Delta \zeta_c|}{|\zeta_c|}\right), \quad (6.1)$$

where:

$$A = \frac{\mu_0 I}{2\pi B_{ref} R_{ref}}, \quad (6.2)$$

it can be seen that the intercept of equation (6.1) can be different among the four orthogonal families only due to the term $\frac{|\Delta \zeta_c|}{|\zeta_c|}$. In the case under study, the intercept is bigger for odd b_n and even a_n , because for these two deformation families conductor displacement $|\Delta \zeta_c|$ is bigger than in the other cases, being the error radii $|\zeta_c|$ nearly the same.

The same methods have been then applied to the whole Firm1 production. Multipolar variations affect all collared coils from Firm1-3 to Firm1-6 with a similar pattern but with a magnitude which is at its maximum for Firm1-6. The analysis of the worst case in the Firm1 series has permitted to have indications of the kind of non-nominality affecting the coil: a variation affecting the inner layer and respecting T-B and L-R symmetry and a displacement of the coil median plane respecting L-R symmetry only. The extrapolation of the distance of the coil defect from the aperture centre has then pointed to the inner layer as the origin of the multipolar variations. Notwithstanding the wrong multipolar struc-

ture, the industrial process for these collared coils has not been stopped, but the couring mould has been revised. After some collared coils have been assembled, multipolar variations in the straight part have been detected again for Firm1-12, as shown in Figure 6.18. The problem remains then to be fixed definitively.

	Aperture 2			
Magnetic length	status ok			
	Average straight positions 2 to 19	Variation straight positions 2 to 19	Heads CS position 1	Heads NCS position 20
Main field Angle	status ok	status ok	status ok	status ok
b2	status ok	status ok	status ok	status ok
b3	status ok	red alarm	status ok	status ok
b4	status ok	yellow alarm	status ok	status ok
b5	status ok	yellow alarm	status ok	status ok
b6	status ok	status ok	status ok	status ok
b7	status ok	yellow alarm	status ok	status ok
b8	status ok	yellow alarm	status ok	status ok
b9	status ok	red alarm	status ok	status ok
b10	status ok	status ok	status ok	status ok
b11	status ok	red alarm	status ok	status ok
b12	status ok	status ok	status ok	status ok
b13	status ok	yellow alarm	status ok	status ok
b14	status ok	status ok	status ok	status ok
b15	status ok	status ok	status ok	status ok
a2	status ok	status ok	status ok	status ok
a3	status ok	status ok	status ok	status ok
a4	status ok	status ok	status ok	status ok
a5	status ok	yellow alarm	status ok	status ok
a6	status ok	yellow alarm	status ok	status ok
a7	status ok	status ok	status ok	status ok
a8	status ok	status ok	status ok	status ok
a9	status ok	red alarm	status ok	status ok
a10	status ok	status ok	status ok	status ok
a11	status ok	yellow alarm	status ok	status ok
a12	status ok	status ok	status ok	status ok
a13	status ok	status ok	status ok	status ok
a14	status ok	status ok	status ok	status ok
a15	status ok	status ok	status ok	status ok
Coil Positioning	yellow alarm			

Figure 6.18 Section of Firm1-12 Alarm Sheet for aperture 2 affected by multipolar variations in the straight part.

6.4 Torsion of the collared coil

Magnetic measurements performed at room temperature on the collared coil Firm3-9 have pointed out a large local variation in the main field direction (see Figure 6.19) around the measuring position 11 (see Figure 6.20) The coil has undergone a rotation around its axis of 2.5 mrad. As it is shown in Figure 6.21, the error affects both apertures. Since the computed σ for the angle variation is 0.5 mrad, then in this case the variation is at 5σ . Errors of this kind may be due to a deformation affecting one of the non-ferromagnetic support on which the collared coil is laid down during magnetic measurements. Due to its laminated structure, in fact, the collared coil has a very low torsional rigidity and the coil can be easily deformed. In this case we expect to recover a correct main field direction in the assembled cold mass.

	Aperture 1					Aperture 2			
Magnetic length	status ok				Magnetic length	status ok			
	Average straight positions 2 to 19	Variation straight positions 2 to 19	Heads CS position 1	Heads NCS position 20		Average straight positions 2 to 19	Variation straight positions 2 to 19	Heads CS position 1	Heads NCS position 20
Main field Angle	status ok	status ok	status ok	status ok	Main field Angle	status ok	status ok	status ok	status ok
b2	status ok	status ok	status ok	status ok	b2	status ok	status ok	status ok	status ok
b3	status ok	status ok	status ok	status ok	b3	status ok	status ok	status ok	status ok

Figure 6.19 Section of Alarm Sheet taken from the magnetic measurements performed on Firm3-9. In a position belonging to the straight part of both apertures, a variation of the main field direction is detected.

	Aperture 1			Aperture 2		
C1/i (mT/KA)	596.471	596.588	596.471	596.471	596.471	596.588
Angle (mrad)	0.181	2.652	1.397	0.433	2.554	1.969
Multipoles	Position 10	Position 11	Position 12	Position 10	Position 11	Position 12
a1	1.811	26.516	13.968	4.335	25.541	19.691
a2	-1.074	-0.701	-0.122	0.945	1.544	1.920

Figure 6.20 Section of Summary data sheet of Firm3-9 magnetic measures. A local deviation of the main field direction value is detected at position 11.

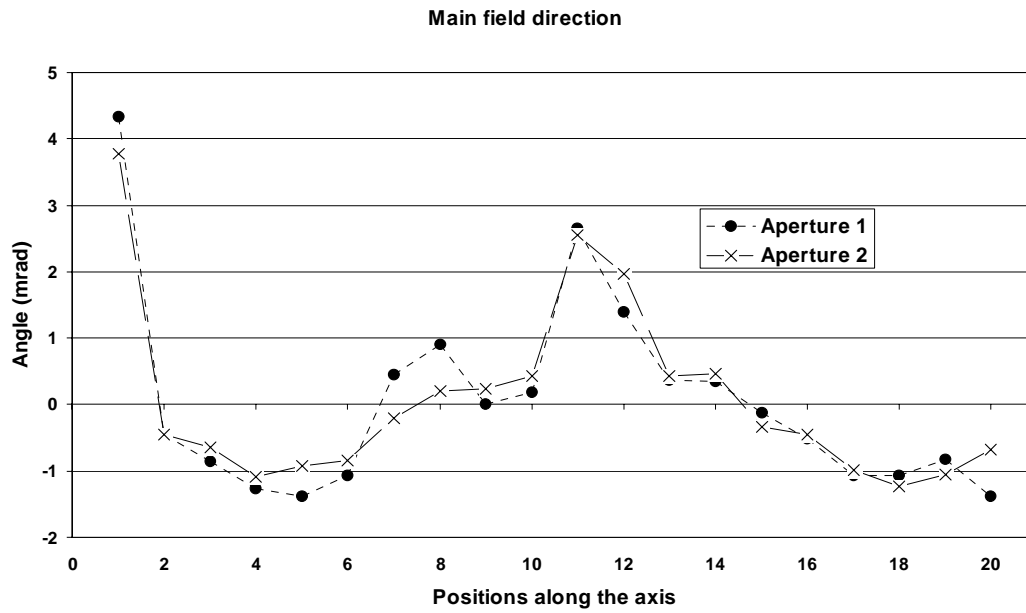


Figure 6.21 Main field direction for inner position along both apertures of Firm1-9. Around position 11 the coil is rotated of about 2.5 mrad.

Conclusions

In the present work, the field quality featured by the main superconducting dipoles of the Large Hadron Collider has been analyzed in order to derive a method to monitor the industrial production of these components. To detect assembly errors or faulty components at an early stage of production, we have developed an automatic tool which analyzes data coming from magnetic measurements data to point out deviations from the expected multipolar structure. Methods of analysis have been studied in the same framework in order to trace back the detected magnetic variations to their causes.

In order to simulate the magnetic effects of manufacturing errors that may happen during the dipole industrial series production, we derived a geometrical model to compute conductors position inside the superconducting coil. Moreover, we developed a method to have indications on the distance of the error from the center of the aperture, based on the ratio of decay of the multipole anomalies. In both cases, we always used the decomposition of coil deformations in orthogonal families, as it has been proposed in the literature [7].

We then statistically analyzed magnetic measurements performed on collared coils to compute acceptance criteria for field quality. At this stage, sensitivity data computed with the geometrical model are used to normalize magnetic measurements to nominal shims, since in some cases the manufacturers have used sizes different from the nominal ones for pre-stress purposes. We decided not to derive control bounds from the beam dynamics, which imposes tolerances to the whole set of the LHC machine. Such tolerances do not fit the need of a quality control since in general they are too loose to be applied to a single magnet in order to derive indications of the quality of the industrial process. Instead, magnetic measurements at room temperature provide a fast way to check the field quality featured by each magnet and they can be used to detect manufacturing errors and drifts affecting the industrial production. In order to state if measured quantities can be described by Gaussian distributions, we performed a normality test which has proved measurements compatibility with that kind of distribution. Control bounds have then been computed for tests to be performed on the collared coil magnetic measurements

at room temperature considering the statistical tails of the distributions describing measured values.

Some data relative to anomalous collared coil have been discarded. Then, control bounds have been placed at $[-k\sigma, +k\sigma]$, where k has been chosen to have at the end of a Gaussian production only a few cases (1 to 3) in the tails out of this range. Outside this range a yellow alarm is set. We also defined a red alarm when data are outside $[-2k\sigma, +2k\sigma]$; this is useful to detect very strong anomalies in field quality that can be related to major problems in the assembly or in components. Each new magnetic measurement can then be compared to the previous production in order to assure production homogeneity. Deviations from the expected magnetic structure are pointed out through colored alarms directly on the measurement file for fast localization of the defect along coil axis and summarized for each test performed and for each aperture.

The automatic tool of analysis has been applied to all the collared coils manufactured till now and deviations from the expected magnetic behavior have been analyzed. Different cases have been found. Strong deviations affecting a wrong measurement have been detected and the measurement has been redone. In another case, large deviations affecting a collared coil suggested that the assembly was affected by a localized defect. After inspection, it has been found to be due to the wrong insertion of a double coil protection sheet into the assembly. Simulations of the defect have been performed in order to analyze such deviations in terms of coil deformations, and a good agreement has been found between the geometrical model developed and the measurement. We then tried to understand magnetic measurements performed on a set of collared coils of a firm which are affected by large deviations along their axis. Analyzing the decoupled multipolar decay, we derived indications that such deviations are due to a defect affecting the coil inner layer and the coil midplane position. It seems that such imperfections can be due to a misalignment of the mould in which coils have been cured. In the last case presented, deviations from the expected magnetic content have been traced back to a local rotation of coil probably due to a failure of the support on which the assembly is laid down during measurement.

The methods of field quality analysis that we have presented in this work will be applied in the future to the monitoring of the cold mass assembly procedures. Furthermore, control bounds computed for monitoring collared coil production will be updated with all available statistics. Finally the database of manufacturing errors which are likely to happen during the industrial series production of the LHC dipole magnet will be enlarged.

Acknowledgements

I wish to acknowledge Professor Del Tin, for giving the opportunity of carrying out this thesis and for his many useful suggestions.

I wish to acknowledge Dott. Scandale and Dott. Todesco for their invaluable help and for the encouragement they provided during the thesis work. Many thanks go also to all CERN personnel of the LHC/MMS group, for having given me the possibility of working in a stimulating and pleasant environment. In particular, thanks to Vittorio Remondino for measurement data and discussion.

Special thanks go to the ASP (Associazione per lo Sviluppo Scientifico e Tecnologico del Piemonte) for the financial support to this collaboration between the Politecnico di Torino and the CERN laboratories.

I wish to thank Boris Bellesia, Luca Bottura, Arnaud Devred, Paolo Ferracin, Paolo Fessia, Giuseppe Gubello, Ramesh Gupta, Marco La China, Cristiano Lanza, John Miles, Stefano Redaelli and Alberto Schiappapietra for precious discussion and suggestions.

Thanks also to Antonio, Boris, Davide, Esther, Eva, Francesco, Fedrico Ravotti, Federico Roncarolo, Georgina, Juan, Luis, Matteo, Marco, Mirko, Rocho and Ubaldo for their precious collaboration outside CERN.

Thanks a lot to my family and to Stefania for having being so patient in the course of my work and for their constant support.

Bibliography

- [1] <http://public.web.cern.ch/Public/Whatiscern.html>.
- [2] CD-ROM, *Superconducting accelerator Magnets*, 1998, MJB Plus.
- [3] S.Myers, *The LEP Collider, from design to approval and commissioning*, CERN-91-08, Geneva.
- [4] The LHC study Group, *Design study of the Large Hadron Collider (LHC) : a multiparticle collider in the LEP tunnel*, Geneva, CERN, 1991 - CERN-91-03.
- [5] The LHC study Group, *The Large Hadron Collider - Conceptual Design*, CERN/AC/95-05 (1995).
- [6] J.Poole, M.Silari, *LEP Dismantling Project - Status report*, CERN, SL-Note-2001-015 MR.
- [7] K.-H.Mess, P.Schmuser, S.Wolff, *Superconducting accelerator magnets*, World Scientific Publishing, 1996.
- [8] S.Wolff, "Superconducting accelerator magnet design", *CERN Accelerator School 94-01*, CERN, 1994, Vol. II, pag. 755-790.
- [9] AA.VV., *Technical specification for the supply of 1158 cold masses of the superconducting dipole magnets for the LHC collider*, LHC Project document No.: LHC-MB-CI-0006, Vol. I.
- [10] A. K. Jain, "Basic theory of magnets", *CERN Yellow Report 98-05*, CERN , 1998.
- [11] R. Wolf, "Field error naming conventions for LHC magnets", *CERN LHC-MMS/98-198 Rev. 2.0*, CERN, 1998, Annex F1.
- [12] O. Bruning, S.Fartoukh, "Field quality specification for the LHC main dipole magnets", *CERN-LHC-Project-Report-501*, Geneva, CERN, 10 Oct 2001, 93p.
- [13] P.Ferracin, W.Scandale, E.Todesco, and R.Wolf, "Modeling of random geometric errors in superconducting magnets with applications to the CERN Large Hadron Collider", *Phys. Rev. ST-AB* 3 (2000) 122403, also in *CERN LHC Project Report 460* (2000).
- [14] J.Billan et al., "Magnetic measurements of the LHC quadrupole and dipole magnets at room temperature", *LHC Project Note 283*, CERN, 2002.

- [15] K.N. Henrichsen, "Overview of magnet measurement methods", *CERN Report 98-05*, CERN, 1998.
- [16] P.Ferracin, O.Pagano, S.Redaeli, W.Scandale, E.Todesco, "Control of field quality for the production of the main LHC dipoles", *LHC Project Report 467*, CERN, 2001.
- [17] A.V. Tollestrup, "The amateur magnet builder's handbook", Fermilab, *UPC 086*, 1979.
- [18] R.Gupta, "Estimating and adjusting field quality in superconducting accelerator magnets", presented at *The LHC Collective Effects Workshop Proceed.*, Montreaux, Switzerland, 1995.
- [19] R.Gupta et al., "Field quality analysis as a tool to monitor magnet production", presented at the *Fifteenth International Conference On Magnet Technology*, 1997, Vancouver, Canada.
- [20] A.Bonito Oliva, P.Gagliardi, R.Penco and P.Valente, "A statistical analysis of the whole Ansaldo "HERA dipoles" production", *CERN-95-05*.
- [21] D.C.Montgomery, *Statistical quality control*, 3rd Ed., J.Wiley & Sons, 1996, Canada.
- [22] R.Russenschuck, T.Tortschanoff, A.Ijspeert, N.Siegel, R.Perin, "Tracing back measured magnetic field imperfections in LHC magnets by means of the inverse problem approach", *CERN 99-01*.
- [23] J.-P.Koutchouk, M.Zorzano, P.Mier, *From LEP to LHC, some important issues*, CERN, SL-Note-2000-007 DI, pp 13-4.
- [24] AA.VV., *Technical specification for the supply of 1158 cold masses of the superconducting dipole magnets for the LHC collider*, LHC Project document No.: LHC-MB-CI-0006, Vol. II, Annex G8.
- [25] A.Devred, et al., "About the Mechanics of SCC Dipole Magnet Prototypes", *AIP Conference Proceedings Series*, 249, NY,1989, pp. 1309-74.
- [26] E.Todesco, L.Bottura, S.Pauletta, V.Remondino, S.Sanfilippo, W.Scandale, "Status report on field quality in the main LHC dipoles", *Proceedings of European Particle Accelerator Conference*, 2002, Paris, France.
- [27] S.Gleis, J.Miles, O.Pagano, W.Scandale and E.Todesco, "Analysis of warm magnetic measurements in a LHC main dipole prototype", *LHC Project Report 352*, Geneva, 1999.

-
- [28] S.Peggs, "Feedback between accelerator physicists and magnet builders", *Particle accelerators*, 54, 1996, OPA, pp.83-92.
- [29] R.Gupta et al., "Tuning shims for high field quality in superconducting magnets", presented at *Magnet Technology 14th*, Tampere, Finland, 1995.
- [30] S.Readelli, *Analysis of the magnetic field perturbations in dipoles and quadrupoles of the Large Hadron Collider (LHC)*, Tesi di Laurea, Facolta di Scienze Matematiche, Fisiche e Naturali, Universita degli Studi di Milano, 2000.
- [31] P.Ferracin, W.Scandale, E.Todesco, D.Tommasini, "Azimutal coil size and field quality in the main CERN Large Hadron Collider dipoles", *Phys. Rev.*, STAB 2002.
- [32] Fortran codes: *Bio.f* and *Bia.f*, by E.Todesco.
- [33] T.Ogitsu, A.Devred, "Influence of azimuthal coil size variations on magnetic field harmonics of superconducting particle accelerator magnets", *Rev. Sci. Instrum.* 65 (6), 1994, AIP, pp. 26-33
- [34] E.Farina, P.Fessia, D.Perini, A.Schiappapietra, L.Senée, "Development and manufacture of the coil end spacers of the LHC pre-series dipoles", *LHC Project Report 535*, CERN, 2002
- [35] <http://www.davidmlane.com/hyperstat>.
- [36] E.Dietrich, A.Schulze, *Statistical procedures for machine and process qualification*, ASQ Quality Press, Wisconsin, USA, 1999.
- [37] W.H.Press, S.A.Teukolsky, B.P.Flannery, W.T.Vetterling, *Numerical recipes in C*, Cambridge University Press, USA, 1988.
- [38] P.Ferracin, private communications.

Appendix A

Stationary circular motion for a particle beam

Using the right-handed reference system of Figure A.1, the equation of motion for a particle subjected to an electromagnetic static field can be derived. Lorentz's equation can be written as following:

$$\frac{d}{dt}(m\vec{v}) = q\vec{E} + q(\vec{v} \wedge \vec{B}) \quad (\text{A.1})$$

where:

- $m = \frac{m_0}{\sqrt{\left(1 - \frac{v^2}{c^2}\right)}}$ is the particle relativistic mass, with m the particle mass at rest, v is the particle speed and c is the light speed.
- q is the particle electric charge;
- E is the electric field:
- B is the magnetic field.

Taking the Lorentz's force component parallel to the x-axis, one gets:

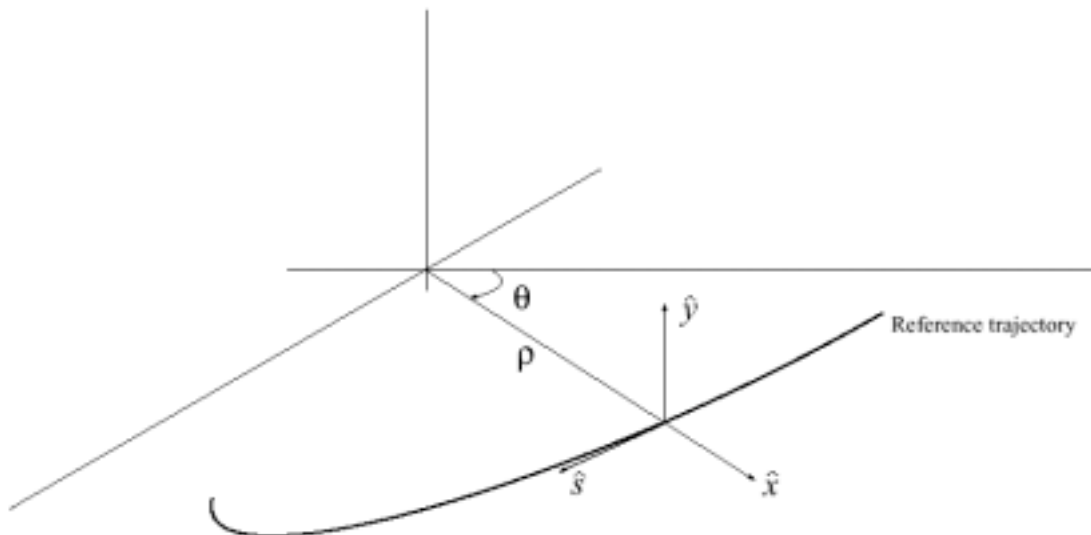


Figure A.1 Reference system for development of equation of motion.

$$\frac{d}{dt}(m\dot{r}) - m r \dot{\theta}^2 = q(E_r + r\dot{\theta}B_y - \dot{y}B_\theta) \quad (\text{A.2})$$

where only components have been considered. r is the circular trajectory radius. For a stationary circular trajectory, E is null (no acceleration), and if $\vec{B} = B_\theta \hat{i}_\theta$ we can write:

$$m\ddot{r} - m \frac{v_\theta^2}{r} = qv_\theta B_y \quad (\text{A.3})$$

where $v_\theta = r\dot{\theta}$ is the azimuthal velocity of the particle. Since the circular trajectory radius is constant, equation (A.3) becomes:

$$mv_0 = -qB_y r \quad (\text{A.4})$$

remembering that $v_\theta = v_0$ for a stationary motion on a circular trajectory, where v_0 is the total particle velocity. Finally, since v_0 is really near c , we can write:

$$mv_0 = \frac{m_0}{\sqrt{1 - \frac{v_0^2}{c^2}}} c \frac{v_0}{c} = \frac{Ev_0}{c^2} = -qB_y r \approx \frac{E}{c} \quad (\text{A.5})$$

from which equation (1.2) can be derived:

$$|B| = \frac{E}{qrc} \quad (\text{A.6})$$

Appendix B

Geometric models for symmetric computations

For field quality analysis purposes, a simplified geometrical model of the LHC dipole coil cross-section of Figure 3.7 was needed. Assumptions had to be made on the elastic modulus of the coil. The two possible extreme assumptions are the following ones:

- *Copper wedges have the same properties of the cables.* This approximation implies that the coil has an homogenous structure.
- *Copper wedges are infinitely rigid if compared to the properties of cables:* This approximation assumes that the whole deformation is taken by cables.

In the geometrical model presented in Section 4.3 for asymmetric computations, the hard copper wedges approximation has been assumed. Here a geometrical model for symmetrical computation using the soft copper wedges approximation is presented in the case of azimuthal coil size variation only. The numerical comparison between sensitivity data of the two models and those of a validated FEM for symmetrical computations is also reported.

2.1 Soft copper wedges model

Let us assume that the compressibility of copper wedges is the same as that of cables. When a polar shim is inserted on the coil being collared, both conductors and copper wedges are squeezed of an amount proportional to the ratio of their angular dimension and the total angular dimension of a layer quadrant. From the design position of conductors given as in Table 3.2 for nominal shims, one has to compute the new positions of conductors after the insertion of a non-nominal shim in the polar region, according to the reference system given in Figure 3.7. We will refer to the usual outer layer of a coil quadrant, but all formulas that will be given can apply to the coil inner layer. With notations used in Figure B.1 for non-nominal position coordinates of blocks, after the insertion of a polar

shim of non nominal thickness $k + \delta_{shim,pol}$ (where k is the nominal thickness), the new angular coordinate for block 2 is the following:

$$\Phi'_2 = \Phi_2 - \frac{\delta_{shim,polar}}{r_i} \frac{\Phi_2}{\Phi_{tot}} \frac{180}{\pi}. \quad (\text{B.1})$$

where Φ_{tot} is computed by the following equation:

$$\Phi_{tot} = \Phi_2 + nc(2) \frac{th_i(2)}{r_i} \frac{180}{\pi}. \quad (\text{B.2})$$

where $nc(2)$ and $th_i(2)$ corresponds to the number and the inner thickness of conductors belonging to block 2. In the inner layer, a shim insertion changes Φ_4 , Φ_5 and Φ_6 but leaves unchanged Φ_3 , like Φ_1 in the outer layer.

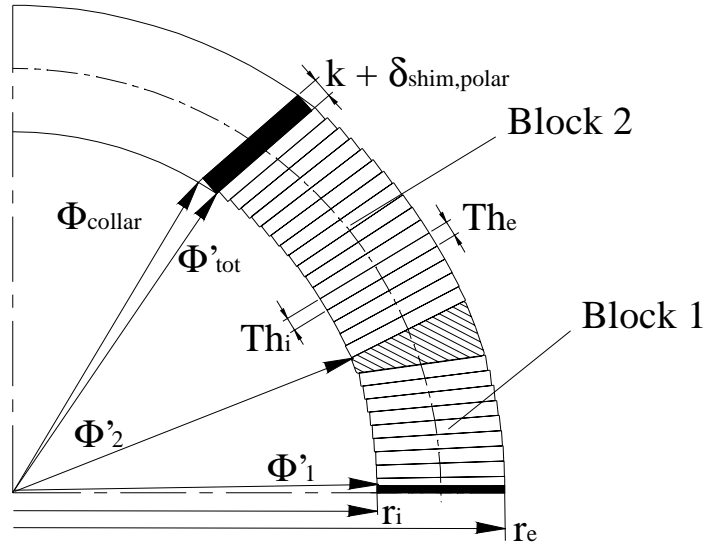


Figure B.1 Notation used to compute conductor displacement in the outer layer of a coil quadrant after the insertion of a polar shim.

To compute cables thickness, we assumed as usual that the block angle α is not modified by the non-nominal shim insertion (see Section 4.3). This assumption implies that cables are squeezed by the same amount both on the inner and on the outer side ($\delta th_i = \delta th_e$). So we can write for block 2:

$$th_i(2) = th_i(2) - \delta_{shim,polar} \frac{th_i(2)}{r_i} \frac{180}{\Phi_{tot}} \frac{180}{\pi}. \quad (\text{B.3})$$

$$th_e(2) = th_e(2) - \delta_{shim,polar} \frac{th_i(2)}{r_i \Phi_{tot}} \frac{180}{\pi}. \quad (\text{B.4})$$

Equation (B.3) and equation (B.4) apply to all the blocks of the coil, since even if the Φ_1 and Φ_3 don't change, cables are uniformly squeezed all along the coil, as well as the copper wedge.

These equations have been implemented in a Fortran code (*shimomo.f*, see Appendix C), that reads an input file (*shimo.dat*, see Appendix C), computes conductor positions and write them on the output file (*magn.inp*, Appendix C) which is read by a magnetostatic model. [32] The latter, then, computes the multipoles for the given arrangement of conductors.

2.1.1 Results and comparison with validated Finite Element Model

In order to compare the two first-order approximations on the copper wedge compressibility, we computed the field errors arising from the use of non-nominal polar shims. Results have then been compared to computations carried with a validated Finite Element Model (FEM), [31]. Magnetic sensitivity values to non-nominal polar shims ($\delta_{shim,polar} = 0.1$ mm) are reported in Table B.1 and Table B.2 for the inner and outer layer. Only sensitivity data relative to allowed multipoles b_3 , b_5 and b_7 are reported together with the main component C_1 , higher order multipoles being weakly dependent on the shim size. [31].

Table B.1 Odd b_n sensitivity to the insertion of a 0.3 mm thick polar shim (nominal thickness: 0.2 mm) in the inner layer according to codes developed under different assumptions. The Finite Element Model (FEM) has been validated and its results are reported for reference. Values are given in units (10^{-4}).

Multipole	Polar shim inserted in the inner layer		
	Hard copper wedges	Soft copper wedges	FEM
C_1	5.76	5.30	5.42
b_3	2.23	1.71	2.07
b_5	-0.39	-0.44	-0.35
b_7	0.15	0.16	0.14

The hard copper wedge approximation overestimates the sensitivity of the main component C_1 to the polar shim insertion on the inner layer (see Table B.1) with respect to the FEM model (+ 6%), while the soft copper wedge underestimate it (- 2.2%). The former approximation better represents polar shims magnetic effect on allowed multipoles (b_3 : + 7%; b_5 : + 10%; b_7 : + 6%) than the latter (b_3 : - 20%; b_5 : + 20%; b_7 : + 12%). A shim insertion in the pole region of the outer layer (see Table B.2) has an effect on the multipolar content of the aperture which is better represented by the hard copper wedge approximation both for the C_1 sensitivity and for the allowed multipoles (C_1 : + 1.5%; b_3 : + 1.5%) than by the soft copper wedge approximation (C_1 : + 5%; b_3 : + 5%). From Table B.2, it is evident that conductor displacements in the outer layer weakly affect higher order multipoles and both approximation are good in evaluating the b_5 and b_7 sensitivity to polar shims non-nominal dimensions.

Table B.2 Multipole variations due to the insertion of a 0.9 mm thick polar shim (nominal thickness: 0.8 mm) in the outer layer according to codes developed under different assumptions. The Finite Element Model (FEM) has been validated and its results are reported for reference. Values are given in units (10^{-4}).

Multipole	Polar shim inserted in the outer layer		
	Hard copper wedges	Soft copper wedges	FEM
C_1	3.83	3.99	3.78
b_3	1.62	1.69	1.60
b_5	-0.07	-0.07	-0.07
b_7	-0.02	-0.02	-0.02

These computations show that sensitivities of multipoles on shim may differ significantly (up to 25%) according to the hard or soft copper wedges approximations. From a mechanical point of view, the hard copper wedges approximation should better modelize the coil deformations. Comparison of sensitivities given by these two approximations with a finite element model based on the actual properties of coil components confirm this hypothesis.

Appendix C

Fortran codes for field quality computations

C.1 Soft copper wedges code

The file *Shimomo.f* for symmetric geometrical computations of conductor positioning inside the coil after a polar shim insertion with the soft copper wedges approximation is the following:

```

Program shimomo
  parameter(nbt=50)
  real r(nbt),p(nbt),a(nbt)
  real th1(nbt),th2(nbt),wi(nbt)
  real ptoti, ptote

  integer nf1(nbt),nf2(nbt)
  integer nc(nbt)
  character*70 str

  pi=datan(1.d0)*4
  open(1,file='base.inp',status='old')
  read(1,*) nbl,nca,ism,riron
  read(1,'(a70)') str
  do i=1,nbl
    read(1,*) nc(i),r(i),p(i),a(i),
    .      wi(i),th1(i),th2(i),nf1(i),nf2(i)
  end do
  close(1)

  open(1,file='shimo.dat',status='old')
  read(1,*) shi,sho
  close(1)
C
C-----
C
  ptoti=p(6)+nc(6)*th1(6)/r(6)*180/3.141592654
  ptote=p(2)+nc(2)*th1(2)/r(2)*180/3.141592654

  p(2)=p(2)-(sho-0.8)/r(2)*180/3.141592654*p(2)/ptote
  p(4)=p(4)-(shi-0.2)/r(4)*180/3.141592654*p(4)/ptoti

```

```
p(5)=p(5)-(shi-0.2)/r(5)*180/3.141592654*p(5)/ptoti
p(6)=p(6)-(shi-0.2)/r(6)*180/3.141592654*p(6)/ptoti
```

```
th2(1)=th2(1)-th1(1)*(sho-0.8)/r(1)/ptote*180/3.141592654
th2(2)=th2(2)-th1(2)*(sho-0.8)/r(2)/ptote*180/3.141592654
th2(3)=th2(3)-th1(3)*(shi-0.2)/r(3)/ptoti*180/3.141592654
th2(4)=th2(4)-th1(4)*(shi-0.2)/r(4)/ptoti*180/3.141592654
th2(5)=th2(5)-th1(5)*(shi-0.2)/r(5)/ptoti*180/3.141592654
th2(6)=th2(6)-th1(6)*(shi-0.2)/r(6)/ptoti*180/3.141592654
```

```
th1(1)=th1(1)*(1-(sho-0.8)/r(1)/ptote*180/3.141592654)
th1(2)=th1(2)*(1-(sho-0.8)/r(2)/ptote*180/3.141592654)
th1(3)=th1(3)*(1-(shi-0.2)/r(3)/ptoti*180/3.141592654)
th1(4)=th1(4)*(1-(shi-0.2)/r(4)/ptoti*180/3.141592654)
th1(5)=th1(5)*(1-(shi-0.2)/r(5)/ptoti*180/3.141592654)
th1(6)=th1(6)*(1-(shi-0.2)/r(6)/ptoti*180/3.141592654)
```

```
C
C-----
C
```

```
open(1,file='magn.inp',status='unknown')
write(1,'(i3,i4,i4,2x,f10.0)') nbl,nca,isym,riron
write(1,'(a70)') str
do i=1,nbl
  write(1,'(i4,2x,3f8.3,f10.1,f10.3,f8.3,i4,i5)')
  .      nc(i),r(i),p(i),a(i),
  .      wi(i),th1(i),th2(i),nf1(i),nf2(i)
end do
close(1)

end
```

The input file *shimo.dat* is the following:

```
C
C insert first inner layer polar shim dimesion
C and then outer layer polar shim dimension.
C
0.2 0.8
```

The output file magn.inp which is loaded by the magnetostatic code is the following:

```
6 2 1 98
nc r phi alp width thick1 thick2 n1 n2
9 43.900 0.157 0.000 15.4 1.616 1.856 2 18
16 43.900 21.90 27.00 15.4 1.616 1.856 2 18
5 28.000 0.246 0.000 15.4 1.973 2.307 2 14
5 28.000 22.02 24.080 15.4 1.973 2.307 2 14
3 28.000 47.710 48.000 15.4 1.973 2.307 2 14
2 28.000 66.710 68.500 15.4 1.973 2.307 2 14
```

C.2 Hard copper wedge code

The file *Shimodis.f* for symmetric geometrical computations of conductor positioning inside the coil after a polar shim insertion with the hard copper wedges approximation is the following:

Program shimodis

```
parameter(nbt=50)
real r(nbt),p(nbt),a(nbt)
real th1(nbt),th2(nbt),wi(nbt)

integer nf1(nbt),nf2(nbt)
integer nc(nbt)
character*70 str

pi=datan(1.d0)*4
open(1,file='base.inp',status='old')
read(1,*) nbl,nca,isym,riron
read(1,'(a70)') str
do i=1,nbl
  read(1,*) nc(i),r(i),p(i),a(i),
  .      wi(i),th1(i),th2(i),nf1(i),nf2(i)
end do
close(1)

open(1,file='shimo.dat',status='old')
read(1,*) shi,sho
```

```

      close(1)
C
C-----
C
      p(2)=p(2)-nc(1)*(sho-0.8)/25/r(2)*180/3.141592654
      p(4)=p(4)-nc(3)*(shi-0.2)/15/r(4)*180/3.141592654
      p(5)=p(5)-(nc(3)+nc(4))*(shi-0.2)/15/r(5)*180/3.141592654
      p(6)=p(6)-(nc(3)+nc(4)+nc(5))*(shi-0.2)/15/r(6)*180/3.141592654
      th1(1)=th1(1)-(sho-0.8)/25
      th1(2)=th1(2)-(sho-0.8)/25
      th1(3)=th1(3)-(shi-0.2)/15
      th1(4)=th1(4)-(shi-0.2)/15
      th1(5)=th1(5)-(shi-0.2)/15
      th1(6)=th1(6)-(shi-0.2)/15
      th2(1)=th2(1)-(sho-0.8)/25
      th2(2)=th2(2)-(sho-0.8)/25
      th2(3)=th2(3)-(shi-0.2)/15
      th2(4)=th2(4)-(shi-0.2)/15
      th2(5)=th2(5)-(shi-0.2)/15
      th2(6)=th2(6)-(shi-0.2)/15
C
C-----
C

      open(1,file='magn.inp',status='unknown')
      write(1,(i3,i4,i4,2x,f10.0)) nbl,nca,isym,riron
      write(1,'(a70)') str
      do i=1,nbl
         write(1,(i4,2x,3f8.3,f10.1,f10.3,f8.3,i4,i5))
         .      nc(i),r(i),p(i),a(i),
         .      wi(i),th1(i),th2(i),nf1(i),nf2(i)
      end do
      close(1)

      end

```

The input file *shimo.dat* and the output file *magn.inp* are the same as for the file *shimomo.f*, reported in Section C.1. Conductor positions written on the outputfile are then loaded by the magnetostatic code.

C.3 Asymmetric code

The file *Shibia.f* for asymmetric geometrical computations of conductor positioning inside a coil with non-nominal azimuthal size and for the insertion of non-nominal polar shim and of polyimide sheet in the median plane with the hard copper wedges approximation is the following:

Program shibia.f

```
parameter(nbt=50)
real r(nbt),p(nbt),a(nbt)
real th1(nbt),th2(nbt),wi(nbt),int(nbt)
real cw(nbt),ptn(nbt),psn(nbt)
real psm(nbt),Apn(nbt),shosx(nbt)
real shisx(nbt),shodx(nbt),shidx(nbt)
real Ap(nbt),ptop(nbt),pbot(nbt),th1m(nbt),th2m(nbt)
real th1n(nbt),th2n(nbt),delta(nbt),dosx(nbt),disx(nbt)
real didx(nbt),dodx(nbt)
integer nf1(nbt),nf2(nbt)
integer nc(nbt)
character*70 str
```

```
pi=datan(1.d0)*4
open(1,file='base.inp',status='old')
read(1,*) nbl,nca,ism,riron
read(1,'(a70)') str
do i=1,nbl
  read(1,*) nc(i),r(i),p(i),a(i),
  .      wi(i),th1(i),th2(i),nf1(i),nf2(i),int(i)
end do
close(1)
open(1,file='biashi.dat',status='old')
do i=1,4
  read(1,*) shosx(i),shisx(i),shidx(i),shodx(i)
end do
do i=1,2
  read(1,*) dosx(i),disx(i),didx(i),dodx(i)
end do
close(1)
```

```
C=====
C computing delta for blocks 1,2,7,8,13,14,19 and 20
do i=1,2
  delta(i)=dodx(1)-dodx(2)
  delta(i+6)=dosx(1)-dosx(2)
```

```

    delta(i+12)=dosx(2)-dosx(1)
    delta(i+18)=dodx(2)-dodx(1)
end do

```

C computing delta for the other blocks

```

do i=3,6
    delta(i)=didx(1)-didx(2)
    delta(i+6)=disx(1)-disx(2)
    delta(i+12)=disx(2)-disx(1)
    delta(i+18)=didx(2)-didx(1)
end do

```

C computing phi for non nominal azimuthal length dimensions

```

do i=0,3
    p(1+i*6)=p(1+i*6)-delta(1+i*6)/r(1+i*6)*180/3.141592654
    p(2+i*6)=p(2+i*6)-delta(2+i*6)/r(2+i*6)*180/3.141592654*
    .   nc(2+i*6)/(nc(1+i*6)+nc(2+i*6))
    p(3+i*6)=p(3+i*6)-delta(3+i*6)/r(3+i*6)*180/3.141592654
    p(4+i*6)=p(4+i*6)-delta(4+i*6)/r(4+i*6)*180/3.141592654*
    .   (nc(4+i*6)+nc(5+i*6)+nc(6+i*6))/(nc(3+i*6)+nc(4+i*6)+
    .   nc(5+i*6)+nc(6+i*6))
    p(5+i*6)=p(5+i*6)-delta(5+i*6)/r(5+i*6)*180/3.141592654*
    .   (nc(5+i*6)+nc(6+i*6))/(nc(3+i*6)+nc(4+i*6)+
    .   nc(5+i*6)+nc(6+i*6))
    p(6+i*6)=p(6+i*6)-delta(6+i*6)/r(6+i*6)*180/3.141592654*
    .   nc(6+i*6)/(nc(3+i*6)+nc(4+i*6)+nc(5+i*6)+nc(6+i*6))
end do

```

C computing th1 for blocks belonging to outer layers

```

do j=0,3
    do i=1,2
        th1(i+j*6)=th1(i+j*6)+delta(i+j*6)/(nc(1+j*6)+nc(2+j*6))
    end do
end do

```

C computing th1 for blocks belonging to inner layers

```

do j=0,3
    do i=3,6
        th1(i+j*6)=th1(i+j*6)+delta(i+j*6)/
    .   (nc(3+j*6)+nc(4+j*6)+nc(5+j*6)+nc(6+j*6))
    end do
end do

```

C computing th2 for blocks belonging to outer layers

```

do j=0,3
    do i=1,2
        th2(i+j*6)=th2(i+j*6)+delta(i+j*6)/(nc(1+j*6)+nc(2+j*6))
    end do
end do

```

```

        end do
    end do

C   computing th2 for blocks belonging to inner layers
    do j=0,3
        do i=3,6
            th2(i+j*6)=th2(i+j*6)+delta(i+j*6)/
                (nc(3+j*6)+nc(4+j*6)+nc(5+j*6)+nc(6+j*6))
        end do
    end do

C   copper wedges fixed dimensions
    cw(1)=2.718437
    cw(2)=1.840442
    cw(3)=5.633472
    cw(4)=6.967788

C   angular amplitude of outer and inner layer
    ptn(1)=113.29006
    ptn(2)=150.89019

C   angular amplitude of conductor occupied layer
    psn(1)=ptn(1)-2*cw(1)-p(1)-p(19)
    psn(2)=ptn(2)-2*(cw(2)+cw(3)+cw(4))-p(3)-p(21)
    psn(3)=ptn(2)-2*(cw(2)+cw(3)+cw(4))-p(9)-p(15)
    psn(4)=ptn(1)-2*cw(1)-p(7)-p(13)

C   angular amplitude of conductors blocks before applying shims
    do i=1,4
        Apn(1+(i-1)*6)=p(2+(i-1)*6)-p(1+(i-1)*6)-cw(1)
        Apn(2+(i-1)*6)=ptn(1)/2-p(2+(i-1)*6)
        Apn(3+(i-1)*6)=p(4+(i-1)*6)-p(3+(i-1)*6)-cw(2)
        Apn(4+(i-1)*6)=p(5+(i-1)*6)-p(4+(i-1)*6)-cw(3)
        Apn(5+(i-1)*6)=p(6+(i-1)*6)-p(5+(i-1)*6)-cw(4)
        Apn(6+(i-1)*6)=ptn(2)/2-p(6+(i-1)*6)
    end do

C   shim difference from nominal dimensions
    shosx(1)=shosx(1)-0.8
    shosx(4)=shosx(4)-0.8
    shisx(1)=shisx(1)-0.2
    shisx(4)=shisx(4)-0.2
    shidx(1)=shidx(1)-0.2
    shidx(4)=shidx(4)-0.2
    shodx(1)=shodx(1)-0.8
    shodx(4)=shodx(4)-0.8

```

```

C   new angular amplitude due to shim insertion (infinitely
C   stiff copper wedges and collars)
psm(1)=psn(1)-(shodx(1)/r(2)+shodx(2)/r(1)+shodx(3)/r(19)
.+shodx(4)/r(20))*180/3.141592654
psm(2)=psn(2)-(shidx(1)/r(6)+shidx(2)/r(3)+shidx(3)/r(21)
.+shidx(4)/r(24))*180/3.141592654
psm(3)=psn(3)-(shisx(1)/r(12)+shisx(2)/r(9)+shisx(3)/r(15)
.+shisx(4)/r(18))*180/3.141592654
psm(4)=psn(4)-(shosx(1)/r(8)+shosx(2)/r(7)+shosx(3)/r(13)
.+shosx(4)/r(14))*180/3.141592654

C   conductor block new angular amplitude computation
C   for blocks belonging to right outer layer
do k=1,2
  do i=1,2
    Ap(i+(k-1)*18)=Apn(i+(k-1)*18)*psm(1)/psn(1)
  end do
end do

C   for blocks belonging to right inner layer
do k=1,2
  do i=3,6
    Ap(i+(k-1)*18)=Apn(i+(k-1)*18)*psm(2)/psn(2)
  end do
end do

C   for blocks belonging to left inner layer
do k=1,2
  do i=9,12
    Ap(i+(k-1)*6)=Apn(i+(k-1)*6)*psm(3)/psn(3)
  end do
end do

C   for blocks belonging to left outer layer
do k=1,2
  do i=7,8
    Ap(i+(k-1)*6)=Apn(i+(k-1)*6)*psm(4)/psn(4)
  end do
end do

C   starting point for geometry reconstruction computation
ptop(1)=ptn(1)/2-shodx(1)/r(2)*180/3.141592654
ptop(2)=ptn(2)/2-shidx(1)/r(6)*180/3.141592654
ptop(3)=ptn(2)/2-shisx(1)/r(12)*180/3.141592654
ptop(4)=ptn(1)/2-shosx(1)/r(8)*180/3.141592654
pbot(1)=ptn(1)/2-shodx(4)/r(20)*180/3.141592654
pbot(2)=ptn(2)/2-shidx(4)/r(24)*180/3.141592654

```

```
pbot(3)=ptn(2)/2-shisx(4)/r(18)*180/3.141592654
pbot(4)=ptn(1)/2-shosx(4)/r(14)*180/3.141592654
```

C computation of phi values

```
p(2)=ptop(1)-Ap(2)
p(6)=ptop(2)-Ap(6)
p(12)=ptop(3)-Ap(12)
p(8)=ptop(4)-Ap(8)
p(14)=pbot(4)-Ap(14)
p(18)=pbot(3)-Ap(18)
p(24)=pbot(2)-Ap(24)
p(20)=pbot(1)-Ap(20)
do i=1,4
  p(1+(i-1)*6)=p(2+(i-1)*6)-cw(1)-Ap(1+(i-1)*6)
  p(5+(i-1)*6)=p(6+(i-1)*6)-cw(4)-Ap(5+(i-1)*6)
  p(4+(i-1)*6)=p(5+(i-1)*6)-cw(3)-Ap(4+(i-1)*6)
  p(3+(i-1)*6)=p(4+(i-1)*6)-cw(2)-Ap(3+(i-1)*6)
end do
do k=1,2
  do i=1,2
    th2(i+(k-1)*18)=th2(i+(k-1)*18)+th1(i+(k-1)*18)*
.(psm(1)/psn(1)-1)
  end do
end do
do k=1,2
  do i=3,6
    th2(i+(k-1)*18)=th2(i+(k-1)*18)+th1(i+(k-1)*18)*
.(psm(2)/psn(2)-1)
  end do
end do
do k=1,2
  do i=9,12
    th2(i+(k-1)*6)=th2(i+(k-1)*6)+th1(i+(k-1)*6)*
.(psm(3)/psn(3)-1)
  end do
end do
do k=1,2
  do i=7,8
    th2(i+(k-1)*6)=th2(i+(k-1)*6)+th1(i+(k-1)*6)*
.(psm(4)/psn(4)-1)
  end do
end do
```

C

```
do k=1,2
  do i=1,2
    th1(i+(k-1)*18)=th1(i+(k-1)*18)*psm(1)/psn(1)
```

```

        end do
    end do
    do k=1,2
        do i=3,6
            th1(i+(k-1)*18)=th1(i+(k-1)*18)*psm(2)/psn(2)
        end do
    end do
    do k=1,2
        do i=9,12
            th1(i+(k-1)*6)=th1(i+(k-1)*6)*psm(3)/psn(3)
        end do
    end do
    do k=1,2
        do i=7,8
            th1(i+(k-1)*6)=th1(i+(k-1)*6)*psm(4)/psn(4)
        end do
    end do
end do

```

```

C=====
open(1,file='magna.inp',status='unknown')
write(1,'(i3,i4,i4,2x,f10.0)') nbl,nca,isym,riron
write(1,'(a70)') str
do i=1,nbl
    write(1,'(i4,2x,3f8.3,f10.1,f10.3,f8.3,i4,i5,f6.0)')
    .      nc(i),r(i),p(i),a(i),
    .      wi(i),th1(i),th2(i),nf1(i),nf2(i),int(i)
end do
close(1)
end

```

The input file *biashi.dat* is the following:

```

0.8 0.2  0.2  0.8
0.0 0.0  0.0  0.0
0.0 0.0  0.0  0.0
0.8 0.2  0.2  0.8
0.0 0.0  0.0  0.0
0.0 0.0  0.0  0.0

```

where each column corresponds to a layer (outer left layer, inner left layer, inner right layer and outer right layer). The first and fourth rows contain used polar shim dimensions for upper and lower poles. The second and third rows contains the used thickness in the median plane. The last two rows contain the difference from nominal value of upper and lower half layer.

The output file magna.inp, which is the input file for the magnetostatic model, is the following:

```

24 2 0 100000.
nc   r   phi   alp   width  thick1  thick2  n1n2  I
  9 43.900 0.157 0.000   15.4   1.620  1.860  2 18  1.
 16 43.900 21.900 27.000   15.4   1.620  1.860  2 18  1.
  5 28.000 0.246 0.000   15.4   1.973  2.307  2 14  1.
  5 28.000 22.020 24.080   15.4   1.973  2.307  2 14  1.
  3 28.000 47.710 49.000   15.4   1.973  2.307  2 14  1.
  2 28.000 66.710 68.500   15.4   1.973  2.307  2 14  1.
  9 43.900 0.157 0.000   15.4   1.620  1.860  2 18 -1.
 16 43.900 21.900 27.000   15.4   1.620  1.860  2 18 -1.
  5 28.000 0.246 0.000   15.4   1.973  2.307  2 14 -1.
  5 28.000 22.020 24.080   15.4   1.973  2.307  2 14 -1.
  3 28.000 47.710 48.000   15.4   1.973  2.307  2 14 -1.
  2 28.000 66.710 68.500   15.4   1.973  2.307  2 14 -1.
  9 43.900 0.157 0.000   15.4   1.620  1.860  2 18 -1.
 16 43.900 21.900 27.000   15.4   1.620  1.860  2 18 -1.
  5 28.000 0.246 0.000   15.4   1.973  2.307  2 14 -1.
  5 28.000 22.020 24.080   15.4   1.973  2.307  2 14 -1.
  3 28.000 47.710 48.000   15.4   1.973  2.307  2 14 -1.
  2 28.000 66.710 68.500   15.4   1.973  2.307  2 14 -1.
  9 43.900 0.157 0.000   15.4   1.620  1.860  2 18  1.
 16 43.900 21.900 27.000   15.4   1.620  1.860  2 18  1.
  5 28.000 0.246 0.000   15.4   1.973  2.307  2 14  1.
  5 28.000 22.020 24.080   15.4   1.973  2.307  2 14  1.
  3 28.000 47.710 48.000   15.4   1.973  2.307  2 14  1.
  2 28.000 66.710 68.500   15.4   1.973  2.307  2 14  1.

```

where each row contains data relative to a block, from number 1 (the first row) to number 24 (the last row) in sequence.

Appendix D

Statistical notes and normality test results

Here some notes on the statistical methods used in the work are reported. For further reading, the reader may address to [35], [21], [36] and [37].

D.1 Normality test

Usually it is assumed that sample data coming from measurements affected only by random errors can be represented by a normal distribution. To assess if a given sample can be really characterized in terms on normal probability function a test is needed. One of the most applied tests is the one of χ^2 , which is a number used to quantify the discrepancy between the measured frequency of a number and the attended frequency as it can be derived from the normal distribution equation of the same measured value. It is defined as follows:

$$\chi^2 = \frac{1}{d} \sum_{k=1}^n \frac{(O_k - E_k)^2}{E_k} \quad (\text{D.1})$$

where O_k is the observed number of measures with a same value (or in a same bin) and E_k is the expected number of measures with the same value (or belonging to the same bin) that results from the normal probability distribution describing a sample binned in n intervals. d is called *freedom degree*, and it is computed as it follows:

$$d = n - c \quad (\text{D.2})$$

where c is the number of parameters that must be computed out of the sample data to calculate E_k . If the sample has been taken from a perfect normal distribution, then $\tilde{\chi}^2 = 0$. But if the sample cannot be described by the normal distribution, no certain indication can be argued from the value of $\tilde{\chi}^2$. A statistical approach must then be used. The sample does not follow a normal distribution if the probability of $\tilde{\chi}^2$ being bigger than computed is

low. The *confidence level* is a number which quantify at what level a statistical hypothesis can be rejected. Usually the confidence level is chosen to be 1% or 5%. The hypothesis that the sample follows the normal distribution (also called *Gaussian* distribution) can then be rejected if the probability that $\tilde{\chi}^2$ is greater than computed is lower than the chosen confidence level. The probability for $\tilde{\chi}^2$ being larger than the computed value $\tilde{\chi}_0^2$ is expressed as follows:

$$P_d(\tilde{\chi}^2 \geq \tilde{\chi}_0^2) = \frac{2}{d} \frac{\int_{\tilde{\chi}_0^2}^{\infty} x^{d-1} e^{-\frac{x^2}{2}} dx}{2^{\frac{d}{2}} \Gamma\left(\frac{d}{2}\right)} \quad (D.3)$$

where $\Gamma\left(\frac{d}{2}\right)$ is defined as follows:

$$\Gamma\left(\frac{d}{2}\right) = \int_0^{\infty} e^{-t} t^{\frac{d}{2}-1} dt \quad (D.4)$$

But if $P_d(\tilde{\chi}^2 \geq \tilde{\chi}_0^2) \geq 5\%$, the hypothesis cannot be rejected and the sample is said to be compatible with the normal distribution. This means that we are not sure that the sample follows a normal distribution, but we can say that the data distribution can be satisfactorily described by a Gaussian probability distribution.

D.2 Normality test results

Results for the normality test are given in Table D.1 for normal multipoles and in Table D.2 for skew multipoles.

Table D.1 Normality test results given for the straight part normal multipoles featured by collared coils manufactured by the three firms during the pre-series.

	Firm1		Firm2		Firm3	
	$\tilde{\chi}_0^2$	$P(\tilde{\chi}^2 > \tilde{\chi}_0^2)$	$\tilde{\chi}_0^2$	$(\tilde{\chi}^2 > \tilde{\chi}_0^2)$	$\tilde{\chi}_0^2$	$P(\tilde{\chi}^2 > \tilde{\chi}_0^2)$
C_1	0.43	100	3.63	90	3.76	88
b_2	3.04	93	4.53	81	1.42	99

Table D.1 Normality test results given for the straight part normal multipoles featured by collared coils manufactured by the three firms during the pre-series.

	Firm1		Firm2		Firm3	
	$\tilde{\chi}_0^2$	$P(\tilde{\chi}^2 > \tilde{\chi}_0^2)$	$\tilde{\chi}_0^2$	$P(\tilde{\chi}^2 > \tilde{\chi}_0^2)$	$\tilde{\chi}_0^2$	$P(\tilde{\chi}^2 > \tilde{\chi}_0^2)$
b_3	3.08	93	0.99	100	0.58	100
b_4	3.40	91	4.23	84	1.84	98
b_5	3.76	88	0.27	100	0.74	100
b_6	0.56	100	4.95	76	0.92	100
b_7	5.21	73	4.34	82	6.55	59
b_8	0.49	100	3.28	92	3.04	93
b_9	4.17	84	0.43	100	0.45	100
b_{10}	1.04	100	0.44	100	1.01	100
b_{11}	0.48	100	3.52	90	0.28	100
b_{12}	0.22	100	0.56	100	0.50	100
b_{13}	3.77	88	3.55	90	1.36	100
b_{14}	0.52	100	0.26	100	0.35	100
b_{15}	0.33	100	0.41	100	2.73	95

Table D.2 Normality test results given for the straight part skew multipoles featured by collared coils manufactured by the three firms during the pre-series.

	Firm1		Firm2		Firm3	
	$\tilde{\chi}_0^2$	$P(\tilde{\chi}^2 > \tilde{\chi}_0^2)$	$\tilde{\chi}_0^2$	$P(\tilde{\chi}^2 > \tilde{\chi}_0^2)$	$\tilde{\chi}_0^2$	$P(\tilde{\chi}^2 > \tilde{\chi}_0^2)$
a_1	0.40	100	3.74	88	0.33	100
a_2	0.10	100	0.47	100	6.23	63
a_3	1.42	99	1.06	100	0.37	100
a_4	0.26	100	0.43	100	13.06	11
a_5	0.63	100	0.30	100	10.29	25
a_6	0.90	100	2.35	97	0.13	100

Table D.2 Normality test results given for the straight part skew multipoles featured by collared coils manufactured by the three firms during the pre-series.

	Firm1		Firm2		Firm3	
	$\tilde{\chi}_0^2$	$P(\tilde{\chi}^2 > \tilde{\chi}_0^2)$	$\tilde{\chi}_0^2$	$P(\tilde{\chi}^2 > \tilde{\chi}_0^2)$	$\tilde{\chi}_0^2$	$P(\tilde{\chi}^2 > \tilde{\chi}_0^2)$
a_7	2.90	94	3.47	90	1.22	100
a_8	0.55	100	0.25	100	0.16	100
a_9	1.45	99	0.85	100	0.27	100
a_{10}	0.41	100	3.29	91	0.77	100
a_{11}	1.37	99	0.50	100	0.5	100
a_{12}	0.68	100	2.00	98	0.34	100
a_{13}	0.36	100	0.74	100	1.12	100
a_{14}	0.10	100	0.21	100	0.78	100
a_{15}	0.86	100	1.54	99	2.74	95

Appendix E

The macro used to monitor collared coil production

The code of the macro used to analyze the magnetic measurements at room temperature performed on the collared coils is the following:

```
Sub collared_coil_analysis()
=====
*****
=====
'
' macro for calculations and check performing on collared coil data
' calculations are made in Worksheets at the bottom for the 2 aperture
'
=====
*****
=====
'
' UPROTECTING SHEETS
'
=====
Sheets("Alarm sheet").Unprotect
Sheets("Work sheet").Unprotect
Sheets("Summary Data").Unprotect
'
=====
'
' PARAMETRES CALCULATION
'
=====
'
' Subtracting shim contribution
' to multipoles b1 b3 b5 b7 b9 b11
'
' multipoles b1 b3 b5 b7 b9 b11 for aperture 1
'
Sheets("Work sheet").Range("b154").Formula = _
    "=average('Summary Data'!d2:s2)*(1-a225*(average('Assembly Data'!j11:k12)-'Assembly Data'!c10)/10000-b225*(average('Assembly Data'!i11:i12,'Assembly Data'!l11:l12)-'Assembly Data'!f10)/10000)"
Sheets("Work sheet").Range("b158").Formula = _
    "=average('Summary Data'!c7:t7)-c225*(average('Assembly Data'!j11:k12)-'Assembly Data'!c10)-d225*(average('Assembly Data'!i11:i12,'Assembly Data'!l11:l12)-'Assembly Data'!f10)"
Sheets("Work sheet").Range("b160").Formula = _
```

```
"=average('Summary Data'!c9:t9)-e225*(average('Assembly Data'!j11:k12)-'Assembly Data'!c10)-f225*(average('Assembly Data'!i11:i12,'Assembly Data'!l11:l12)-'Assembly Data'!f10)"
Sheets("Work sheet").Range("b162").Formula = _
"=average('Summary Data'!c11:t11)-g225*(average('Assembly Data'!j11:k12)-'Assembly Data'!c10)-h225*(average('Assembly Data'!i11:i12,'Assembly Data'!l11:l12)-'Assembly Data'!f10)"
Sheets("Work sheet").Range("b164").Formula = _
"=average('Summary Data'!c13:t13)-i225*(average('Assembly Data'!j11:k12)-'Assembly Data'!c10)-j225*(average('Assembly Data'!i11:i12,'Assembly Data'!l11:l12)-'Assembly Data'!f10)"
Sheets("Work sheet").Range("b166").Formula = _
"=average('Summary Data'!c15:t15)-k225*(average('Assembly Data'!j11:k12)-'Assembly Data'!c10)-l225*(average('Assembly Data'!i11:i12,'Assembly Data'!l11:l12)-'Assembly Data'!f10)"
```

'multipoles b1 b3 b5 b7 b9 b11 for aperture 2

```
Sheets("Work sheet").Range("b189").Formula = _
"=average('Summary Data'!aa2:ap2)*(1-a225*(average('Assembly Data'!o11:p12)-'Assembly Data'!c10)/10000-b225*(average('Assembly Data'!n11:n12,'Assembly Data'!q11:q12)-'Assembly Data'!f10)/10000)"
Sheets("Work sheet").Range("b193").Formula = _
"=average('Summary Data'!z7:aq7)-c225*(average('Assembly Data'!o11:p12)-'Assembly Data'!c10)-d225*(average('Assembly Data'!n11:n12,'Assembly Data'!q11:q12)-'Assembly Data'!f10)"
Sheets("Work sheet").Range("b195").Formula = _
"=average('Summary Data'!z9:aq9)-e225*(average('Assembly Data'!o11:p12)-'Assembly Data'!c10)-f225*(average('Assembly Data'!n11:n12,'Assembly Data'!q11:q12)-'Assembly Data'!f10)"
Sheets("Work sheet").Range("b197").Formula = _
"=average('Summary Data'!z11:aq11)-g225*(average('Assembly Data'!o11:p12)-'Assembly Data'!c10)-h225*(average('Assembly Data'!n11:n12,'Assembly Data'!q11:q12)-'Assembly Data'!f10)"
Sheets("Work sheet").Range("b199").Formula = _
"=average('Summary Data'!z13:aq13)-i225*(average('Assembly Data'!o11:p12)-'Assembly Data'!c10)-j225*(average('Assembly Data'!n11:n12,'Assembly Data'!q11:q12)-'Assembly Data'!f10)"
Sheets("Work sheet").Range("b201").Formula = _
"=average('Summary Data'!z15:aq15)-k225*(average('Assembly Data'!o11:p12)-'Assembly Data'!c10)-l225*(average('Assembly Data'!n11:n12,'Assembly Data'!q11:q12)-'Assembly Data'!f10)"
```

```
'=====
'
' CHART ANS SHEET FORMATTING
'=====
'
```

```
'*****
'Formatting previous yellow and red cells in Summary sheet'
'in Work sheet and in Alarm sheet
'*****
```

```
Worksheets("Summary Data").Range("B2:v44,y2:as44").Interior.ColorIndex = xlNone
Worksheets("Work sheet").Range("b151:w219,b221").Interior.ColorIndex = xlNone
With Worksheets("Alarm sheet").Range("b5,g5,b8:e37,g8:j37,b38:b39,g38:g39")
    .FormulaR1C1 = "status ok"
    .Interior.ColorIndex = 4
End With
With Worksheets("Alarm sheet").Range("b9,g9")
    .ClearContents
    .Interior.ColorIndex = xlNone
    .Interior.Pattern = xlUp
End With
```

```
*****
'cross section evaluation
*****
new_cs_bound = Worksheets("Work sheet").Range("b228").Value
answer = StrConv(new_cs_bound, 1)
If Worksheets("Assembly Data").Range("e2").Value = 2 Then
  If answer = "NO" Then
    For i = 1 To 3
      Sheets(10 + i).Unprotect
      Sheets(10 + i).Activate
      b3_s = Range("b12").Value
      b5_s = Range("b14").Value
      b7_s = Range("b16").Value
      b9_s = Range("b18").Value
      b11_s = Range("b20").Value
      b3_cs = Range("j12").Value
      b5_cs = Range("j14").Value
      b7_cs = Range("j16").Value
      b9_cs = Range("j18").Value
      b11_cs = Range("j20").Value
      b3_ncs = Range("n12").Value
      b5_ncs = Range("n14").Value
      b7_ncs = Range("n16").Value
      b9_ncs = Range("n18").Value
      b11_ncs = Range("n20").Value
      Range("b12").Value = b3_s - 4
      Range("b14").Value = b5_s - 1.3
      Range("b16").Value = b7_s + 0.3
      Range("b18").Value = b9_s + 0.2
      Range("b20").Value = b11_s + 0
      Range("j12").Value = b3_cs - 1.6
      Range("j14").Value = b5_cs + 0.7
      Range("j16").Value = b7_cs + 0.4
      Range("j18").Value = b9_cs + 0.3
      Range("j20").Value = b11_cs + 0
      Range("n12").Value = b3_ncs - 8.1
      Range("n14").Value = b5_ncs + 0.7
      Range("n16").Value = b7_ncs + 0.2
      Range("n18").Value = b9_ncs + 0.2
      Range("n20").Value = b11_ncs + 0
      Sheets(10 + i).Protect DrawingObjects:=True, Contents:=True, Scenarios:=True
    Next i
    Worksheets("Work sheet").Range("b228").Value = "yes"
  End If
End If
*****
'changing name from firm sheet for bound to Bound Sheet
'in order to use different bound values for different
'firm
*****
foglio = 0
If Worksheets("Original data").Range("c4").FormulaR1C1 = "Alstom" Then
  Sheets("Alstom Bound").Name = "Bound sheet"
  foglio = 1
```

```

ElseIf Worksheets("Original data").Range("c4").FormulaR1C1 = "Ansaldo" Then
    foglio = 2
    Sheets("Ansaldo Bound").Name = "Bound sheet"
Else
    Sheets("Noell Bound").Name = "Bound Sheet"
    foglio = 3
End If
'====='
'Version Evaluation
'====='
M_v = Sheets("Assembly Data").Range("m20").Value
Macro_version = StrConv(M_v, 1)
y_al_str3 = "yellow alarm"
y_al_num3 = 6
If Macro_version = "CERN" Then
    y_al_str = "yellow alarm"
    y_al_num1 = 6
    y_al_num2 = 6
Else
    y_al_str = "status ok"
    y_al_num1 = 4
    y_al_num2 = xlNone
End If
'====='
'====='
'
'
'   MAIN FIELD COMPONENT MODULE
'
'====='
'====='
'====='
'dB/B checks for inner points from position 3 to 18'
'for both aperture.
'====='
For i = 1 To 2
    For j = 1 To 16
        If Sheets("Work sheet").Cells(154 + (i - 1) * 35, 4 + j).Value > _
            Sheets("Bound sheet").Cells(46, 7).Value Or _
            Sheets("Work sheet").Cells(154 + (i - 1) * 35, 4 + j).Value < _
            Sheets("Bound sheet").Cells(46, 6).Value Then
            If Sheets("Alarm sheet").Cells(8, 3 + (i - 1) * 5).Interior.ColorIndex = 4 Then
                With Sheets("Alarm sheet").Cells(8, 3 + (i - 1) * 5)
                    .FormulaR1C1 = y_al_str
                    .Interior.ColorIndex = y_al_num1
                End With
            End If
            Sheets("Work sheet").Cells(154 + (i - 1) * 35, 4 + j).Interior.ColorIndex = y_al_num2 `yellow
            Sheets("Summary Data").Cells(2, 3 + j + (i - 1) * 23).Interior.ColorIndex = y_al_num2 `yellow
        End If
        If Sheets("Work sheet").Cells(154 + (i - 1) * 35, 4 + j).Value > _
            Sheets("Bound sheet").Cells(46, 9).Value Or _
            Sheets("Work sheet").Cells(154 + (i - 1) * 35, 4 + j).Value < _
            Sheets("Bound sheet").Cells(46, 8).Value Then
            With Sheets("Alarm sheet").Cells(8, 3 + (i - 1) * 5)

```



```

        .FormulaR1C1 = "red alarm"
        .Interior.ColorIndex = 3
    End With
    Sheets("Work sheet").Cells(154 + (i - 1) * 35, 4 + j).Interior.ColorIndex = 3 'red
    Sheets("Summary Data").Cells(2, 3 + j + (i - 1) * 23).Interior.ColorIndex = 3 'red
End If
Next j
Next i
*****

'dB/B check for horn positions
'for both aperture
'alarm cell same than that for inner pos.
*****

For i = 1 To 2
    For j = 1 To 2
        If Sheets("Work sheet").Cells(154 + (i - 1) * 35, 4 + (j - 1) * 17).Value > _
            Sheets("Bound sheet").Cells(46, 19).Value Or _
            Sheets("Work sheet").Cells(154 + (i - 1) * 35, 4 + (j - 1) * 17).Value < _
            Sheets("Bound sheet").Cells(46, 18).Value Then
            If Sheets("Alarm sheet").Cells(8, 3 + (i - 1) * 5).Interior.ColorIndex = 4 Then
                With Sheets("Alarm sheet").Cells(8, 3 + (i - 1) * 5)
                    .FormulaR1C1 = y_al_str
                    .Interior.ColorIndex = y_al_num1
                End With
            End If
            Sheets("Work sheet").Cells(154 + (i - 1) * 35, 4 + (j - 1) * 17).Interior.ColorIndex = y_al_num2
            Sheets("Summary Data").Cells(2, 3 + (j - 1) * 17 + (i - 1) * 23).Interior.ColorIndex = y_al_num2
        End If
        If Sheets("Work sheet").Cells(154 + (i - 1) * 35, 4 + (j - 1) * 17).Value > _
            Sheets("Bound sheet").Cells(46, 21).Value Or _
            Sheets("Work sheet").Cells(154 + (i - 1) * 35, 4 + (j - 1) * 17).Value < _
            Sheets("Bound sheet").Cells(46, 20).Value Then
            With Sheets("Alarm sheet").Cells(8, 3 + (i - 1) * 5)
                .FormulaR1C1 = "red alarm"
                .Interior.ColorIndex = 3
            End With
            Sheets("Work sheet").Cells(154 + (i - 1) * 35, 4 + (j - 1) * 17).Interior.ColorIndex = 3
            Sheets("Summary Data").Cells(2, 3 + (j - 1) * 17 + (i - 1) * 23).Interior.ColorIndex = 3
        End If
    Next j
Next i
*****

'checking mean dB/B between heads
'for both aperture
*****

For i = 1 To 2
    If Sheets("Work sheet").Cells(152 + (i - 1) * 35, 2).Value > _
        Sheets("Bound sheet").Cells(43, 3).Value Or _
        Sheets("Work sheet").Cells(152 + (i - 1) * 35, 2).Value < _
        Sheets("Bound sheet").Cells(43, 2).Value Then
        With Sheets("Alarm sheet").Cells(8, 4 + (i - 1) * 5)
            .FormulaR1C1 = y_al_str
            .Interior.ColorIndex = y_al_num1
        End With
    End If
Next i

```

```

With Sheets("Alarm sheet").Cells(8, 5 + (i - 1) * 5)
    .FormulaR1C1 = y_al_str
    .Interior.ColorIndex = y_al_num1
End With
Sheets("Work sheet").Cells(152 + (i - 1) * 35, 2).Interior.ColorIndex = y_al_num2 `yellow
Sheets("Summary Data").Cells(2, 21 + (i - 1) * 23).Interior.ColorIndex = y_al_num2 `yellow
Sheets("Summary Data").Cells(2, 2 + (i - 1) * 23).Interior.ColorIndex = y_al_num2 `yellow
End If
If Sheets("Work sheet").Cells(152 + (i - 1) * 35, 2).Value > _
    Sheets("Bound sheet").Cells(43, 5).Value Or _
    Sheets("Work sheet").Cells(152 + (i - 1) * 35, 2).Value < _
    Sheets("Bound sheet").Cells(43, 4).Value Then
With Sheets("Alarm sheet").Cells(8, 4 + (i - 1) * 5)
    .FormulaR1C1 = "red alarm"
    .Interior.ColorIndex = 3
End With
With Sheets("Alarm sheet").Cells(8, 5 + (i - 1) * 5)
    .FormulaR1C1 = "red alarm"
    .Interior.ColorIndex = 3
End With
Sheets("Work sheet").Cells(152 + (i - 1) * 35, 2).Interior.ColorIndex = 3
Sheets("Summary Data").Cells(2, 21 + (i - 1) * 23).Interior.ColorIndex = 3
Sheets("Summary Data").Cells(2, 2 + (i - 1) * 23).Interior.ColorIndex = 3
End If
Next i
*****
`dB/B for head1 CS
`for both aperture
*****
For i = 1 To 2
    If Sheets("Work sheet").Cells(154 + (i - 1) * 35, 3).Value > _
        Sheets("Bound sheet").Cells(46, 11).Value Or _
        Sheets("Work sheet").Cells(154 + (i - 1) * 35, 3).Value < _
        Sheets("Bound sheet").Cells(46, 10).Value Then
        If Sheets("Alarm sheet").Cells(8, 4 + (i - 1) * 5).Interior.ColorIndex = 4 Then
            With Sheets("Alarm sheet").Cells(8, 4 + (i - 1) * 5)
                .FormulaR1C1 = y_al_str
                .Interior.ColorIndex = y_al_num1
            End With
            Sheets("Summary Data").Cells(2, 2 + (i - 1) * 23).Interior.ColorIndex = y_al_num2 `yellow
        End If
        Sheets("Work sheet").Cells(154 + (i - 1) * 35, 3).Interior.ColorIndex = y_al_num2 `yellow
    End If
    If Sheets("Work sheet").Cells(154 + (i - 1) * 35, 3).Value > _
        Sheets("Bound sheet").Cells(46, 13).Value Or _
        Sheets("Work sheet").Cells(154 + (i - 1) * 35, 3).Value < _
        Sheets("Bound sheet").Cells(46, 12).Value Then
        With Sheets("Alarm sheet").Cells(8, 4 + (i - 1) * 5)
            .FormulaR1C1 = "red alarm"
            .Interior.ColorIndex = 3
        End With
        Sheets("Work sheet").Cells(154 + (i - 1) * 35, 3).Interior.ColorIndex = 3 `red
        Sheets("Summary Data").Cells(2, 2 + (i - 1) * 23).Interior.ColorIndex = 3 `red
    End If
End If

```

```
Next i
*****
'dB/B for head20 NCS
'for both aperture
*****
For i = 1 To 2
  If Sheets("Work sheet").Cells(154 + (i - 1) * 35, 22).Value > _
    Sheets("Bound sheet").Cells(46, 15).Value Or _
    Sheets("Work sheet").Cells(154 + (i - 1) * 35, 22).Value < _
    Sheets("Bound sheet").Cells(46, 14).Value Then
  If Sheets("Alarm sheet").Cells(8, 5 + (i - 1) * 5).Interior.ColorIndex = 4 Then
    With Sheets("Alarm sheet").Cells(8, 5 + (i - 1) * 5)
      .FormulaR1C1 = y_al_str
      .Interior.ColorIndex = y_al_num1
    End With
    Sheets("Summary Data").Cells(2, 21 + (i - 1) * 23).Interior.ColorIndex = y_al_num2 'yellow
  End If
  Sheets("Work sheet").Cells(154 + (i - 1) * 35, 22).Interior.ColorIndex = y_al_num2 'yellow
End If
If Sheets("Work sheet").Cells(154 + (i - 1) * 35, 22).Value > _
  Sheets("Bound sheet").Cells(46, 17).Value Or _
  Sheets("Work sheet").Cells(154 + (i - 1) * 35, 22).Value < _
  Sheets("Bound sheet").Cells(46, 16).Value Then
  With Sheets("Alarm sheet").Cells(8, 5 + (i - 1) * 5)
    .FormulaR1C1 = "red alarm"
    .Interior.ColorIndex = 3
  End With
  Sheets("Work sheet").Cells(154 + (i - 1) * 35, 22).Interior.ColorIndex = 3 'red
  Sheets("Summary Data").Cells(2, 21 + (i - 1) * 23).Interior.ColorIndex = 3 'red
End If
Next i
*****
'checking mean value calculated out of inner
'positions 3 to 18
*****
For i = 1 To 2
  If Sheets("Work sheet").Cells(154 + (i - 1) * 35, 2).Value > _
    Sheets("Bound sheet").Cells(46, 3).Value Or _
    Sheets("Work sheet").Cells(154 + (i - 1) * 35, 2).Value < _
    Sheets("Bound sheet").Cells(46, 2).Value Then
  With Sheets("Alarm sheet").Cells(8, 2 + (i - 1) * 5)
    .FormulaR1C1 = y_al_str3
    .Interior.ColorIndex = y_al_num3
  End With
  Sheets("Work sheet").Cells(154 + (i - 1) * 35, 2).Interior.ColorIndex = y_al_num3 'yellow
  Sheets("Summary Data").Cells(2, 22 + (i - 1) * 23).Interior.ColorIndex = y_al_num3 'yellow
End If
If Sheets("Work sheet").Cells(154 + (i - 1) * 35, 2).Value > _
  Sheets("Bound sheet").Cells(46, 5).Value Or _
  Sheets("Work sheet").Cells(154 + (i - 1) * 35, 2).Value < _
  Sheets("Bound sheet").Cells(46, 4).Value Then
  With Sheets("Alarm sheet").Cells(8, 2 + (i - 1) * 5)
    .FormulaR1C1 = "red alarm"
    .Interior.ColorIndex = 3
```

```

End With
Sheets("Work sheet").Cells(154 + (i - 1) * 35, 2).Interior.ColorIndex = 3 `red
Sheets("Summary Data").Cells(2, 22 + (i - 1) * 23).Interior.ColorIndex = 3 `red
End If
Next i
'=====
'
' ANGLE (Main Field Direction)
'=====
'=====
'=====
'Checking angle deviation from the mean value
'calculated on positions 2:19
'for positions 2:19 and for both aperture
'=====
For i = 1 To 2
  For j = 1 To 18
    If Sheets("Work sheet").Cells(156 + (i - 1) * 35, 3 + j).Value _
      > Sheets("Bound sheet").Cells(49, 7).Value Or _
      Sheets("Work sheet").Cells(156 + (i - 1) * 35, 3 + j).Value _
      < Sheets("Bound sheet").Cells(49, 6).Value Then
      If Sheets("Alarm sheet").Cells(9, 3 + (i - 1) * 5).Interior.ColorIndex = 4 Then
        With Sheets("Alarm sheet").Cells(9, 3 + (i - 1) * 5)
          .FormulaR1C1 = y_al_str
          .Interior.ColorIndex = y_al_num1
        End With
      End If
      Sheets("Work sheet").Cells(156 + (i - 1) * 35, 3 + j).Interior.ColorIndex = y_al_num2 `yellow
      Sheets("Summary Data").Cells(3, 2 + j + (i - 1) * 23).Interior.ColorIndex = y_al_num2 `yellow
    End If
    If Sheets("Work sheet").Cells(156 + (i - 1) * 35, 3 + j).Value _
      > Sheets("Bound sheet").Cells(49, 9).Value Or _
      Sheets("Work sheet").Cells(156 + (i - 1) * 35, 3 + j).Value _
      < Sheets("Bound sheet").Cells(49, 8).Value Then
      With Sheets("Alarm sheet").Cells(9, 3 + (i - 1) * 5)
        .FormulaR1C1 = "red alarm"
        .Interior.ColorIndex = 3
      End With
      Sheets("Work sheet").Cells(156 + (i - 1) * 35, 3 + j).Interior.ColorIndex = 3 `red
      Sheets("Summary Data").Cells(3, 2 + j + (i - 1) * 23).Interior.ColorIndex = 3 `red
    End If
  Next j
Next i
'=====
'Checking angle value
'For Head CS for both aperture
'=====
For i = 1 To 2
  If Sheets("Work sheet").Cells(156 + (i - 1) * 35, 3).Value > _
    Sheets("Bound sheet").Cells(49, 11).Value Or _
    Sheets("Work sheet").Cells(156 + (i - 1) * 35, 3).Value _
    < Sheets("Bound sheet").Cells(49, 10).Value Then
    If Sheets("Alarm sheet").Cells(9, 4 + (i - 1) * 5).Interior.ColorIndex = 4 Then
      With Sheets("Alarm sheet").Cells(9, 4 + (i - 1) * 5)

```

```

        .FormulaR1C1 = y_al_str
        .Interior.ColorIndex = y_al_num1
    End With
End If
Sheets("Work sheet").Cells(156 + (i - 1) * 35, 3).Interior.ColorIndex = y_al_num2 `yellow
Sheets("Summary Data").Cells(3, 2 + (i - 1) * 23).Interior.ColorIndex = y_al_num2 `yellow
End If
If Sheets("Work sheet").Cells(156 + (i - 1) * 35, 3).Value > _
    > Sheets("Bound sheet").Cells(49, 13).Value Or _
    Sheets("Work sheet").Cells(156 + (i - 1) * 35, 3).Value < _
    < Sheets("Bound sheet").Cells(49, 12).Value Then
    With Sheets("Alarm sheet").Cells(9, 4 + (i - 1) * 5)
        .FormulaR1C1 = "red alarm"
        .Interior.ColorIndex = 3
    End With
    Sheets("Work sheet").Cells(156 + (i - 1) * 35, 3).Interior.ColorIndex = 3 `red
    Sheets("Summary Data").Cells(3, 2 + (i - 1) * 23).Interior.ColorIndex = 3 `red
End If
Next i
*****
`Checking angle value
`for head20 NCS for both aperture
*****
For i = 1 To 2
    If Sheets("Work sheet").Cells(156 + (i - 1) * 35, 22).Value > _
        Sheets("Bound sheet").Cells(49, 15).Value Or _
        Sheets("Work sheet").Cells(156 + (i - 1) * 35, 22).Value < _
        < Sheets("Bound sheet").Cells(49, 14).Value Then
        If Sheets("Alarm sheet").Cells(9, 5 + (i - 1) * 5).Interior.ColorIndex = 4 Then
            With Sheets("Alarm sheet").Cells(9, 5 + (i - 1) * 5)
                .FormulaR1C1 = y_al_str
                .Interior.ColorIndex = y_al_num1
            End With
        End If
        Sheets("Work sheet").Cells(156 + (i - 1) * 35, 22).Interior.ColorIndex = y_al_num2 `yellow
        Sheets("Summary Data").Cells(3, 21 + (i - 1) * 23).Interior.ColorIndex = y_al_num2 `yellow
    End If
    If Sheets("Work sheet").Cells(156 + (i - 1) * 35, 22).Value > _
        Sheets("Bound sheet").Cells(49, 17).Value Or _
        Sheets("Work sheet").Cells(156 + (i - 1) * 35, 22).Value < _
        < Sheets("Bound sheet").Cells(49, 16).Value Then
        With Sheets("Alarm sheet").Cells(9, 5 + (i - 1) * 5)
            .FormulaR1C1 = "red alarm"
            .Interior.ColorIndex = 3
        End With
        Sheets("Work sheet").Cells(156 + (i - 1) * 35, 22).Interior.ColorIndex = 3 `red
        Sheets("Summary Data").Cells(3, 21 + (i - 1) * 23).Interior.ColorIndex = 3 `red
    End If
Next i
*****
`Checking angle deviation between the two apertures `
`considering angle `integrals`: FIELD COLINEARITY `
*****
If Sheets("Work sheet").Cells(221, 2).Value > _

```

```

Sheets("Bound sheet").Cells(42, 9).Value Or _
Sheets("Work sheet").Cells(221, 2).Value < _
Sheets("Bound sheet").Cells(42, 8).Value Then
With Sheets("Alarm sheet").Cells(39, 2)
    .FormulaR1C1 = y_al_str3
    .Interior.ColorIndex = y_al_num3
End With
Sheets("Work sheet").Cells(221, 2).Interior.ColorIndex = y_al_num3 `yellow
Sheets("Summary Data").Range("v3,as3").Interior.ColorIndex = y_al_num3 `yellow
End If
If Sheets("Work sheet").Cells(221, 2).Value > _
    Sheets("Bound sheet").Cells(42, 11).Value Or _
    Sheets("Work sheet").Cells(221, 2).Value _
    < Sheets("Bound sheet").Cells(42, 10).Value Then
With Sheets("Alarm sheet").Cells(39, 2)
    .FormulaR1C1 = "red alarm"
    .Interior.ColorIndex = 3
End With
Sheets("Work sheet").Cells(221, 2).Interior.ColorIndex = 3 `red
Sheets("Summary Data").Range("v3,as3").Interior.ColorIndex = 3 `red
End If
'=====
'
'    MULTIPOLES
'=====
'=====
'=====
'
'checking multipoles deviation from the mean value
'calculated out of positions 2:19
'for positions 2 to 19 and for both aperture
'=====
For k = 1 To 2
For i = 1 To 28
For j = 1 To 18
    If Sheets("Work sheet").Cells(156 + i + (k - 1) * 35, 3 + j).Value _
        > Sheets("Bound sheet").Cells(49 + i, 7).Value Or _
        Sheets("Work sheet").Cells(156 + i + (k - 1) * 35, 3 + j).Value _
        < Sheets("Bound sheet").Cells(49 + i, 6).Value Then
        If Sheets("Alarm sheet").Cells(9 + i, 3 + (k - 1) * 5).Interior.ColorIndex = 4 Then
            With Sheets("Alarm sheet").Cells(9 + i, 3 + (k - 1) * 5)
                .FormulaR1C1 = y_al_str
                .Interior.ColorIndex = y_al_num1
            End With
        End If
        Sheets("Work sheet").Cells(156 + i + (k - 1) * 35, 3 + j).Interior.ColorIndex = y_al_num2 `yellow
        If i < 15 Then
            Sheets("Summary Data").Cells(5 + i, 2 + j + (k - 1) * 23).Interior.ColorIndex = y_al_num2
        Else
            Sheets("Summary Data").Cells(8 + i, 2 + j + (k - 1) * 23).Interior.ColorIndex = y_al_num2
        End If
    End If
End If
If Sheets("Work sheet").Cells(156 + i + (k - 1) * 35, 3 + j).Value _
    > Sheets("Bound sheet").Cells(49 + i, 9).Value Or _
    Sheets("Work sheet").Cells(156 + i + (k - 1) * 35, 3 + j).Value _

```

```

    < Sheets("Bound sheet").Cells(49 + i, 8).Value Then
With Sheets("Alarm sheet").Cells(9 + i, 3 + (k - 1) * 5)
    .FormulaR1C1 = "red alarm"
    .Interior.ColorIndex = 3
End With
Sheets("Work sheet").Cells(156 + i + (k - 1) * 35, 3 + j).Interior.ColorIndex = 3 `red
If i < 15 Then
    Sheets("Summary Data").Cells(5 + i, 2 + j + (k - 1) * 23).Interior.ColorIndex = 3
Else
    Sheets("Summary Data").Cells(8 + i, 2 + j + (k - 1) * 23).Interior.ColorIndex = 3
End If
End If
Next j
Next i
Next k
*****
`checking multipoles deviation from the mean value
`calculated out of positions 2:19
`for head CS position 1 and for both aperture
*****
For k = 1 To 2
For i = 1 To 28
    If Sheets("Work sheet").Cells(156 + i + (k - 1) * 35, 3).Value _
        > Sheets("Bound sheet").Cells(49 + i, 11).Value Or _
        Sheets("Work sheet").Cells(156 + i + (k - 1) * 35, 3).Value < _
        Sheets("Bound sheet").Cells(49 + i, 10).Value Then
    If Sheets("Alarm sheet").Cells(9 + i, 4 + (k - 1) * 5).Interior.ColorIndex = 4 Then
        With Sheets("Alarm sheet").Cells(9 + i, 4 + (k - 1) * 5)
            .FormulaR1C1 = y_al_str
            .Interior.ColorIndex = y_al_num1
        End With
    End If
    Sheets("Work sheet").Cells(156 + i + (k - 1) * 35, 3).Interior.ColorIndex = y_al_num2 `yellow
    If i < 15 Then
        Sheets("Summary Data").Cells(5 + i, 2 + (k - 1) * 23).Interior.ColorIndex = y_al_num2
    Else
        Sheets("Summary Data").Cells(8 + i, 2 + (k - 1) * 23).Interior.ColorIndex = y_al_num2
    End If
End If
If Sheets("Work sheet").Cells(156 + i + (k - 1) * 35, 3).Value _
    > Sheets("Bound sheet").Cells(49 + i, 13).Value Or _
    Sheets("Work sheet").Cells(156 + i + (k - 1) * 35, 3).Value _
    < Sheets("Bound sheet").Cells(49 + i, 12).Value Then
With Sheets("Alarm sheet").Cells(9 + i, 4 + (k - 1) * 5)
    .FormulaR1C1 = "red alarm"
    .Interior.ColorIndex = 3
End With
Sheets("Work sheet").Cells(156 + i + (k - 1) * 35, 3).Interior.ColorIndex = 3 `red
If i < 15 Then
    Sheets("Summary Data").Cells(5 + i, 2 + (k - 1) * 23).Interior.ColorIndex = 3
Else
    Sheets("Summary Data").Cells(8 + i, 2 + (k - 1) * 23).Interior.ColorIndex = 3
End If
End If

```

```

Next i
Next k
*****
'checking multipoles deviation from the mean value
'calculated out of positions 2:19
'for head NCS position 20 and for both aperture
*****
For k = 1 To 2
For i = 1 To 28
  If Sheets("Work sheet").Cells(156 + i + (k - 1) * 35, 22).Value _
    > Sheets("Bound sheet").Cells(49 + i, 15).Value Or _
    Sheets("Work sheet").Cells(156 + i + (k - 1) * 35, 22).Value _
    < Sheets("Bound sheet").Cells(49 + i, 14).Value Then
  If Sheets("Alarm sheet").Cells(9 + i, 5 + (k - 1) * 5).Interior.ColorIndex = 4 Then
    With Sheets("Alarm sheet").Cells(9 + i, 5 + (k - 1) * 5)
      .FormulaR1C1 = y_al_str
      .Interior.ColorIndex = y_al_num1
    End With
  End If
  Sheets("Work sheet").Cells(156 + i + (k - 1) * 35, 22).Interior.ColorIndex = y_al_num2 `yellow
  If i < 15 Then
    Sheets("Summary Data").Cells(5 + i, 21 + (k - 1) * 23).Interior.ColorIndex = y_al_num2
  Else
    Sheets("Summary Data").Cells(8 + i, 21 + (k - 1) * 23).Interior.ColorIndex = y_al_num2
  End If
End If
If Sheets("Work sheet").Cells(156 + i + (k - 1) * 35, 22).Value _
  > Sheets("Bound sheet").Cells(49 + i, 17).Value Or _
  Sheets("Work sheet").Cells(156 + i + (k - 1) * 35, 22).Value _
  < Sheets("Bound sheet").Cells(49 + i, 16).Value Then
  With Sheets("Alarm sheet").Cells(9 + i, 5 + (k - 1) * 5)
    .FormulaR1C1 = "red alarm"
    .Interior.ColorIndex = 3
  End With
  Sheets("Work sheet").Cells(156 + i + (k - 1) * 35, 22).Interior.ColorIndex = 3 `red
  If i < 15 Then
    Sheets("Summary Data").Cells(5 + i, 21 + (k - 1) * 23).Interior.ColorIndex = 3
  Else
    Sheets("Summary Data").Cells(8 + i, 21 + (k - 1) * 23).Interior.ColorIndex = 3
  End If
End If
Next i
Next k
*****
'checking multipoles mean value
'calculated out of positions 2:19
'for both aperture
*****
For k = 1 To 2
For i = 1 To 28
  If Sheets("Work sheet").Cells(156 + i + (k - 1) * 35, 2).Value _
    > Sheets("Bound sheet").Cells(49 + i, 3).Value Or _
    Sheets("Work sheet").Cells(156 + i + (k - 1) * 35, 2).Value _
    < Sheets("Bound sheet").Cells(49 + i, 2).Value Then

```



```

If Sheets("Alarm sheet").Cells(9 + i, 2 + (k - 1) * 5).Interior.ColorIndex = 4 Then
  With Sheets("Alarm sheet").Cells(9 + i, 2 + (k - 1) * 5)
    .FormulaR1C1 = y_al_str3
    .Interior.ColorIndex = y_al_num3
  End With
End If
Sheets("Work sheet").Cells(156 + i + (k - 1) * 35, 2).Interior.ColorIndex = y_al_num3 `yellow
If i < 15 Then
  Sheets("Summary Data").Cells(5 + i, 22 + (k - 1) * 23).Interior.ColorIndex = y_al_num3
Else
  Sheets("Summary Data").Cells(8 + i, 22 + (k - 1) * 23).Interior.ColorIndex = y_al_num3
End If
End If
If Sheets("Work sheet").Cells(156 + i + (k - 1) * 35, 2).Value _
  > Sheets("Bound sheet").Cells(49 + i, 5).Value Or _
  Sheets("Work sheet").Cells(156 + i + (k - 1) * 35, 2).Value _
  < Sheets("Bound sheet").Cells(49 + i, 4).Value Then
  With Sheets("Alarm sheet").Cells(9 + i, 2 + (k - 1) * 5)
    .FormulaR1C1 = "red alarm"
    .Interior.ColorIndex = 3
  End With
  Sheets("Work sheet").Cells(156 + i + (k - 1) * 35, 2).Interior.ColorIndex = 3 `red
  If i < 15 Then
    Sheets("Summary Data").Cells(5 + i, 22 + (k - 1) * 23).Interior.ColorIndex = 3
  Else
    Sheets("Summary Data").Cells(8 + i, 22 + (k - 1) * 23).Interior.ColorIndex = 3
  End If
End If
End If
Next i
Next k
'=====
'=====
' COIL POSITIONING
'=====
'=====
For i = 1 To 2
  If Sheets("Summary Data").Cells(43, 2 + (i - 1) * 23).Value > 0.03 Then
    With Sheets("Alarm sheet").Cells(38, 2 + (i - 1) * 5)
      .FormulaR1C1 = y_al_str3
      .Interior.ColorIndex = y_al_num3
    End With
    Sheets("Summary Data").Cells(43, 2 + (i - 1) * 23).Interior.ColorIndex = y_al_num3
  End If
  If Sheets("Summary Data").Cells(43, 2 + (i - 1) * 23).Value > 0.06 Then
    With Sheets("Alarm sheet").Cells(38, 2 + (i - 1) * 5)
      .FormulaR1C1 = "red alarm"
      .Interior.ColorIndex = 3
    End With
    Sheets("Summary Data").Cells(43, 2 + (i - 1) * 23).Interior.ColorIndex = 3
  End If
End If
Next i

```

```
'=====
'=====
'   MAGNETIC LENGTH
'=====
'=====
For i = 1 To 2
  If Sheets("Summary Data").Cells(41, 2 + (i - 1) * 23).Value > _
    Sheets("Bound sheet").Cells(42, 3).Value Or _
    Sheets("Summary Data").Cells(41, 2 + (i - 1) * 23).Value < _
    Sheets("Bound sheet").Cells(42, 2).Value Then
    With Sheets("Alarm sheet").Cells(5, 2 + (i - 1) * 5)
      .FormulaR1C1 = y_al_str3
      .Interior.ColorIndex = y_al_num3
    End With
    Sheets("Summary Data").Cells(41, 2 + (i - 1) * 23).Interior.ColorIndex = y_al_num3 `yellow
  End If
  If Sheets("Summary Data").Cells(41, 2 + (i - 1) * 23).Value > _
    Sheets("Bound sheet").Cells(42, 5).Value Or _
    Sheets("Summary Data").Cells(41, 2 + (i - 1) * 23).Value _
    < Sheets("Bound sheet").Cells(42, 4).Value Then
    With Sheets("Alarm sheet").Cells(5, 2 + (i - 1) * 5)
      .FormulaR1C1 = "red alarm"
      .Interior.ColorIndex = 3
    End With
    Sheets("Summary Data").Cells(41, 2 + (i - 1) * 23).Interior.ColorIndex = 3 `red
  End If
Next i
'=====
'=====
'   PROTECTING SHEETS
'=====
'=====
  Sheets("Alarm sheet").Protect DrawingObjects:=True, Contents:=True, Scenarios:=True
  Sheets("Work sheet").Protect DrawingObjects:=True, Contents:=True, Scenarios:=True
  Sheets("Summary Data").Protect DrawingObjects:=True, Contents:=True, Scenarios:=True
'=====
'=====
'   ALARM RESULTS AND FINAL FORMATTING
'=====
'=====
If foglio = 1 Then
  Sheets("Bound sheet").Name = "Alstom Bound"
ElseIf foglio = 2 Then
  Sheets("Bound sheet").Name = "Ansaldo Bound"
ElseIf foglio = 3 Then
  Sheets("Bound sheet").Name = "Noell Bound"
End If
foglio = 0
Worksheets("Alarm sheet").Activate

End Sub
```

Appendix F

Measurement data of Firm1 defected collared coils

In the following pages, measurement data are reported for some collared coils manufactured at Firm1 which feature large multipolar variations along the coil straight part due to a manufacturing tool defect. The *Alarm sheet* and *Summary data* sheets are reported.

Firm1-3 Alarm sheet:

File name			HEMIBB_A001 - 1000003 cc.xls			
Component ID			HEMIBB_A001		1000003	
Date of test Ap 1			01.05.01		01.05.01	
Magnetic length			Aperture 1		Aperture 2	
Magnetic length	Main field Angle	Average central positions 1 to 20	Central positions 2 to 19		Central positions 2 to 19	
			position 1	position 1	position 1	position 20
Main field Angle	Main field Angle	Average central positions 1 to 20	Central positions 2 to 19		Central positions 2 to 19	
			position 1	position 1	position 1	position 20
b2		status ok	status ok	status ok	status ok	status ok
b3		status ok	status ok	status ok	status ok	status ok
b4		status ok	status ok	status ok	status ok	status ok
b5		status ok	status ok	status ok	status ok	status ok
b6		status ok	status ok	status ok	status ok	status ok
b7		status ok	status ok	status ok	status ok	status ok
b8		status ok	status ok	status ok	status ok	status ok
b9		status ok	status ok	status ok	status ok	status ok
b10		status ok	status ok	status ok	status ok	status ok
b11		status ok	status ok	status ok	status ok	status ok
b12		status ok	status ok	status ok	status ok	status ok
b13		status ok	status ok	status ok	status ok	status ok
b14		status ok	status ok	status ok	status ok	status ok
b15		status ok	status ok	status ok	status ok	status ok
a2		status ok	status ok	status ok	status ok	status ok
a3		status ok	status ok	status ok	status ok	status ok
a4		status ok	status ok	status ok	status ok	status ok
a5		status ok	status ok	status ok	status ok	status ok
a6		status ok	status ok	status ok	status ok	status ok
a7		status ok	status ok	status ok	status ok	status ok
a8		status ok	status ok	status ok	status ok	status ok
a9		status ok	status ok	status ok	status ok	status ok
a10		status ok	status ok	status ok	status ok	status ok
a11		status ok	status ok	status ok	status ok	status ok
a12		status ok	status ok	status ok	status ok	status ok
a13		status ok	status ok	status ok	status ok	status ok
a14		status ok	status ok	status ok	status ok	status ok
a15		status ok	status ok	status ok	status ok	status ok
Coil Positioning	Coil Positioning	status ok	yellow alarm			
Field Collinearity	Field Collinearity	status ok	yellow alarm			

Firm1-3-Ap.1 Summary Data:

File	HCM001 - 1000003															Aperture 1 - Collared coils															Integrals
C1A (m/mKA)	596.597	597.025	596.970	597.890	596.520	596.618	596.550	596.544	596.639	596.614	597.079	596.110	596.194	596.597	595.861	595.425	596.004	0.0068													
Angle (rad)	-1.2232	1.2296	1.2296	1.2343	1.2343	0.9271	0.9271	-0.2422	-0.2422	0.2558	0.2558	-0.3238	-0.3238	-0.2384	-0.2384	-0.8128	-0.2282	0.0003													
Multipliers	Problem 1	Problem 2	Problem 3	Problem 4	Problem 5	Problem 6	Problem 7	Problem 8	Problem 9	Problem 10	Problem 11	Problem 12	Problem 13	Problem 14	Problem 15	Problem 16	Problem 17	Problem 18	Problem 19	Problem 20											
01	0.0000	0.0000	0.0000	0.0000	0.0000	0.0000	0.0000	0.0000	0.0000	0.0000	0.0000	0.0000	0.0000	0.0000	0.0000	0.0000	0.0000	0.0000	0.0000	0.0000											
02	-0.4822	-0.5097	-1.4312	-1.5258	-0.8208	-0.2286	-0.1208	-0.1284	-0.3291	-0.2284	-0.2291	-1.2262	-1.2262	-0.2282	-0.2282	0.7282	0.7282	-0.8208	-0.8208	-1.2262											
03	5.2771	5.2771	1.0250	1.0250	4.2542	4.2542	2.7280	2.7280	1.2292	1.2292	4.8254	2.2282	2.2282	4.8254	1.2292	4.8254	4.8254	4.8254	4.8254	5.2771											
04	-0.0005	-0.0005	0.0005	0.0005	-0.0005	-0.0005	-0.0005	-0.0005	-0.0005	-0.0005	-0.0005	0.0005	0.0005	-0.0005	-0.0005	0.0005	0.0005	0.0005	0.0005	0.0005											
05	0.0071	0.0071	0.0071	0.0071	-0.0071	-0.0071	-0.0071	-0.0071	0.0071	0.0071	0.0071	0.0071	0.0071	-0.0071	-0.0071	0.0071	0.0071	0.0071	0.0071	0.0071											
06	0.0005	0.0005	0.0005	0.0005	0.0005	0.0005	0.0005	0.0005	0.0005	0.0005	0.0005	0.0005	0.0005	0.0005	0.0005	0.0005	0.0005	0.0005	0.0005	0.0005											
07	0.0005	0.0005	0.0005	0.0005	0.0005	0.0005	0.0005	0.0005	0.0005	0.0005	0.0005	0.0005	0.0005	0.0005	0.0005	0.0005	0.0005	0.0005	0.0005	0.0005											
08	-0.2282	-0.2282	-0.2282	-0.2282	-0.2282	-0.2282	-0.2282	-0.2282	-0.2282	-0.2282	-0.2282	-0.2282	-0.2282	-0.2282	-0.2282	-0.2282	-0.2282	-0.2282	-0.2282	-0.2282											
09	0.0005	0.0005	0.0005	0.0005	0.0005	0.0005	0.0005	0.0005	0.0005	0.0005	0.0005	0.0005	0.0005	0.0005	0.0005	0.0005	0.0005	0.0005	0.0005	0.0005											
10	-0.2282	-0.2282	-0.2282	-0.2282	-0.2282	-0.2282	-0.2282	-0.2282	-0.2282	-0.2282	-0.2282	-0.2282	-0.2282	-0.2282	-0.2282	-0.2282	-0.2282	-0.2282	-0.2282	-0.2282											
11	0.0005	0.0005	0.0005	0.0005	0.0005	0.0005	0.0005	0.0005	0.0005	0.0005	0.0005	0.0005	0.0005	0.0005	0.0005	0.0005	0.0005	0.0005	0.0005	0.0005											
12	0.0005	0.0005	0.0005	0.0005	0.0005	0.0005	0.0005	0.0005	0.0005	0.0005	0.0005	0.0005	0.0005	0.0005	0.0005	0.0005	0.0005	0.0005	0.0005	0.0005											
13	0.0005	0.0005	0.0005	0.0005	0.0005	0.0005	0.0005	0.0005	0.0005	0.0005	0.0005	0.0005	0.0005	0.0005	0.0005	0.0005	0.0005	0.0005	0.0005	0.0005											
14	0.0005	0.0005	0.0005	0.0005	0.0005	0.0005	0.0005	0.0005	0.0005	0.0005	0.0005	0.0005	0.0005	0.0005	0.0005	0.0005	0.0005	0.0005	0.0005	0.0005											
15	0.0005	0.0005	0.0005	0.0005	0.0005	0.0005	0.0005	0.0005	0.0005	0.0005	0.0005	0.0005	0.0005	0.0005	0.0005	0.0005	0.0005	0.0005	0.0005	0.0005											
16	0.0005	0.0005	0.0005	0.0005	0.0005	0.0005	0.0005	0.0005	0.0005	0.0005	0.0005	0.0005	0.0005	0.0005	0.0005	0.0005	0.0005	0.0005	0.0005	0.0005											
17	-0.2282	-0.2282	-0.2282	-0.2282	-0.2282	-0.2282	-0.2282	-0.2282	-0.2282	-0.2282	-0.2282	-0.2282	-0.2282	-0.2282	-0.2282	-0.2282	-0.2282	-0.2282	-0.2282	-0.2282											
18	0.0005	0.0005	0.0005	0.0005	0.0005	0.0005	0.0005	0.0005	0.0005	0.0005	0.0005	0.0005	0.0005	0.0005	0.0005	0.0005	0.0005	0.0005	0.0005	0.0005											
19	0.0005	0.0005	0.0005	0.0005	0.0005	0.0005	0.0005	0.0005	0.0005	0.0005	0.0005	0.0005	0.0005	0.0005	0.0005	0.0005	0.0005	0.0005	0.0005	0.0005											
20	-0.2282	-0.2282	-0.2282	-0.2282	-0.2282	-0.2282	-0.2282	-0.2282	-0.2282	-0.2282	-0.2282	-0.2282	-0.2282	-0.2282	-0.2282	-0.2282	-0.2282	-0.2282	-0.2282	-0.2282											
0x (mm)	-0.51	-0.44	-0.31	-0.20	-0.27	-0.42	-0.34	-0.39	-0.41	-0.33	-0.29	-0.27	-0.26	-0.30	-0.25	-0.30	-0.25	-0.41	-0.32	-0.35											
0y (mm)	-1.23	0.34	-0.64	-0.46	-0.34	-0.43	-0.39	-0.62	-0.31	-0.95	-0.40	-0.61	-0.54	-0.44	-0.33	-0.50	-0.56	-0.48	-0.36	-0.71											
Mag. (m)	14.4451																														
TF (mTm/A)	556.884																														
Cell pos. (mm)	0.0300																														
Current (A)	15.2700																														

Firm1-4 Alarm sheet:

File name		HCMBB_A001-10000014_cc.xls	
Component ID		HCMBB_A001	
Date of test Ap 1		05.06.01	
Serial Number		1000004	
Date of test Ap 2		05.06.01	
Magnetic length		Aperture 2	
Magnetic length		Magnetic length	
Main field Angle		Main field Angle	
b2	status ok	status ok	status ok
b3	status ok	status ok	status ok
b4	status ok	status ok	status ok
b5	status ok	status ok	status ok
b6	status ok	status ok	status ok
b7	status ok	status ok	status ok
b8	status ok	status ok	status ok
b9	status ok	status ok	status ok
b10	status ok	status ok	status ok
b11	status ok	status ok	status ok
b12	status ok	status ok	status ok
b13	status ok	status ok	status ok
b14	status ok	status ok	status ok
b15	status ok	status ok	status ok
a2	status ok	status ok	status ok
a3	status ok	status ok	status ok
a4	status ok	status ok	status ok
a5	status ok	status ok	status ok
a6	status ok	status ok	status ok
a7	status ok	status ok	status ok
a8	status ok	status ok	status ok
a9	status ok	status ok	status ok
a10	status ok	status ok	status ok
a11	status ok	status ok	status ok
a12	status ok	status ok	status ok
a13	status ok	status ok	status ok
a14	status ok	status ok	status ok
a15	status ok	status ok	status ok
Coil Positioning	status ok	Coil Positioning	status ok
Field Collinearity	status ok	Field Collinearity	status ok
Average central positions 1 to 20		Average central positions 2 to 19	
Heads MCS position 20		Heads CS position 1	
Heads MCS position 20		Heads CS position 20	

Firm1-5 Alarm sheet:

File name		HCMBB_A001-1000005.xls			
Component ID	HCMBB_A001	Serial Number	1000005		
Date of test Ap 1	06/07/01	Date of test Ap 2	06/07/01		
Magnetic length		Aperture 2			
Main field Angle	Average central positions 1 to 20	Central positions 2 to 19	Heads CS position 1	Heads NCS position 20	
	status ok	status ok	status ok	status ok	
b2	status ok	status ok	status ok	status ok	
b3	status ok	status ok	status ok	status ok	
b4	status ok	status ok	status ok	status ok	
b5	status ok	status ok	status ok	status ok	
b6	status ok	status ok	status ok	status ok	
b7	status ok	yellow alarm	status ok	status ok	
b8	status ok	status ok	status ok	status ok	
b9	status ok	yellow alarm	status ok	status ok	
b10	status ok	status ok	status ok	status ok	
b11	status ok	status ok	status ok	status ok	
b12	status ok	status ok	status ok	status ok	
b13	status ok	yellow alarm	status ok	status ok	
b14	status ok	status ok	status ok	status ok	
b15	status ok	status ok	status ok	status ok	
a2	status ok	status ok	status ok	status ok	
a3	status ok	yellow alarm	status ok	status ok	
a4	status ok	status ok	status ok	status ok	
a5	status ok	yellow alarm	status ok	status ok	
a6	status ok	status ok	status ok	status ok	
a7	status ok	status ok	status ok	status ok	
a8	status ok	status ok	status ok	status ok	
a9	status ok	status ok	status ok	status ok	
a10	status ok	status ok	status ok	status ok	
a11	status ok	status ok	status ok	status ok	
a12	status ok	status ok	status ok	status ok	
a13	status ok	status ok	status ok	status ok	
a14	status ok	status ok	status ok	status ok	
a15	status ok	status ok	status ok	status ok	
Coil Positioning Field Collinearity	yellow alarm				
Coil Positioning	status ok				

Measurement data of Firm1 defected collared coils

Firm1-5-Ap.2 Summary data:

File		Aperture 2 - Collared coils																		Integrals
HCHB_A001 - 1000005		Aperture 2 - Collared coils																		100000
Ct1 (mT/KA)		Aperture 2 - Collared coils																		1.618
Angle (rad)		Aperture 2 - Collared coils																		0.563
Multipoles		Aperture 2 - Collared coils																		0.270
E1		Aperture 2 - Collared coils																		1.079
E2		Aperture 2 - Collared coils																		-0.111
E3		Aperture 2 - Collared coils																		0.812
E4		Aperture 2 - Collared coils																		0.048
E5		Aperture 2 - Collared coils																		0.253
E6		Aperture 2 - Collared coils																		0.000
E7		Aperture 2 - Collared coils																		0.717
E8		Aperture 2 - Collared coils																		0.000
E9		Aperture 2 - Collared coils																		0.000
E10		Aperture 2 - Collared coils																		0.000
E11		Aperture 2 - Collared coils																		0.000
E12		Aperture 2 - Collared coils																		0.000
E13		Aperture 2 - Collared coils																		0.000
E14		Aperture 2 - Collared coils																		0.000
E15		Aperture 2 - Collared coils																		0.000
E16		Aperture 2 - Collared coils																		0.000
E17		Aperture 2 - Collared coils																		0.000
E18		Aperture 2 - Collared coils																		0.000
E19		Aperture 2 - Collared coils																		0.000
E20		Aperture 2 - Collared coils																		0.000
E21		Aperture 2 - Collared coils																		0.000
E22		Aperture 2 - Collared coils																		0.000
E23		Aperture 2 - Collared coils																		0.000
E24		Aperture 2 - Collared coils																		0.000
E25		Aperture 2 - Collared coils																		0.000
E26		Aperture 2 - Collared coils																		0.000
E27		Aperture 2 - Collared coils																		0.000
E28		Aperture 2 - Collared coils																		0.000
E29		Aperture 2 - Collared coils																		0.000
E30		Aperture 2 - Collared coils																		0.000
E31		Aperture 2 - Collared coils																		0.000
E32		Aperture 2 - Collared coils																		0.000
E33		Aperture 2 - Collared coils																		0.000
E34		Aperture 2 - Collared coils																		0.000
E35		Aperture 2 - Collared coils																		0.000
E36		Aperture 2 - Collared coils																		0.000
E37		Aperture 2 - Collared coils																		0.000
E38		Aperture 2 - Collared coils																		0.000
E39		Aperture 2 - Collared coils																		0.000
E40		Aperture 2 - Collared coils																		0.000
E41		Aperture 2 - Collared coils																		0.000
E42		Aperture 2 - Collared coils																		0.000
E43		Aperture 2 - Collared coils																		0.000
E44		Aperture 2 - Collared coils																		0.000
E45		Aperture 2 - Collared coils																		0.000
E46		Aperture 2 - Collared coils																		0.000
E47		Aperture 2 - Collared coils																		0.000
E48		Aperture 2 - Collared coils																		0.000
E49		Aperture 2 - Collared coils																		0.000
E50		Aperture 2 - Collared coils																		0.000
E51		Aperture 2 - Collared coils																		0.000
E52		Aperture 2 - Collared coils																		0.000
E53		Aperture 2 - Collared coils																		0.000
E54		Aperture 2 - Collared coils																		0.000
E55		Aperture 2 - Collared coils																		0.000
E56		Aperture 2 - Collared coils																		0.000
E57		Aperture 2 - Collared coils																		0.000
E58		Aperture 2 - Collared coils																		0.000
E59		Aperture 2 - Collared coils																		0.000
E60		Aperture 2 - Collared coils																		0.000
E61		Aperture 2 - Collared coils																		0.000
E62		Aperture 2 - Collared coils																		0.000
E63		Aperture 2 - Collared coils																		0.000
E64		Aperture 2 - Collared coils																		0.000
E65		Aperture 2 - Collared coils																		0.000
E66		Aperture 2 - Collared coils																		0.000
E67		Aperture 2 - Collared coils																		0.000
E68		Aperture 2 - Collared coils																		0.000
E69		Aperture 2 - Collared coils																		0.000
E70		Aperture 2 - Collared coils																		0.000
E71		Aperture 2 - Collared coils																		0.000
E72		Aperture 2 - Collared coils																		0.000
E73		Aperture 2 - Collared coils																		0.000
E74		Aperture 2 - Collared coils																		0.000
E75		Aperture 2 - Collared coils																		0.000
E76		Aperture 2 - Collared coils																		0.000
E77		Aperture 2 - Collared coils																		0.000
E78		Aperture 2 - Collared coils																		0.000
E79		Aperture 2 - Collared coils																		0.000
E80		Aperture 2 - Collared coils																		0.000
E81		Aperture 2 - Collared coils																		0.000
E82		Aperture 2 - Collared coils																		0.000
E83		Aperture 2 - Collared coils																		0.000
E84		Aperture 2 - Collared coils																		0.000
E85		Aperture 2 - Collared coils																		0.000
E86		Aperture 2 - Collared coils																		0.000
E87		Aperture 2 - Collared coils																		0.000
E88		Aperture 2 - Collared coils																		0.000
E89		Aperture 2 - Collared coils																		0.000
E90		Aperture 2 - Collared coils																		0.000
E91		Aperture 2 - Collared coils																		0.000
E92		Aperture 2 - Collared coils																		0.000
E93		Aperture 2 - Collared coils																		0.000
E94		Aperture 2 - Collared coils																		0.000
E95		Aperture 2 - Collared coils																		0.000
E96		Aperture 2 - Collared coils																		0.000
E97		Aperture 2 - Collared coils																		0.000
E98		Aperture 2 - Collared coils																		0.000
E99		Aperture 2 - Collared coils																		0.000
E100		Aperture 2 - Collared coils																		0.000

Alarm sheet of HCMBB_A001-01000006:

File name		HCMBB_A001-01000006.xls	
Component ID	HCMBB_A001	Serial Number	1000006
Date of test Ap 1	12.09.01	Date of test Ap 2	12.09.01
Magnetic length		Aperture 2	
Magnetic length		status ok	
Main field Angle	Average central positions 1 to 20	Central positions 2 to 19	Heads CS position 1
	status ok	status ok	status ok
Main field Angle	Average central positions 1 to 20	Central positions 2 to 19	Heads NCS position 20
	status ok	status ok	status ok
b2	status ok	red alarm	status ok
b3	status ok	red alarm	status ok
b4	status ok	yellow alarm	status ok
b5	status ok	red alarm	status ok
b6	status ok	yellow alarm	status ok
b7	status ok	red alarm	status ok
b8	status ok	red alarm	status ok
b9	status ok	red alarm	status ok
b10	status ok	status ok	status ok
b11	status ok	red alarm	status ok
b12	status ok	status ok	status ok
b13	status ok	red alarm	status ok
b14	status ok	status ok	status ok
b15	status ok	yellow alarm	status ok
a2	status ok	red alarm	status ok
a3	status ok	status ok	status ok
a4	status ok	red alarm	status ok
a5	status ok	yellow alarm	status ok
a6	status ok	red alarm	status ok
a7	status ok	yellow alarm	status ok
a8	status ok	red alarm	status ok
a9	status ok	yellow alarm	status ok
a10	status ok	status ok	status ok
a11	status ok	yellow alarm	status ok
a12	status ok	yellow alarm	status ok
a13	status ok	status ok	status ok
a14	status ok	status ok	status ok
a15	status ok	yellow alarm	status ok
Coil Positioning	red alarm		status ok
Field Collinearity	status ok		

